

Department für Augenheilkunde Tübingen
Universitäts-Augenklinik

**Development of dry eye models to test a new treatment
option for dry eye disease**

**Thesis submitted as requirement to fulfill the degree
“Doctor of Philosophy” in *Experimental Medicine* (PhD)**

**at the
Faculty of Medicine
Eberhard Karls Universität
Tübingen**

**presented by
Rocha Teixeira Netto, Alice**

2024

Dean: Professor Dr. B. Pichler

1st reviewer: Professor Dr. K. U. Bartz-Schmidt

2nd reviewer: Professor Dr. F. Schaeffel

Date of oral examination: 28.02.2024

Dedications

I dedicate this thesis to my family, especially my parents, Roseli and Joaquim, and my sister, Elisa, who supported me unconditionally in all my decisions. In addition, I dedicate it to my grandmothers, aunts, and cousin, who have been encouraging me during these years, even from a great distance.

Table of contents

1 Introduction	1
1.1 Ocular anatomy	1
1.2 Corneal anatomy	1
1.3 Regenerative function of the limbal region.....	3
1.4 Tear film anatomy	4
1.5 Function and composition of corneal epithelial cells	5
1.5.1 Function of the glycocalyx of the ocular surface epithelium	5
1.5.2 Tight junctions	6
1.6 Corneal diseases	6
1.7 Dry eye disease	8
1.7.1 Causes of dry eye disease	9
1.7.2 Inflammation process in dry eye disease	10
1.8 State of the art of dry eye models	12
1.9 Treatment approaches.....	15
1.10 DNA-Nanoparticles (NPs).....	17
1.10.1 Drug delivery with DNA-NP	17
1.11 Aim of this thesis.....	19
2 Materials and Methods.....	21
2.1 Materials	21
2.1.1 Products	21
2.1.2 Equipments	23
2.1.3 Programs.....	24
2.2 Methods	25
2.2.1 Organ culture	25
2.2.1.1 Preparation of porcine corneas.....	25
2.2.1.2 <i>Ex vivo</i> dry eye model: incubation at low humidity.....	26

2.2.1.3 <i>Ex vivo</i> dry eye model: treatment with dexamethasone and hyaluronic acid.....	26
2.2.1.4 <i>Ex vivo</i> dry eye model: treatment with DNA-Nanoparticles.....	27
2.2.2 Culture of an <i>in vitro</i> model	27
2.2.2.1 Preparation of an <i>in vitro</i> human corneal model (SkinEthic™ HCE).....	27
2.2.2.2 <i>In vitro</i> human corneal model for dry eye disease: incubation at low humidity and treatment with NPs.....	27
2.2.3 Cell culture	28
2.2.3.1 Isolation and cultivation of porcine primary corneal cells: outgrowth method.....	28
2.2.3.2 Passaging corneal cells	30
2.2.3.3 Cell quantification after immunostaining	30
2.2.4 Preparation of DNA-Nanoparticles	31
2.2.5 Histology	31
2.2.5.1 Production of cryosections.....	31
2.2.5.2 Periodic acid-Schiff (PAS) staining	32
2.2.5.3 Hematoxylin-eosin (HE) staining.....	32
2.2.5.4 4',6-diamidino-2-phenylindole (DAPI) Staining	33
2.2.5.5 Histological analysis: thickness of corneal epithelium.....	33
2.2.5.6 Histological analysis: analysis of corneal epithelium integrity	34
2.2.5.7 Analysis of NPs' fluorescence.....	36
2.2.6 Molecular methods	36
2.2.6.1 Quantitative Real-Time PCR of porcine corneas	36
2.2.6.2 Quantitative Real-Time PCR of corneal cell cultures	38
2.2.6.3 IL-1 β enzyme-linked immunosorbent assay (ELISA)	39
2.2.6.4 TdT-Mediated dUTP-Biotin Nick End Labeling (TUNEL) Assay	40
2.2.6.5 Porcine cytokine antibody array.....	41
2.2.6.6 Immunostaining of corneal cell cultures.....	42
2.2.7 Statistical analysis	43
3 Results	45

3.1 Chapter 1: Development of an <i>ex vivo</i> porcine dry eye model.....	45
3.1.1 Corneal damage and corneal thinning are consequences of low humidity.....	45
3.1.2 Inflammation in the porcine model is induced by low humidity	47
3.1.3 Tight junctions and glycocalyx markers are upregulated in samples cultivated at LH	51
3.1.4 Apoptosis of porcine corneal cells is induced by LH.....	52
3.1.5 Treatment with dexamethasone counteracts LH effects and with hyaluronic acid eye drops counteracts only partially	54
3.2 Chapter 2: Testing of DNA Nanoparticles in the dry eye model.....	59
3.2.1 The DNA-Nanoparticles protect the <i>in vitro</i> human corneal model by adhesion to the corneal epithelium.....	59
3.2.2 The DNA-Nanoparticles adhere to the stressed <i>in vitro</i> human corneal model and to controls for up to 24 h.....	60
3.2.3 The DNA-Nanoparticles adhere to the stressed porcine corneas	63
3.2.4 DNA-Nanoparticles hinder corneal epithelial apoptosis caused by low humidity.....	65
3.2.5 Treatment with NPs 100 μ M counteracts upregulation of <i>galectin-3</i>	67
3.3 Chapter 3: Establishment of a porcine corneal cell culture	69
3.3.1 Establishment of the outgrowth method	69
3.3.2 Cell cultures cultivated with FBS contain higher amounts of cells	71
3.3.3 Cultures cultivated without FBS contain mainly epithelial cells and keratocytes.....	73
4 Discussion	78
4.1 An <i>ex vivo</i> model for dry eye disease	78
4.2 Inflammation is induced in the dry eye model	80
4.3 Upregulation of tight junctions and glycocalyx markers in the dry eye model.....	82
4.4 Apoptosis is induced in the dry eye model.....	82

4.5 Treatment with dexamethasone can reverse the effects of low humidity, while hyaluronic acid partially reverses it.....	83
4.6 NPs adhere to the epithelial surface of stressed <i>in vitro</i> and <i>ex vivo</i> models.....	85
4.7 NPs prevent apoptosis at <i>ex vivo</i> porcine DED model.....	89
4.8 NPs 100 μ M prevent upregulation of <i>galectin-3</i> caused by LH.....	89
4.9 Corneal cell isolation with the outgrowth method: differences in cell cultures cultured with FBS and without it.....	91
4.10 The outgrowth method provides a mixed cell culture that can be useful in studying toxicology of new ocular drugs.....	93
4.11 Conclusion.....	95
5 Summary.....	96
6 German Summary.....	98
7 Bibliography.....	101
8 Declaration of own contributions.....	112
9 Publications.....	114
10 Acknowledgements.....	115

List of abbreviations

ADDE	aqueous-deficient dry eye
Ang1	angiopoetin-1
APC	antigen-presenting cells
Atto 488	attometer range 488 nanometers
BSA	bovine serum albumin
C	Celsius
CAMs	cell adhesion molecules
cDNA	complementary DNA
CD4	cluster of differentiation 4
CK3	cytokeratin 3
CK12	cytokeratin 12
CL	contact lens
CMC	critical micelle concentration
CRD	carbohydrate recognition domains
CXCL8	chemokine C-X-C motif ligand-8
DAPI	4',6-diamidino-2-phenylindole
DED	dry eye disease
Dexa	dexamethasone
DNA	deoxyribonucleic acid
EDE	evaporative dry eye
EDTA	ethylenediamine tetraacetic acid
ELISA	enzyme-linked immunosorbent assay
EVEIT	<i>ex vivo</i> eye irritation test
FBS	fetal bovine serum
FGF21	fibroblast growth factor 21
GRs	glucocorticoid receptors
h	hour(s)
HA	hyaluronic acid
HCl	hydrochloric acid
HE	hematoxylin and eosin
HH	high humidity
HHS	harris hematoxylin solutions
IFN- β	interferon-beta
IFN- γ	interferon-gamma
I κ B	NF- κ B inhibitor
IL-1	interleukin 1
IL-6	interleukin 6
IL-8	interleukin 8
IL-1 β	interleukin 1 beta
IL-17	interleukin 17
JAM	junctional adhesion molecule
Kan-NP	kanamycin loaded nanoparticle
kDa	kilodalton

LASIK	laser-assisted in situ keratomileusis
LESC	limbal epithelial stem cell
LH	low humidity
M	molarity
MAPK	mitogen-activated protein kinase
MgCl ₂	magnesium dichloride
MGD	meibomian gland dysfunction
MIF	macrophage migration inhibitory factor
min	minute(s)
mL	milliliters
μL	microliters
mm	millimeters
μM	micromolar
μm	micrometers
MMP	metalloproteinase
MMP9	metalloproteinase 9
mRNA	messenger RNA
MUC	mucin(s)
NaCl	sodium chloride
NF-κB	nuclear factor kappa-light-chain-enhancer of activated B cells
ng	nanogram
NK	natural killer
NLRP3	NLR family pyrin domain containing 3
NOD	nonobese diabetic
NP(s)	DNA-Nanoparticle(s)
PAS	periodic acid–Schiff
PBS	phosphate-buffered saline
PCR	polymerase chain reaction
PFA	paraformaldehyde
pg	picograms
PS	penicillin-streptomycin
qRT-PCR	quantitative real-time PCR
RNA	ribonucleic acid
ROS	reactive oxygen species
s	second(s)
TAE	tris base, acetic acid, EDTA
TBS	tris buffered saline
TBS-T	tris buffered saline with Tween 20
T/E	trypsin/ EDTA
Th0	naive T cell
Th1	T helper 1
Th17	T helper 17
TLR	toll like receptor
TNF-α	tumor necrosis factor-alpha
TUNEL	TdT-Mediated dUTP-Biotin Nick End Labeling
VEGF-C	vascular endothelial growth factor C

VEGF-D	vascular endothelial growth factor D
v/v	volume per volume
x g	relative centrifugal force in units of gravity
ZO-1	zonula occludens-1
ZO-2	zonula occludens-2
ZO-3	zonula occludens-3
w/v	weight per volume

List of figures

Figure 1: Schematic representation of the layers of the human eye.	1
Figure 2: Schematic representation of corneal anatomy.	3
Figure 3: Schematic representation of tear film anatomy.	5
Figure 4: Dry eye is characterized by an inflammatory vicious cycle.	9
Figure 5: Simplified representation of inflammation process in DED.	12
Figure 6: Method of forming and loading the NPs.	18
Figure 7: Porcine corneal preparation.	25
Figure 8: Corneal cell outgrowth method.	29
Figure 9: The virtual meter used for corneal epithelial measurement.	34
Figure 10: Evaluation of the corneal epithelial integrity of PAS images. ...	35
Figure 11: Corneal damage and corneal thinning occur as a consequence of exposure to LH.	46
Figure 12: Inflammatory markers are expressed in samples incubated at LH in comparison to the ones incubated at HH.	48
Figure 13: Tight junction and glycocalyx markers are upregulated due to LH.	51
Figure 14: Porcine corneas incubated for 12 h and for 24 h at LH had apoptosis of corneal epithelial cells stimulated.	53
Figure 15: LH effects on porcine corneas are counteracted by dexamethasone.	56
Figure 16: The effects caused by LH are partially neutralized by hyaluronic acid (HA).	58
Figure 17: <i>In vitro</i> human corneal model (SkinEthic™ HCE) underwent structural damage when incubated with pristine Atto 488 at LH as control and presented mild damage when treated with NP-Atto 488 and incubated at LH.	60
Figure 18: NPs adhered to the stressed <i>in vitro</i> human corneal tissue for up to 24 h.	62
Figure 19: NPs adhered to the stressed porcine corneal epithelium.	64
Figure 20: NPs hinder apoptosis caused by LH.	66
Figure 21: Upregulation of <i>galectin-3</i> was prevented in corneas treated with NP 100 μM and submitted to LH.	68

Figure 22: Corneal cell isolation with the outgrowth method.	71
Figure 23: The average number of cells per week during outgrowth cultivation.	72
Figure 24: Cell cultures cultivated with FBS and without it contained corneal epithelial cells.	74
Figure 25: Cell cultures cultivated without FBS showed more keratocan and lumican expression.	76
Figure 26: Pie chart representing the proportion of distinct cell types.	77
Figure 27: A summary of the results of <i>ex vivo</i> incubations of porcine corneas at LH for 12 h, 24 h, and 48 h.	83

List of tables

Table 1: Products and manufacturers	21
Table 2: Equipments and manufacturers	23
Table 3: Primer pairs in 5'-3' directions used for a quantitative real-time PCR of porcine corneas	38
Table 4: “Primer pairs in 5'-3' directions used for quantitative real-time PCR of corneal cells (Netto et al., 2023, p. 9)”	39
Table 5: Primary and secondary antibodies and dilutions used for immunostaining	43
Table 6: Cytokines released in the media of samples submitted to LH for 24 h and 48 h	50

1 Introduction

1.1 Ocular anatomy

The human eye is the organ responsible for the vision. It measures around 22 to 27 mm in anteroposterior diameter and 69 to 85 mm in circumference (Kels et al., 2015). The eye is composed of three main layers (Snell & Lemp, 1998). The cornea, the sclera, and their zone of interdigitation, known as the limbus, are part of one layer of the eyeball. The second eye layer is the middle uveal layer, which is considered the central vascular layer of the eyeball and contains the iris, ciliary body, and choroid. The third one comprises the retina, which is the interior layer of the eye (Figure 1) (Kels et al., 2015).

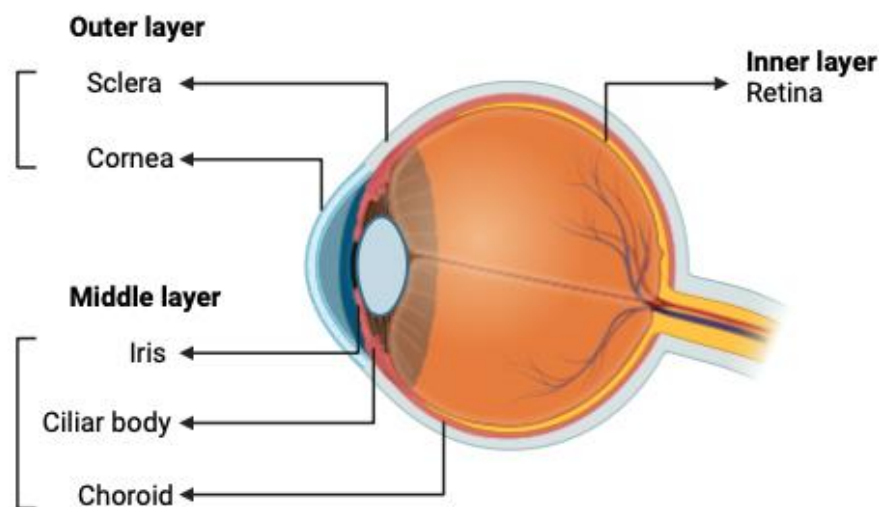


Figure 1: **Schematic representation of the layers of the human eye.**

The outer layer is comprised of the sclera and cornea, the middle layer is formed by the iris, ciliary body, and choroid, and the inner layer contains the retina. Created with BioRender.com.

1.2 Corneal anatomy

The cornea and the sclera are the cover of the eyeball. Despite being transparent, the cornea lacks blood vessels and protects the eye against

infections because of its structural barrier (DeMonte & Kim, 2011 apud Netto et al., 2022). The cornea's refractive power is approximately 40-44 diopters, which makes it two-thirds of the total refractive power of the eye (Sridhar 2017). It is covered with a tear film, and they together make an appropriate anterior refractive surface for the eye (Sridhar 2017). The cornea in turn is composed of many layers, such as epithelium, Bowman's layer, stroma, Descemet's membrane, and endothelium (Figure 2) (DeMonte & Kim, 2011). In 2013, a sixth corneal layer was discovered between the stroma and Descemet's membrane, called Dua's layer, also known as pre-Descemet's layer (Dua et al., 2013).

The corneal epithelium, formed of a nonkeratinized stratified squamous epithelium, has five to seven layers and is derived from the surface ectoderm. The epithelium has three types of cells: superficial cells, wing cells, and basal cells. The superficial cells, connected by tight junctions, form two to three layers and are flat polygonal cells with microvilli on the surface. The wing cells form two to three layers and hence the name, have a wing-like shape. The deeper layer of the corneal epithelium is a single layer composed of basal cells, which can be cuboidal or columnar. These cells have a lot of organelles and are the only corneal epithelial cells that are capable of mitosis, besides the stem cells and transiently amplifying cells. The basal cells generate the wing and superficial cells (Sridhar, 2017).

About 90% of the cornea is made up of the middle layer, the stroma, which consists of a stromal matrix of collagen fibrils and keratocytes (Wentz-Hunter et al., 2001 apud Netto et al., 2023). A single layer of cells called endothelium covers the posterior layer, and these cells are responsible for keeping the transparency of the cornea by controlling the circulation of aqueous humor into the cornea (Kinoshita et al., 2018 apud Netto et al., 2023).

Cytokeratins, such as cytokeratin 3 (CK3) and cytokeratin 12 (CK12), are expressed by corneal epithelial cells, and tight junctions formed by zonula occludens 1 (ZO-1) and occludin are also present in these cells (Ban et al., 2003; Shi et al., 2020 apud Netto et al., 2023). Vimentin belongs to the intermediate filament type III, which forms part of the cytoskeleton. A basal

expression of this protein can be found in keratocytes, fibroblasts, and myofibroblasts (Chaurasia et al., 2009 apud Netto et al., 2023). Moreover, the undifferentiated epithelial cells at the proliferative rim of the cornea express vimentin as well (Castro-Muñozledo et al., 2017 apud Netto et al. 2023). At the stroma, keratocytes produce keratan sulfate-containing proteoglycans known as keratocan and lumican (España et al., 2003 apud Netto et al., 2023). Activated corneal keratocytes differentiate into fibroblasts when the epithelial barrier is breached, exposing the stroma (Fukuda, 2020 apud Netto et al., 2023).

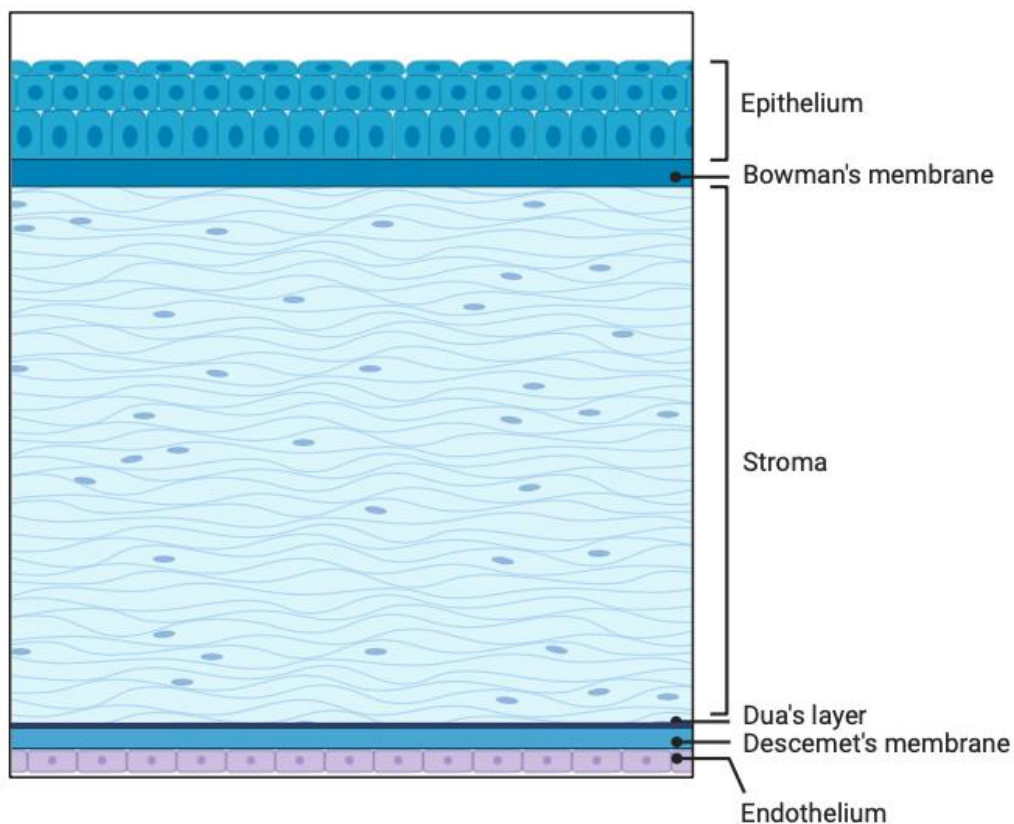


Figure 2: **Schematic representation of corneal anatomy.**

The cornea comprises of the following layers: epithelium, which is the most external; Bowman's membrane; stroma; Descemet's membrane; and endothelium. Recently, it was discovered and incorporated a sixth layer to the cornea, Dua's layer, placed between the stroma and Descemet's membrane. Created with BioRender.com.

1.3 Regenerative function of the limbal region

The corneoscleral limbus is the place where corneal stem cells reside. A stem cell repository is believed to be located in the limbal palisades of Vogt and

interpalisade ridges (Dua & Azuara-Blanco, 2000). Treatment of limbal insufficiency, which can result from frequent ocular diseases like chemical burns or rare ocular diseases like ocular cicatricial pemphigoid, can be challenging. The cornea cannot regenerate its layers of cells without the limbal region (Schlötzer-Schrehardt & Kruse, 2005; Yoon et al., 2014 apud Netto et al., 2023). This area is responsible for originating almost every cell type of the cornea. As a result of limbal insufficiency, conjunctival epithelial ingrowth, inflammation, and destruction of the basal membrane cause vision loss. Thus, limbal epithelial stem cell therapy (LESC) can be considered a viable alternative to limbal insufficiency treatment (Bremond-Gignac et al., 2018 apud Netto et al., 2023). Consequently, methods for the expansion of limbal epithelial stem cells (LESCs) *ex vivo* are needed (Netto et al., 2023).

1.4 Tear film anatomy

The tear film is composed of a complex of different chemicals that are secreted by multiple sources, such as the cornea, and it comprises three distinct layers. The most external layer originates from the secretion of meibomian glands, which is an oily secretion. This secretion is a subtle refractive surface as well as a barrier against the evaporation of the tear film. The middle layer is formed by the lacrimal gland and numerous accessory lacrimal glands that are disseminated within the conjunctiva stroma. The third layer, which stays in contact with the corneal superficial epithelial cells, is the mucin layer, which is produced by the conjunctival goblet cells and by the epithelial cells of the cornea, and the conjunctiva (Figure 3). The tear film is responsible for the lubrication and hydration of the ocular surface and is the first layer interacting with incoming light. It is also important because it provides oxygen, immunoglobulins, lysozymes, lactoferrin, and α - and β -defensins (Gipson, 2007; Sridhar, 2017).

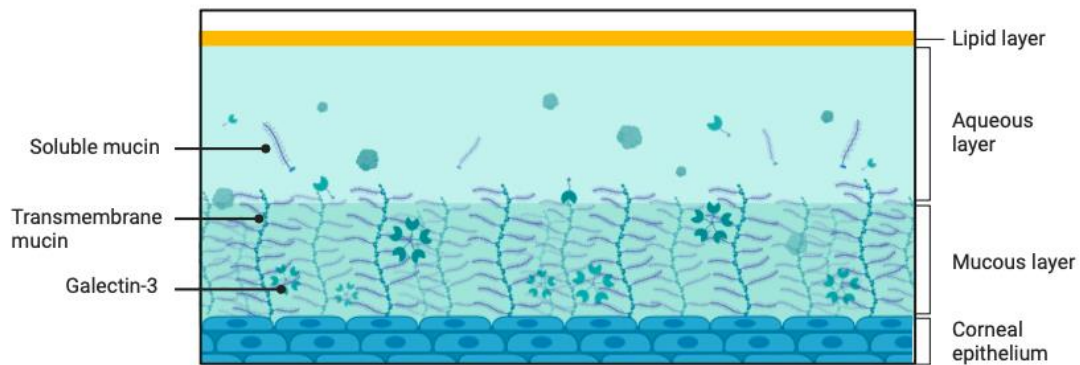


Figure 3: **Schematic representation of tear film anatomy.** The tear film comprises of three layers. The most external is the lipid layer, followed by the aqueous and mucous layers. Created with BioRender.com.

1.5 Function and composition of corneal epithelial cells

The external layer of the superficial corneal cells comprises microvilli and microplicae, that help to increase the surface area of the interface between tears and cells. The epithelial cell surface retains the tear film (Sridhar, 2017; Bron et al., 2017). The tear film fills small irregularities in the cell surface, creating a smooth and uniform cover, thus creating an ideal surface for the correct refraction of light (Gipson, 2007). This cell layer is connected by tight junctions and also has a barrier formed by dense, apical glycocalyx, rich in transmembrane mucins, that plays an important role as a lubricant, reducing attrition at the corneal surface and helps to combat microbial colonization (Bron et al., 2017 apud Netto et al., 2022).

1.5.1 Function of the glycocalyx of the ocular surface epithelium

Transmembrane mucins (MUC), such as MUC1, MUC4, and MUC16, and a soluble lectin, galectin-3 are part of the epithelial glycocalyx. The mucin exodomains are glycosylated, making the plasma membranes hydrophilic instead of hydrophobic and providing moistening of the epithelium (Bron et al., 2017). Structurally, galectin-3 has carbohydrate recognition domains (CRD) that

attach to MUC1 and MUC16 and generate a galectin-glycoprotein lattice. This complex is responsible for a protective barrier function and also for the regulation of cell-cell, cell-matrix, and cell-pathogen interactions (Bron et al., 2017; Uchino et al., 2015 apud Netto et al., 2022).

1.5.2 Tight junctions

The epithelial cells of the cornea are interconnected through tight junctions that form a barrier and prevent the tear film from entering the intercellular spaces (DelMonte & Kim, 2011). They also help stabilize the epithelial cell structure by connecting the cytoskeletons of the epithelial cells (Anderson & Van Itallie, 2009). Two protein classes form tight junctions. The first class is composed of transmembrane proteins, which connect the membranes of the neighbor cells and the tight junction-associated proteins. The second class consists of tight junction-associated proteins, which are intracellular proteins located on the cytoplasmic side. Occludin, claudin, and junctional adhesion molecule (JAM) are known as transmembrane proteins. ZO-1, ZO-2, and ZO-3 are zonula occludens proteins that bind transmembrane proteins and the cytoskeleton, stabilizing tight junctions (Bäumli, 2008 apud Netto et al., 2022).

In the corneal epithelium, tight junctions are involved in several signaling pathways that regulate their assembly, maintenance, and function. Inflammatory signaling causes changes in the corneal epithelial barrier, affects transcript and protein levels of tight junctions proteins, and impacts their subcellular localization (Leong & Tong, 2015; Contreras-Ruiz et al., 2012).

1.6 Corneal diseases

Corneal diseases are considered an important cause of blindness in the world, 6.7 million people worldwide are estimated to have visual impairment

correlated with corneal diseases (Porth et al., 2019 apud Netto et al., 2023). Several diseases and injuries can affect the cornea, including ulcerative lesions, keratoconus, leukoma, bullous keratopathy, dystrophies (the most common being Fuchs'), infections, inflammations, and perforations. Symptoms may include opacification, moderate or severe impairment of vision, and even blindness (Hamrah et al., 2015 apud Netto et al., 2023).

Some corneal diseases are more prevalent in developing countries. Corneal edema after cataract surgery was reported to be a cause of visual impairment, especially in a low-income elderly population in São Paulo, Brazil, and the importance of a good quality cataract surgery and of a cautious post-operative follow-up was strengthened (Porth et al., 2019; Araújo Filho et al., 2008). Trachoma is an ocular infection caused by *Chlamydia trachomatis* that is also more prevalent in developing countries. Repeated bacterial infections since childhood lead to chronic conjunctival inflammation. Afterward, scarring of the conjunctiva occurs, resulting in the inward turning of the eyelashes and causing them to scratch the cornea (trichiasis). This harms the corneal surface and can ultimately cause visual impairment and corneal opacification (Ramadhani et al., 2016).

Regarding developed countries, the most common corneal diseases are keratoconus, Fuchs' dystrophy, and dry eye disease. Keratoconus is a corneal ectasia defined by progressive thinning of the corneal stroma, irregular astigmatism, and reduced visual acuity (Santodomingo-Rubido et al., 2022; Cavas-Martínez et al., 2017). In Fuchs' corneal endothelial dystrophy, there is a reduction of corneal endothelial cells and abnormal growth of the extracellular matrix in Descemet's membrane, known as guttae. This will cause corneal edema and reduced vision (Ong Tone et al., 2021). Dry eye disease (DED) is a chronic disease that involves an insufficient amount or poor quality of tear film (Rouen & White, 2018).

1.7 Dry eye disease

Dry eye is a multifactorial illness that influences the ocular surface and tear fluid (Lemp & Foulks, 2007). Some symptoms of dry eye are: foreign body sensation in the eye, burning eyes, itching, and photosensitivity (Zeev et al., 2014). In general, 5-35% of the population worldwide suffers from dry eye, depending on age (Lemp & Foulks, 2007). This chronic eye disease is currently treated primarily with eye drops applied several times a day (Zhang et al., 2017). There are, however, many side effects associated with these eye drops after application, such as ocular allergies or blurred vision, which results in lower compliance (Robin & Muir, 2019 apud Netto et al. 2022).

It is currently unknown what triggers the pathomechanisms of dry eye. Studies indicate that chronic dry eyes are defined by elevated osmolarity of the tear film and inflammatory processes that affect both the lacrimal gland and the ocular surface (Barabino et al., 2012 apud Netto et al., 2022). When the cornea is not sufficiently moistened, it can lead to severe corneal damage, as the membranes of the corneal epithelial cells are destroyed by the drought and thereby lose the intercellular connections (Gilbard et al., 1984). An inflammatory vicious cycle is described in DED (Yamaguchi, 2018). Tear film instability initiates the cycle and leads to hyperosmolarity of the tear film (Pflugfelder & de Paiva, 2017 apud Netto et al., 2022). One possible pathomechanism of DED is the activation of stress-activated protein kinases by the hyperosmolarity of the tear film or the drying out of the ocular surface, culminating with the release of pro-inflammatory cytokines, matrix metalloproteinases, and pro-apoptotic factors (De Paiva et al., 2009; Pflugfelder et al., 2005 apud Netto et al., 2022). Pro-inflammatory cytokines trigger inflammatory reactions that activate further signaling cascades and ultimately lead to cell death (Rajalakshmy et al., 2014). Similarly, pro-apoptotic factors trigger cell death. Furthermore, when matrix metalloproteinases are activated, they break down the extracellular matrix, leading to a disruption in cell-cell adhesion (Pflugfelder et al., 2005 apud Netto et al., 2022). As a result of these processes, the corneal tissue loses its stability

and integrity (Figure 4) (Dursun et al., 2002; Pflugfelder et al., 2005 apud Netto et al., 2022).

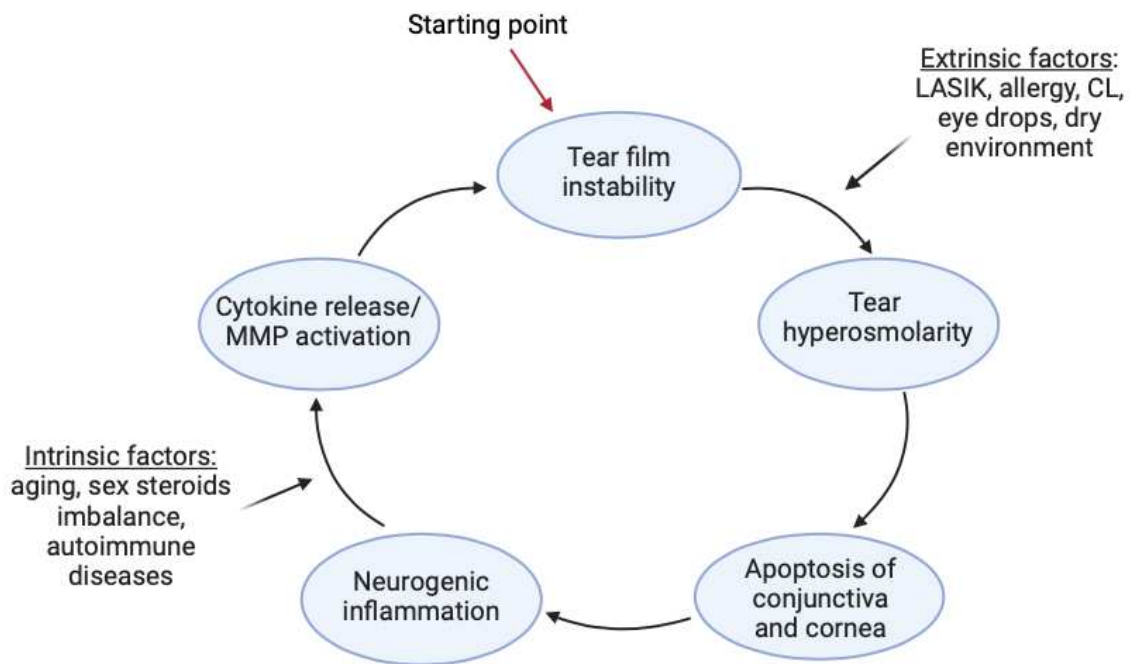


Figure 4: **Dry eye is characterized by an inflammatory vicious cycle.**

The initiating event that triggers inflammatory events in DED occurs when the tear film loses its homeostasis. Stopping the vicious cycle of inflammation is a crucial step toward treating it. Tear film instability and hyperosmolarity, leading to apoptosis of corneal and conjunctival cells, neurogenic inflammation, and cytokine release causing inflammation in the ocular surface, are parts of the cycle. Stress to the surface of the eye is generated by intrinsic and extrinsic factors, which accelerate the vicious cycle and aggravate dry eye. The red arrow indicates starting point of the vicious cycle. LASIK: laser-assisted in situ keratomileusis. CL: contact lens. MMP: metalloproteinase. Created with BioRender.com.

Figure adapted from: <https://doi.org/10.1167/iovs.17-23651> (Yamaguchi, 2018).

1.7.1 Causes of dry eye disease

Hyperosmolarity of the tear film and tear instability are the main conductors of DED (Lemp & Foulks, 2007). Two major subtypes of DED are described: evaporative dry eye (EDE) and aqueous-deficient dry eye (ADDE). The EDE occurs as a consequence of exaggerated evaporation of the tear film, causing hyperosmolarity, but the tear function is normal in this case. A well-known example of EDE is the case of meibomian gland dysfunction (MGD), in which lipid deficiency in the tear film causes a higher rate of tear evaporation. In

ADDE, the tear film evaporation rate is normal, but tear secretion is reduced. This is the case, for example, of age-related DED, in which the lacrimal glands secrete fewer tears. However, it is important to note that these subtypes of DED can be present at the same time in one disease, for example, as it occurs in Sjögren syndrome (Bron et al., 2017).

It is also important to highlight that ocular surface hyperosmolarity is influenced by both the environment and personal behavior. External factors include environmental humidity, temperature, and wind velocity, while on a personal level, blink rate, lid aperture size, and medication influence tear secretion (Bron et al., 2017; Rouen & White, 2018; Milner et al., 2017; Stapleton et al., 2017). When it comes to environmental influence in DED, low humidity (LH) is a well-known risk factor since it increases tear evaporation (Rouen & White, 2018; Milner et al., 2017; Stapleton et al., 2017).

1.7.2 Inflammation process in dry eye disease

Desiccating stress and hyperosmolarity of tear fluid trigger an innate immune pathway by activation of the NLR family pyrin domain containing 3 (NLRP3) inflammasome and Toll-like receptors (TLRs) (Tsubota et al., 2020 apud Netto et al. 2022). Hyperosmolarity of the tear fluid generates reactive oxygen species (ROS), which activate NLRP3 (Park et al., 2019). Ultimately, interleukin 1 beta (IL-1 β), a pro-inflammatory cytokine, is secreted and matured as a result of NLRP3 activation (Chi et al., 2017 apud Netto et al. 2022). Tear hyperosmolarity also triggers many events in the corneal epithelial cells through the activation of mitogen-activated protein kinase (MAPK) that triggers nuclear factor kappa-light-chain-enhancer of activated B cells (NF- κ B), which is involved in the cellular response stimulated by stress, cytokines, and free radicals. NF- κ B is also stimulated by TLR signaling pathways, and it triggers the secretion of IL-1 β and tumor necrosis factor- alpha (TNF- α) (Tsubota et al., 2020 apud Netto et al., 2022). Hence, matrix metalloproteinase 9 (MMP9) is activated by both IL-1 β and TNF- α (Corrales et al., 2006; Bron et al., 2017 apud Netto et al., 2022).

MMP9 cleaves tight junction components such as occludin and ZO-1 and glycocalyx components such as galectin-3 (Uchino et al., 2015 apud Netto et al., 2022). Consequently, these factors induce the loss of corneal epithelial cells and increase the permeability of corneal epithelium (Figure 5) (Bron et al., 2017 apud Netto et al., 2022).

In the innate immune response, epithelial cells and macrophages will secrete other pro-inflammatory cytokines and chemokines such as interleukin-8 (IL-8), also called chemokine C-X-C motif ligand-8 (CXCL8) (Tsubota et al., 2020; Enríquez-de-Salamanca et al., 2010). In addition, as part of the innate immune response, natural killer (NK) cells stimulate the maturation of antigen-presenting cells (APCs) through secretion of IFN- γ and other pro-inflammatory cytokines such as TNF- α , interleukin-1 (IL-1) and interleukin-6 (IL-6) (Bron et al., 2017; Tsubota et al., 2020).

Once APCs have been activated, they migrate to local lymph nodes and activate naive T cells (Th0) that differentiate into IL-17-secreting T helper cell 17 (Th17) and interferon gamma (IFN- γ) secreting Th1 cells, initiating the adaptive immune response. These cells move back to the conjunctiva and release IFN- γ and IL-17, upregulating the synthesis of chemokines, cell adhesion molecules (CAMs), and vascular endothelial growth factor VEGF-C and VEGF-D. These processes will ultimately cause disruption of the corneal epithelial barrier and reduction of conjunctival goblet cells (Bron et al., 2017; Tsubota et al., 2020; Stevenson et al., 2012). Moreover, the T cell infiltration in the ocular surface perpetuates the chronic inflammation that is found in DED (Tsubota et al., 2020).

Apoptosis of corneal cells is also a consequence of the inflammatory processes in DED. There are intrinsic and extrinsic pathways that can induce apoptosis of ocular surface cells in DED. The stress-associated mitogen-activated protein kinase pathway is an intrinsic pathway related to this disease. Tumor necrosis factor and Fas/Fas ligand are increased in DED and modulate the extrinsic pathway (Stevenson et al., 2012; Tsubota et al., 2020).

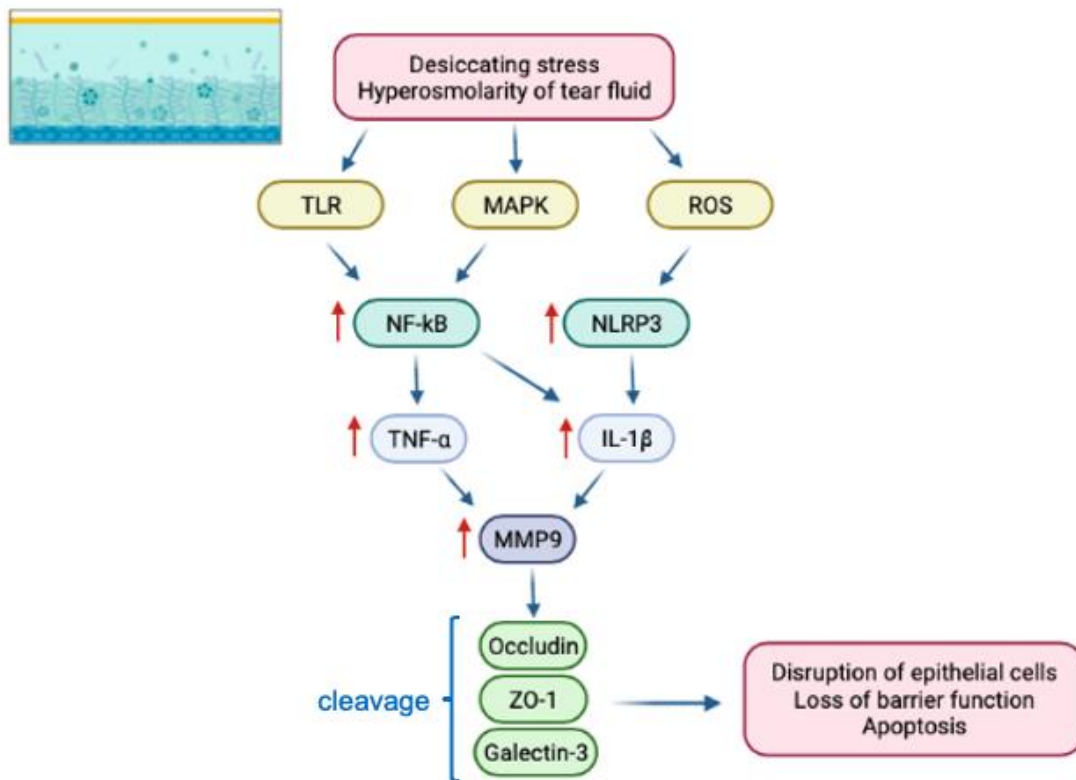


Figure 5: **Simplified representation of inflammation process in DED.**

Tear hyperosmolarity stimulates a cascade of events in the epithelial cells of the ocular surface, involving NF- κ B signaling pathways and the generation of inflammatory cytokines, such as IL-1 β , TNF- α and proteases, such as MMP9. Both IL-1 β and TNF- α upregulate the production of MMP9. Then, MMP9 cleaves tight junction components, such as occludin and ZO-1, and glycocalyx components, such as galectin-3. Consequently, these factors induce the loss of corneal epithelial cells and increase the permeability of corneal epithelium. Hyperosmolarity also generates ROS, which activates NLRP3. NLRP3 ultimately leads to the maturation and secretion of the pro-inflammatory cytokine IL-1 β and is also involved in the apoptosis mechanism (Netto et al., 2022). These mediators and tear hyperosmolarity will generate goblet cell and epithelial cell depletion and deterioration of the epithelial glycocalyx. Created with BioRender.com.

1.8 State of the art of dry eye models

In vivo dry eye models have already been proposed. Mouse models of lacrimal inflammation (dacryoadenitis) have been suggested. For example, the nonobese diabetic (NOD) mouse model can be used as a model for secondary Sjögren syndrome. In this model, there is a lymphocytic infiltration of CD4⁺ Th1 cells in the lacrimal gland (Takahashi et al., 1997; Barabino & Dana, 2004). Another mouse model for Sjögren's syndrome is the MRL/lpr mouse, in which

CD4⁺ T cells also infiltrate the lacrimal gland (Van Blokland & Versnel, 2002; Barabino & Dana, 2004). Dogs, cats, rabbits, mice, and monkeys models were proposed based on the surgical removal of the lacrimal gland (Barabino & Dana, 2004 apud Netto et al. 2022). However, it was observed that the removal of this gland did not cause significant modifications of the ocular surface signs. This might occur due to the fact that the accessory lacrimal glands compensate the amount of tears (Barabino & Dana, 2004). In rabbits, hyper evaporative dry eye models have been developed by implanting lid specula or sutures to prevent them from blinking. Dry spots on the rabbit corneal epithelial surface were observed already after two hours of implantation of the lid specula. However, it is important to note that DED is a chronic event, so due to the acuteness of the stimulated dry eye, this model is not ideal for investigating DED pathogenesis (Fujihara et al., 1995; Barabino & Dana, 2004). The tear film is protected by lipids that are produced by meibomian glands and deposited onto the aqueous phase each time the eyes blink. Therefore, a rabbit model was suggested in which meibomian glands orifices were cauterized. While this model is useful for investigating how meibomian gland dysfunction affects the surface of the eye, it should be ideally performed in an environment with constant temperature, humidity, and airflow (Gilbard et al., 1989; Barabino & Dana, 2004). A combined lacrimal insufficiency and evaporative dry eye mouse model was established with the use of transdermal scopolamine and the display of constant airflow. Scopolamine inhibits cholinergic (muscarinic) receptors in the lacrimal gland causing a reduction of aqueous production. Hence, in this model, it was identified modification of aqueous tear production and corneal barrier function similar to human DED (Dursun et al., 2002; Barabino & Dana, 2004).

Although several *ex vivo* models have been established previously, they are either laborious or difficult to set up, thus reducing the reproducibility efficiency (Netto et al., 2022). For instance, based on the *ex vivo* eye irritation test (EVEIT), rabbit corneas can be cultivated, and lesions can be introduced via dental drill. Using a special culture chamber with a micro pumping system for the medium supply, the corneas can be incubated in an incubator at 32 °C

and saturated humid air to simulate DED (Schrage et al., 2012). Although relatively simple, the technique does require a special pumping system, and the lesions produced through dental drills are not uniform in many cases.

Similarly, the whole porcine eyes can be received from a local abattoir and fixed in a holder. To reproduce dry eye disease, the flow of tears and blinking at long intervals using a ventilator can be simulated. Moreover, a computer-controlled mechanical arm system has also been explored in the literature to simulate blinking and lacrimation. The mechanical arm had the ability to move the eyelid of the porcine eye and apply phosphate-buffered saline (PBS). However, this apparatus makes the study more variable due to the elevated number of factors involved and more expensive (Chan et al., 2014 apud Netto et al., 2022).

Ex vivo porcine dry eye models were also developed based on corneal exposure to air room temperature with constant humidity of 55-65% for different time points (Choy, To et al., 2004). The same research group developed a porcine dry eye model in which lacrimation and blinking were simulated with the help of a mechanical arm (Choy, Cho et al., 2004; Choy et al., 2006; Choy et al., 2008). A modification of the previous methods was created by Hasegawa et al. For that, porcine eyes were incubated in a chamber maintained at 20-22 °C and 40-50% humidity without airflow. Artificial tears composed of sodium hyaluronate and castor oil were evaluated in this model (Hasegawa et al., 2014). The main advantages of this method are the reduction of the number of *in vivo* animals used to test potential new drugs, the ability to gather a large volume of data on new therapies in a short period of time, and it allows the fast evaluation of these new therapies. However, this model is not able to assess blinking and corneal wound healing, which are better to be studied in *in vivo* animals. Due to postmortem modifications presented by the dry eye model, long-term and adverse effects of the new therapeutic options cannot be assessed as well. As a result, this porcine model provides a useful way to screen potential drugs before testing on animals in the long run (Hasegawa et al., 2014).

In conclusion, *in vivo* studies are more expensive, and there has been opposition to the use of animals for research purposes. *Ex vivo* experiments are less expensive and can be used to study the influence of an individual factor in dry eye syndrome. Because of that, there is a need for the development of a simple, robust, and easily reproducible *ex vivo* model for DED (Netto et al., 2022).

1.9 Treatment approaches

Since there are different types of DED, there are distinct types of treatment (Rouen & White, 2018). In general, the goal is to restore the homeostasis of the tear film (Nelson et al., 2017). Simple lifestyle changes such as taking breaks from staring at a computer screen, increasing humidity at home or workplace, and avoiding environments with dry air can help alleviate symptoms (Rouen & White, 2018). Some studies have shown that nutritional supplementation of essential fatty acids, such as omega-3, helps alleviate symptoms because they have an anti-inflammatory effect and help to increase the lipid layer of the tear film, thus reducing its evaporation (Stapleton et al., 2017; Rouen & White, 2018).

Due to the multifactorial nature of dry DED, it is often difficult to identify and eliminate the causative triggers, so treating the symptoms is usually the best option. Generally, a treatment with tear substitutes in the form of eye drops can be used. Most lubricating eye drops have an aqueous base mixed with viscosity-enhancing agents that help increase ocular lubrication and extend the retention time on the eye. These agents are: carbomer 940 (polyacrylic acid), carboxymethyl cellulose, dextran, hyaluronic acid (HA), hydroxypropyl-guar, hydroxypropyl methylcellulose, polyvinyl alcohol, polyvinyl pyrrolidone and polyethylene glycol (Jones et al., 2017).

The use of artificial tears composed of hyaluronic acid (HA) is widespread, and the efficacy of HA to moisturize the eye surface and to improve DED symptoms was already demonstrated (Choi et al., 2015; Vogel et al., 2010

apud Netto et al., 2022). HA can also heal wounds and bind to ocular surface cells (Jones et al., 2017).

Corticosteroids present a therapeutic effect against the inflammation processes that occur at DED. Because of that, dexamethasone (dexa), a corticosteroid, is used to treat inflammatory symptoms (Pflugfelder, 2004; Nagelhout et al., 2005 apud Netto et al., 2022). Glucocorticoids attach to their inactive cytosolic receptors (GRs), ultimately hindering the expression of cytokines and adhesion molecules. The activated GRs move to the cell nucleus, directly interacting with DNA elements to modulate transcriptional events. Moreover, activated GRs counteract the activity of NF- κ B. Different mechanisms were described for that: firstly, glucocorticoids stimulate transcription and protein synthesis of NF- κ B inhibitor, I κ B. Secondly, activated GRs hinder NF- κ B attachment to DNA through protein-protein interactions (Almawi & Melemedjian, 2002).

Another medication that also has an anti-inflammatory role and is an immunomodulating drug is Cyclosporin A, which is a fungal derived-peptide (Jones et al., 2017; Pflugfelder, 2004). This drug has been used to treat moderate to severe DED (Jones et al., 2017).

A treatment approach used for retaining tears at the ocular surface is the punctal plug. It is used to occlude the punctal opening or the canaliculus, reducing the drainage of tears in the case of ADDE (Jones et al., 2017).

Regarding artificial tears, the efficacy and tolerability of the various tear substitutes are perceived very differently from person to person. In general, the retention time of all eye drops on the ocular surface is very low (Davies, 2000). To ensure sufficient moistening of the cornea, a common feature and, at the same time a disadvantage, of all therapies is the multiple applications per day, resulting in reduced compliance. In addition, most eye drops, due to their high viscosity, cause blurred vision, which is very uncomfortable for the patient. For this reason, the need for new, effective treatment options that ensure adequate humidification despite low application frequency remains very high.

1.10 DNA-Nanoparticles (NPs)

Because of the disadvantages and side effects of the current eye drops described before, the Schnichels Lab at the University Eye Hospital of Tübingen, together with chemists from the University of Groningen (AG Prof. Dr. Herrmann), have developed a platform technology for eye drops based on DNA-Nanoparticles (NPs) that have a high affinity for the eye.

DNA-Nanoparticles consist of lipid-modified DNA strands that form micelles with hydrophobic cores and hydrophilic coronas (Figure 6). The lipid-modified DNA strands are formed by four alkyl-modified 2'-deoxyuridine nucleotides (U). The U-modified DNA strands contain amphiphilic properties, and when they are introduced into an aqueous environment, the strands self-assemble into micellar nanoparticles. Additionally, these nanoparticles can be easily equipped with therapeutic moieties, making them useful as drug delivery platforms. Another feature of the NPs is that they present intrinsic affinity for the ocular surface (Willem de Vries et al., 2018; Schnichels et al., 2021).

1.10.1 Drug delivery with DNA-NP

There are a number of methods for loading drugs onto DNA-Nanoparticles, including hydrophobic interactions with the micelle's lipid core, covalent bonding with a complementary DNA strand, or hybridization with aptamers on the DNA nanoparticles' corona (Figure 6). An aptamer is a small DNA or RNA oligomer that acts as a link between a drug and the NPs by selectively binding to it. The DNA itself does not function therapeutically or genetically and is easily degradable. This biodegradation profile sets these DNA-Nanoparticles apart from most polymeric or inorganic nanoparticles developed for drug delivery (Arora et al., 2012; Chen et al., 2009; Willem de Vries et al., 2018). The DNA-Nanoparticles are protected with a patent in Europe and a patent application in the U.S. (WO2015041520).

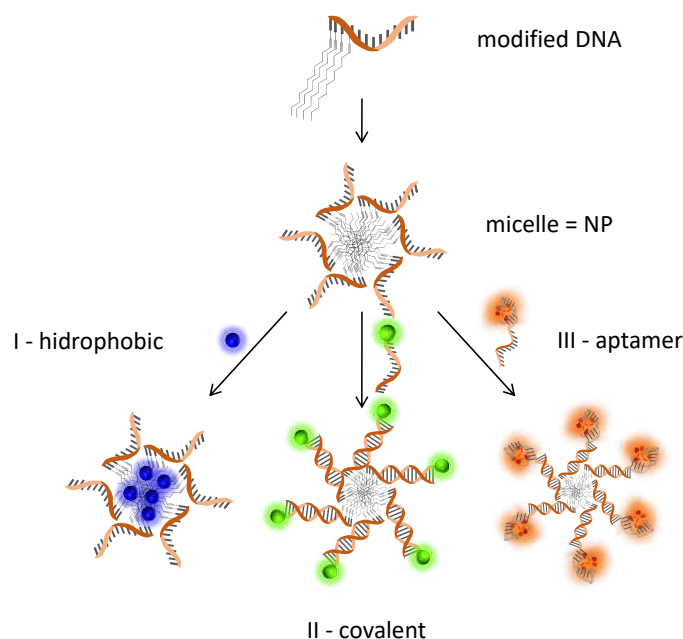


Figure 6: **Method of forming and loading the NPs.**

As a first step, several amphiphilic lipid-DNA strands self-assemble to form NPs. Functionalization of the NPs can take place via hydrophobic interactions with the core (blue I), covalent interactions with complementary DNA strands (green II), or aptamers (orange III). Adapted with permission from ACS Appl. Mater. Interfaces 2021, 13, 8, 9445–9456. Copyright 2023 American Chemical Society.

A proof-of-principle study showed that the NPs bind strongly to animal and human corneas. Initially, fluorescently labeled NPs successfully adhered to porcine corneas, but a fluorescent dye used as a control did not show any affinity (Willem de Vries et al., 2018). Additionally, it was shown that the NPs behave similarly on human corneal tissue even when combined with a drug. Through aptameric interactions, the NPs were loaded with the aminoglycoside antibiotic Kanamycin. Even two hours after the application of these eye drops on the human corneal tissue, a significant amount of the Kanamycin-loaded NP (Kan-NP) could be detected. On the other hand, five minutes after application, the unformulated antibiotic had not been detected on the tissue (Willem de Vries et al., 2018).

1.11 Aim of this thesis

As mentioned before, DED has a high prevalence among the world's population, and the main initial treatment option currently is the use of lubricating eye drops. Because of that, there is a need to establish a simple, robust, and not expensive dry eye model on which candidate therapeutics can be tested. Moreover, DED is a chronic disease that requires constant treatment, for example, using eye drops several times a day. However, these eye drops often cause local side effects like ocular allergies or blurred vision after their application due to the high viscosity of these eye drops. Hence, these facts lead to reduced compliance (Hermann et al., 2011 apud Netto et al., 2022). Therefore, testing new therapeutic options for DED is needed.

In this thesis, the first aim is to establish an easy-to-reproduce *ex vivo* porcine model for DED. This porcine model offers the unique possibility of viewing the entire tissue complex of a cornea while being able to better mimic the *in vivo* conditions, thus avoiding *in vivo* experiments. *Ex vivo* experiments do rely on animal tissue, however, it is worth noting that the eyes used in such experiments are obtained from a local abattoir where the animals are primarily slaughtered for nutritional purposes (Netto et al., 2022).

A further aim of this thesis is to test if the DNA-Nanoparticles (NPs), whose safety has already been demonstrated *in vitro* (Willem de Vries et al., 2018), are a potential new treatment option for DED. For this purpose, the porcine corneal dry eye model established, and a 3D *in vitro* corneal model (SkinEthic™ HCE) were treated with the NPs and submitted to LH stress. Next, the *ex vivo* and *in vitro* models were evaluated histologically and characterized by suitable markers.

Finally, the last aim of this thesis is to establish an *in vitro* corneal cell model that can be used in the future to test new therapeutic options for corneal diseases, such as corneal infection or DED. To produce an *in vitro* corneal model, corneal limbal isolation and primary corneal cell cultivation were performed (Netto et al., 2023). Methods to isolate primary corneal cells have been previously used in our laboratory, involving the isolation of corneal

explants and the use of dispase (Yoeruek et al., 2007; Sobolewska et al., 2015). Therefore, the method developed in this thesis is an adaptation of the protocols that were previously used, and it was called the outgrowth method. Moreover, cell cultures cultivated with fetal bovine serum (FBS) and without are compared (Netto et al., 2023). Due to ethical concerns surrounding the use of laboratory animals in research, it is necessary to explore alternative methods that can be employed (Hurst et al., 2020 apud Netto et al., 2023). Hence, an advantage of the method described is that the porcine eyes used were not derived from animals exclusively used for research grounds (Netto et al., 2023).

2 Materials and Methods

2.1 Materials

2.1.1 Products

Table 1: **Products and manufacturers.**

Product	Manufacturer	Product's number
Artelac® Splash EDO®	Bausch-Lomb, Heidelberg, Germany	
Bovine serum albumin (BSA)	PanReac AppliChem ITW Reagent, Darmstadt, Germany	A1391,0500
Cell counting slides	Wolflabs (Olympus), Pocklington, UK	N5232100
CnT-Prime	CellnTec-Advanced Cell Systems, Bern, Switzerland	CnT-PR114211
T25 culture flask with ventilation screw cap	Greiner Bio-One GmbH, Frickenhausen, Germany	690175
Culture Medium II with Dextran T500	Pan Biotech, Aidenbach, Germany	P04-09702
DexaEDO®	Bausch-Lomb; Heidelberg, Germany	
Disposable cup 100 mL	Sarstedt, Nümbrecht, Germany	75.563
Disposable safety scalpel #11	Aesculap AG, Tuttlingen, Germany	BA811SU
DNAse I	Aplichem, Darmstadt, Germany	APA3778-0500
Eosin Y	Sigma Aldrich, Taufkirchen, Germany	230251
Ethylenediamine tetraacetic acid (EDTA)	Carl Roth, Karlsruhe, Germany	8040
Dulbecco's Phosphate Buffered Saline (PBS)	Gibco™ Thermo-Fisher, Karlsruhe, Germany	10010056
Eppendorf Safe-Lock tube 1.5 mL	Eppendorf, Hamburg, Germany	0030120086
Ethanol absolute for analysis	VWR, Darmstadt, Germany	K48829 383710
Eukitt®	Sigma Aldrich, Taufkirchen, Germany	03989
Fetal bovine serum (FBS)	Thermo-Fischer, Karlsruhe,	10100147

	Germany	
Fluorsave™	Merck Milipore, Darmstadt, Germany	345789
Harris Hematoxylin	Sigma-Aldrich, Taufenkirchen, Germany	HHS-32
Hydrochloric acid-alcohol	Applichem, Darmstadt, Germany	257097
Iodine Braunol®	B. Braun, Melsungen, Germany	190970
iTaq Universal SYBR® Green Supermix	Bio-Rad, Feldkirchen, Germany	1725124
Lumit™ IL-1β Human Immunoassay	Promega, Walldorf, Germany	#W6010
Methanol	Honeywell, Offenbach, Germany	67.56.1
Maintenance Medium	Episkin, Lyon, France	19SMM023
Microscope slide	R. Langenbrinck GmbH, Emmendingen, Germany	03-0060
MgCl ₂	Sigma Aldrich, Taufkirchen, Germany	M8266-100G
MultiMACS™ cDNA Synthesis Kit	Miltenyi Biotec, Köln, Germany	130-094-410
NaCl	VWR, Darmstadt, Germany	27810.295
NanoBiT® IL-1β Immunoassay Kit	Promega, Walldorf, Germany	CS2032A01
Needle 20G Sterican®	B Braun, Melsungen, Germany	4657519
Needle 25G Sterican®	B Braun, Melsungen, Germany	9186166
Paraformaldehyde (PFA)	Merck Milipore, Darmstadt, Germany	1040051000
Penicillin-streptomycin (PS) 100 mL	Thermo-Fischer, Karlsruhe, Germany	15140148
Periodic Acid Solution	Carl Roth, Karlsruhe, Germany	HP00.1
RayBio® C Series Porcine Cytokine Array 1	Ray-Biotech, Peachtree Corners, GA, USA	AAP-CYT-1-4
Schiff's reagent	Carl Roth, Karlsruhe, Germany	X900.1
SkinEthic™ HCE	Episkin, Lyon, France	HCS/S/5
SsoAdvanced Universal SYBR® Green Supermix	Bio-Rad, Feldkirchen, Germany	1725270
Syringe 1 mL	BD Plastik™, Madrid, Spain	303172
Tissue-Tek	Sakura Finetek, Torrance, CA, USA	4583

Tween 20 Polyoxyethylene (20) Sorbitan Monolaurate	Serva Electrophoresis GmbH, Heidelberg, Germany	39796.01
Tris acetate	Sigma Aldrich, Taufkirchen, Germany	T1258
Trizma®-Base	Sigma Aldrich, Taufkirchen, Germany	93362
Triton X-100	Sigma Aldrich, Taufkirchen, Germany	#9002-93-1
Trypsin/EDTA (T/E)	Gibco™ Thermo-Fischer, Karlsruhe, Germany	25200072
Tube 15 mL	Greiner Bio-One, Frickenhausen, Germany	188271
Tube 50 mL	Greiner Bio-One, Frickenhausen, Germany	210261
TUNEL assay	Roche Diagnostics, Mannheim, Germany	11684817910
Xylol	VWR, Darmstadt, Germany	28975-325
4',6-diamidino-2-phenylindole (DAPI)	Thermo-Fischer, Karlsruhe, Germany	D1306
6-well plate, Cellstar®	Greiner Bio-One, Frickenhausen, Germany	M9062-100EA
8-well chamber slides, Nunc® Lab-Tek® II	Merck Milipore, Darmstadt, Germany	154534
96-well plate, Falcon®, white/clear	Corning, Keiserslautern, Germany	CLS3922-100EA
96-well PCR plate full-skirted	Nippon Genetics, Düren, Germany	FG-180250

2.1.2 Equipments

Table 2: **Equipments and manufacturers.**

Equipment	Manufacturer	Model
Centrifuge VWR Mega Star 3.0R	VWR, Darmstadt, Germany	521.1752
Cryostat	LEICA, Wetzlar, Germany	CM 1900
Heracell 150i CO ₂ incubator	Thermo-Fischer, Karlsruhe, Germany	50116050

Heratherm Oven	Thermo-Fischer, Karlsruhe, Germany	51028112
Hygrometer	InFactory	145616
MultiMACS™M96 Separator	Miltenyi Biotec, Köln, Germany	130-091-937
M200 NanoQuant spectrophotometer	Tecan, Männerdorf, Switzerland	Infinite 200
Multimode microplate reader	Tecan, Männerdorf, Switzerland	Tecan Spark
Olympus R1 SLI Cell counter	Olympus corporation, Center Valley, PA, USA	K23009240
Scale	Sartorius, Göttingen, Germany	LA 120 S
Thermal cycler Bio-Rad CFX96™ Real-Time System	Bio-Rad, Feldkirchen, Germany	1845097
VWR Thermal Shake Touch	VWR, Darmstadt, Germany	89232-908
Zeiss Axio Observer	Carl Zeiss, Oberkochen, Germany	491916-0002-000
Zeiss Axio Imager Z1 Apotome Microscope with Mrm digital camera	Carl Zeiss, Oberkochen, Germany	p1739

2.1.3 Programs

- GraphPad Prism™ Version 8.2.1, GraphPad Software, Inc., San Diego, California, USA.
- ImageJ™ Software (ImageJ, U. S. National Institutes of Health, Bethesda, MD, USA, <https://imagej.nih.gov/ij/>, 30 November 2021) Version 2.0.0-rc-68/1.52e
- Biorender (<https://biorender.com>), Biorender, Inc., Toronto, Canada.
- ZEN Imaging Software Version 2.6 (blue edition), Zeiss, Oberkochen, Germany.

2.2 Methods

2.2.1 Organ culture

2.2.1.1 Preparation of porcine corneas

Porcine eyes were obtained from a local abattoir in Balingen, Germany. After the euthanization of the pigs, the eyes were enucleated and cooled at 4 °C for two hours until being used. To prepare for the experiment, the pig eyes were allowed to reach room temperature, and any surrounding muscles and tissues were removed. The eyes were disinfected in iodine 5% (v/v) diluted in Milli-Q water for 5 min. After that, the eyes were washed five times in 1x phosphate-buffered saline (PBS) with 2% penicillin-streptomycin (PS). The porcine corneas were extracted from the eyes with a scalpel, scissors, and forceps. A cut was made around the cornea, leaving a narrow part of the sclera around it. The cornea samples were placed in 6-well plates with the corneal epithelium facing upwards with 800 μ L of medium (Culture Medium II) supplemented with 2% PS (Figure 7) (Netto et al., 2022).

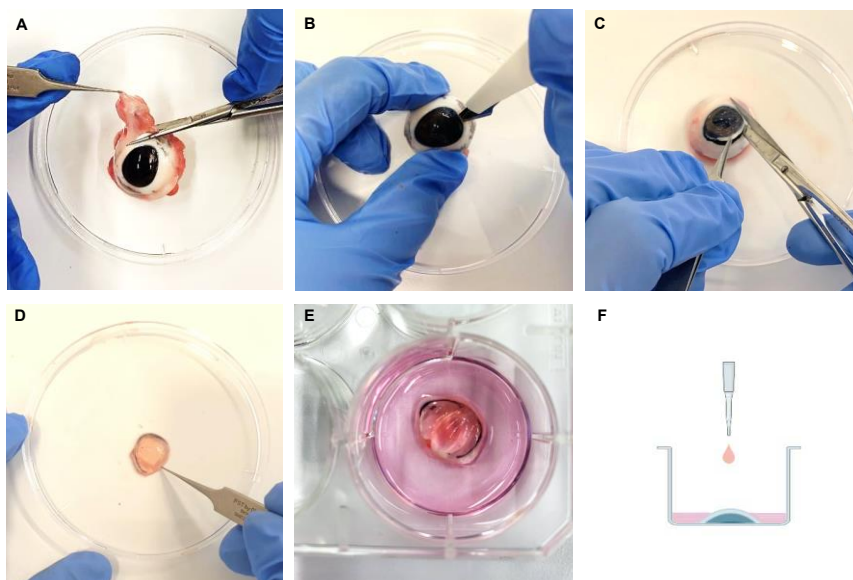


Figure 7: **Porcine corneal preparation.**

(A) Muscles and tissues around the eye were discarded. (B-C) To remove the cornea, a cut was made around it first with a scalpel and then with scissors. (D) A narrow part of the sclera was

left around the cornea. (E) The corneas were incubated in a 6-well plate facing upwards, and Culture Medium II was added. (F) The schematic figure depicts the air-lifting technique, porcine cornea is placed in a 6-well plate facing upwards, and culture media in pink meets the corneal epithelium surface. Figure F was created with BioRender.com. Figure published at <https://doi.org/10.3390/ijms23094567> (Netto et al., 2022).

2.2.1.2 *Ex vivo* dry eye model: incubation at low humidity

The corneas were divided into two groups, and each cornea received 800 μ L of medium (Culture Medium II) supplemented with 2% PS. This amount of medium covered the surface of the porcine corneal epithelium so that the medium moisturized the apical epithelium cells, and the air made contact with this thin layer of medium (Ban et al., 2003) (Figure 7 F). Controls were cultivated in a 6-well plate at 37 °C and 95% humidity (high humidity, HH), whereas dry eye corneas were cultivated at 37 °C and 30% humidity (low humidity, LH) for 12, 24, or 48 h (Netto et al., 2022). For culturing the corneas in LH, a drying oven was used as an incubator (Heratherm Oven, Thermo-Fischer). One day before incubation, a disposable cup with 50 mL of Milli-Q water was placed at the bottom of the incubator so that the humidity could be maintained around 30%. The humidity was monitored during the experiment with a digital hygrometer.

2.2.1.3 *Ex vivo* dry eye model: treatment with dexamethasone and hyaluronic acid

To explore whether it is possible to reverse the damage caused by LH, samples were treated with one drop of dexamethasone (1.3 mg/mL, DexaEDO®, Bausch-Lomb, Heidelberg, Germany) every 12 h or with one drop of hyaluronic acid (0.2%, Artelac® Splash EDO®, Bausch-Lomb, Heidelberg, Germany) every 6 h. Corneas were cultivated at LH, with or without treatment, while the controls were cultivated at HH, with or without treatment, for 24 h (Netto et al., 2022).

2.2.1.4 *Ex vivo* dry eye model: treatment with DNA-Nanoparticles

To investigate whether the damage caused by LH could be prevented, corneas (HH and LH) were treated with 50 μ L of DNA-Nanoparticles (NPs) 50 μ M, 100 μ M, or with buffer and incubated in 6-well plates for 24 h. Untreated corneas were incubated at LH as well as HH for the same period and served as controls. For histology, the NPs were attached to a fluorescent green dye Atto 488 (NP-Atto 488), and the untreated samples were incubated with pristine Atto 488.

2.2.2 Culture of an *in vitro* model

2.2.2.1 Preparation of an *in vitro* human corneal model (SkinEthic™ HCE)

The *in vitro* human corneal model (SkinEthic™ HCE) is produced from transformed human corneal keratinocytes, resulting in a tissue similar to the human cornea epithelium with basal, wing, and mucus production cells (Alépée et al., 2016). The artificial human corneal epithelium was delivered to the laboratory, transferred to a 6-well plate, and incubated with 1 mL of Maintenance Medium SkinEthic™ overnight at 37 °C and 95% humidity.

2.2.2.2 *In vitro* human corneal model for dry eye disease: incubation at low humidity and treatment with NPs

The next day after the delivery as describe in 2.2.2.1, one group of SkinEthic™ HCE samples was treated with NP-Atto 488 50 μ M and incubated at extreme LH (15% humidity and 37 °C) or at HH (95% humidity and 37 °C) for 30 minutes. For this group, a lower humidity was used, but the incubation time was also shorter. Untreated controls were incubated with the pristine florescent dye Atto 488 and cultivated under the same two conditions for the same period of time. The second group of *in vitro* human corneal samples was treated with NP-

Atto 488 and incubated at LH (30% humidity at 37 °C) or at HH (95% humidity and 37 °C) for 24 h. Control samples treated with pristine Atto 488 were also cultivated under the same two conditions for 24 h. Afterward, the samples were frozen in aluminum cups filled with tissue-Tek in liquid nitrogen and stored at -28 °C. The samples received the NP-Atto 488, and the untreated samples received Atto 488 due to further histological analysis. For the second group of samples, after Hematoxylin-eosin (HE) or after 4',6-diamidino-2-phenylindole (DAPI) staining, mosaic pictures were done with the Zeiss Axio Imager Z1 Apotome Microscope with Mrm digital camera.

2.2.3 Cell culture

2.2.3.1 Isolation and cultivation of porcine primary corneal cells: outgrowth method

Porcine eyes were collected from a local abattoir in Balingen just after the euthanization of the animals, were stored and cooled during transportation to the laboratory. Direct contact between the eyes and the ice was avoided. At the laboratory, the eyes were stored at 4 °C until being used. To perform the outgrowth method, the porcine eye was removed from the refrigerator, and muscles and tissues around the eye were removed with scissors and forceps (Figure 8 A). The eye was disinfected in iodine 5% (v/v) diluted in Milli-Q water for 5 min in a disposable cup. Next, it was washed five times in PBS with 2% PS. In a petri dish, the porcine cornea was extracted from the eye with a scalpel, scissors, and forceps by cutting circularly around the cornea, leaving a thin part of the sclera around it (Figures 8 B-C). The rest of the eye was discarded, and the cornea was washed in PBS with PS. The cornea was first cut in half and then each half in three parts. The center of the cornea was extracted, leaving a strip of approximately 2 mm of corneal tissue and 2 mm of sclera (Figures 8 D-F). The strips were cut in small explants. The explants of one eye were placed in a T25 culture flask with a ventilation screw cap (Figure 8 G), 15-20 explants were used per culture flask. After 5 min, the cornea

explants adhered to the surface of the flask and 1 mL of culture medium (CnT-Prime + 2% PS) was carefully added, one drop per explant, so that the explants do not detach from the flask. In some samples, 10% FBS was added to the culture medium, and the cultivation of corneal cells with FBS and without it was compared. The flasks were incubated in an incubator at 37 °C with 5% CO₂ overnight. On the next day, 3 mL of culture medium was carefully added to the flask and incubated in an incubator at 37 °C with 5% CO₂ for 4-5 weeks. The culture medium was changed twice per week. To change the medium, the old medium was carefully aspirated to avoid detachment of corneal explants, and 4 mL of new culture medium was slowly added. The cells achieved 70%-80% confluency in approximately four weeks (Netto et al., 2023).

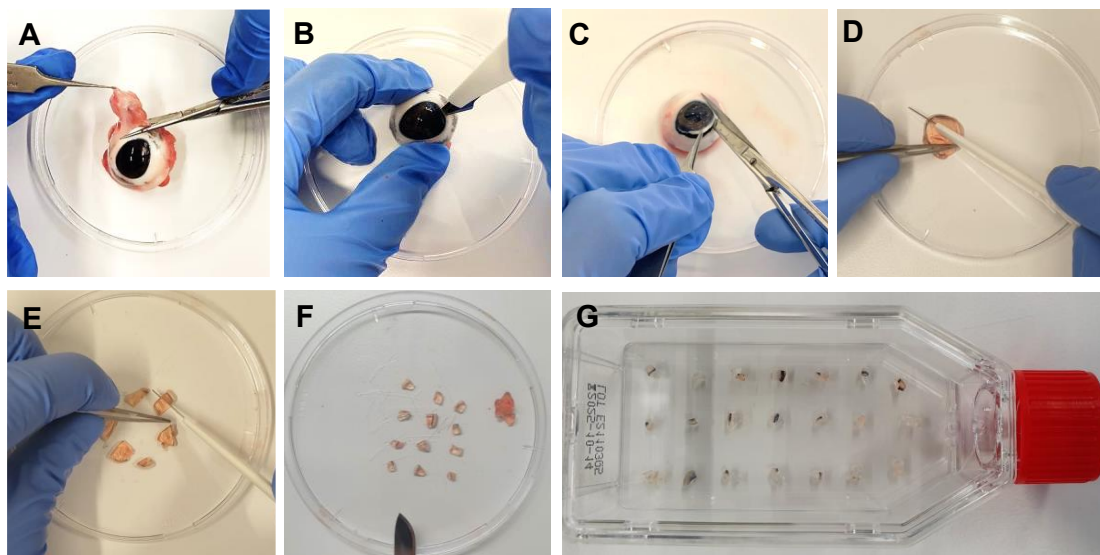


Figure 8: Corneal cell outgrowth method.

(A) Muscles and tissues around the eye were discarded. (B-C) To remove the cornea, first an incision was made in the sclera with a scalpel, then the cornea was completely extracted with scissors. (D) The cornea was cut in half. (E-F) Each cornea half was cut in pieces, and the center of the cornea was removed so that a strip of approximately 2 mm of corneal tissue and 2 mm of sclera was done. (G) The small cornea explants were placed in a T25 culture flask with a ventilator screw cap. After 5 min, when the cornea explants adhered to the surface of the flask, 1 mL of culture medium was added (CnT-Prime + 2% PS), one drop per explant. Optionally, 10% FBS was added to the medium, depending on the purpose of the culture. Figure published at: <https://doi.org/10.3390/mps6030050> (Netto et al., 2023).

2.2.3.2 Passaging corneal cells

After four to five weeks of cultivation, the corneal cells were split. For that, corneal explants were removed from the flask with the help of forceps. The culture medium was aspirated, and the cells were washed with 4 mL of PBS. Next, PBS was aspirated, 1 mL of trypsin/EDTA (T/E) was added, and the flask was incubated in an incubator at 37 °C with 5% CO₂ for 5 min. After that, the cells were mechanically detached by tapping on the side of the bottle, and 2 mL of T/E-stopping solution was added (CnT-Prime + 2% PS + 10% FBS). The entire content of the flask was pipetted into a 15 mL falcon and centrifuged at room temperature, 300 x g, for 5 min. The supernatant was carefully aspirated, and the cell content was resuspended with 1 mL of culture medium (CnT-Prime + 2% PS with or without FBS, depending if the explants were previously incubated with serum or not). Cells at first passage were counted, diluted accordingly, and seeded in chamber slides for immunostaining or frozen without medium in 1.5 mL tubes for qRT-PCR. 25,000-50,000 cells were seeded in 8-well chamber slides (Netto et al., 2023).

2.2.3.3 Cell quantification after immunostaining

A quantification of epithelial cells and keratocytes in the cell cultures was performed. A cell count was performed with semi-automated counter software ImageJ™, the total number of cells per picture was quantified by counting the cells' nuclei manually, and CK3, lumican, and keratocan positive cells were counted as well. The software ImageJ™ has a function that allows one to mark with an "X" the nucleus of each cell every time one clicks. Therefore, when cell counting is finished, it provides the total number of clicks per image. A calculation of the ratio of CK3-positive cells to total cells was done to obtain the percentage of epithelial cells. The same procedure was done to obtain the percentage of keratocytes, and an average between lumican and keratocan-positive cells was calculated. A minimum of two wells per condition were

stained with each marker separately, and a minimum of five pictures per staining and per condition was used for analysis (Netto et al., 2023).

2.2.4 Preparation of DNA-Nanoparticles

A buffer mix comprising 100 μL of 50x TAE stock (containing 2,5 M of Tris-acetate and 50 mM of ethylenediamine tetraacetic acid (EDTA)), 200 μL of NaCl (5 M), and 100 μL of MgCl_2 (1 M) was prepared in an Eppendorf tube.

A DNA single strand formed by four alkyl-modified 2'-deoxyuridine nucleotides (U) and eight bases (adenine-cytosine-guanine-thymine) was synthesized using standard automated solid-phase phosphoramidite coupling methods on an ÄKTA oligopilot plus (GE Healthcare) DNA synthesizer (Sequence 5'→3': UUUUGCGGATTC). This gave the DNA strand, which was actually hydrophilic, a hydrophobic side. The hydrophobic section of the DNA single strand caused multiple strands to assemble into micelles in solution. The micelles were prepared in 1x buffer mix and deionized water at a concentration of 100 μM and 50 μM . One equivalent of the complementary DNA was added and hybridized using a thermal gradient (90 °C for 30 min, then -1 °C every two minutes until room temperature). For fluorescence analysis, the complementary strand was coupled with the dye Atto 488 (U4T-Atto 488 = NP labeled with a covalently bound fluorescent dye Atto 488) (Willem de Vries et al., 2018).

2.2.5 Histology

2.2.5.1 Production of cryosections

After incubating the samples for the determined time, they were frozen with Tissue-Tek (Sakura Finetek, Torrance, CA, USA) in liquid nitrogen and stored at -28 °C. Frozen porcine corneal samples and the *in vitro* human corneal model were used to generate cryosections. Cryosections were

generated with a Cryostat (Leica), with a thickness of 12 μm , and three sections of each porcine cornea were placed on a microscope slide. Slices were dried at room temperature for 15 min and further stored at $-28\text{ }^{\circ}\text{C}$ until further processing (Netto et al., 2022). Regarding the *in vitro* human corneal model, four sections were placed on each slide. The slides were also stored unfixed at $-28\text{ }^{\circ}\text{C}$ until further processing.

2.2.5.2 Periodic acid-Schiff (PAS) staining

Periodic acid-Schiff (PAS) staining was used to verify the glycocalyx content of the porcine corneal tissue samples. The cryosections were fixed with ice-cold methanol for 10 min and the slides were incubated in 1% periodic acid for 10 min. “The acid was washed with running water, and the samples were incubated for 10 min with Schiff’s reagent and washed under running water again. The slides were placed in a container filled with Harris Hematoxylin Solutions (HHS) for 10 min, and differentiated with hydrochloric acid-alcohol solution for 3 s. After that, they were washed and left in the water for 10 min to remove the excess staining (Netto et al., 2022, p. 16).” The samples were dehydrated first with two times 96% (v/v) ethanol and then with two times 99% (v/v) ethanol. The sections were immersed into a row of xylene (four vessels filled with xylene) and embedded with Eukitt®. The Zeiss Axio Imager Z1 Apotome Microscope with Mrm digital camera was used for imaging.

2.2.5.3 Hematoxylin-eosin (HE) staining

Hematoxylin-eosin (HE) staining was used to visualize the different structures and components of the tissue under the microscope. Hematoxylin stains all acidic or basophilic structures, such as cell nuclei, and eosin stains all acidophilic or basic components of cell structures, such as cytoplasm and extracellular matrix. The cryosections were fixed in ice-cold methanol for 10 min

and washed in Milli-Q water twice for 1 min. Afterward, the sections were stained with HHS for 10 min and washed twice with water. “Next, the slides were differentiated in hydrochloric acid-alcohol solution for 3 s, washed with water for 10 min, and placed in Eosin Y for 2 min. After that, the cryosections were dehydrated using an ascending ethanol series (70% (v/v), two times 96% (v/v), two times 99% (v/v)), and in a series of four times xylene. Finally, the samples were embedded with Eukitt® (Netto et al., 2022, p. 16).” The Zeiss Axio Imager Z1 Apotome Microscope with Mrm digital camera was used for imaging.

2.2.5.4 4',6-diamidino-2-phenylindole (DAPI) Staining

4',6-diamidino-2-phenylindole (DAPI) staining was used to visualize the nuclei of cells. Cryosections were fixed in ice-cold methanol for 10 min at room temperature. After briefly air drying the slides, they were washed three times in TBS (1x) for 10 min. 100 μ L of DAPI solution (0.2 μ g/mL DAPI was diluted 1:20 in PBS) was pipetted onto each slide and incubated for 5 min at room temperature in the dark. This was followed by a washing process twice with TBS (1x) for 5 min and for another 5 min in water. After briefly air-drying the slides, they were covered with one drop of Fluorsave™, and a cover slip was placed on top. The Zeiss Axio Imager Z1 Apotome Microscope with Mrm digital camera was used for imaging.

2.2.5.5 Histological analysis: thickness of corneal epithelium

An image-analyzing system (ZEN Imaging Software, Carl Zeiss, Germany) was used to measure the thickness of the porcine corneal epithelium. HE pictures were used for the measurement. A virtual meter was used, and one end of the meter was allocated to the bottom of the corneal basal cells, and the other end was allocated to the top of the superficial corneal cells (Figure 9). To

reduce variability, the mean of six measures per picture and six pictures of 200-fold magnification per sample was used for the analysis of porcine corneas. The thickness average of each picture was plotted on a graph, and the average thickness per condition was calculated. The number of samples used for quantification was: $n = 8$ for 12 h LH and HH, $n = 7$ for 24 h LH, $n = 8$ for 24 h HH, $n = 5$ for 48 h LH and HH (Netto et al., 2022).

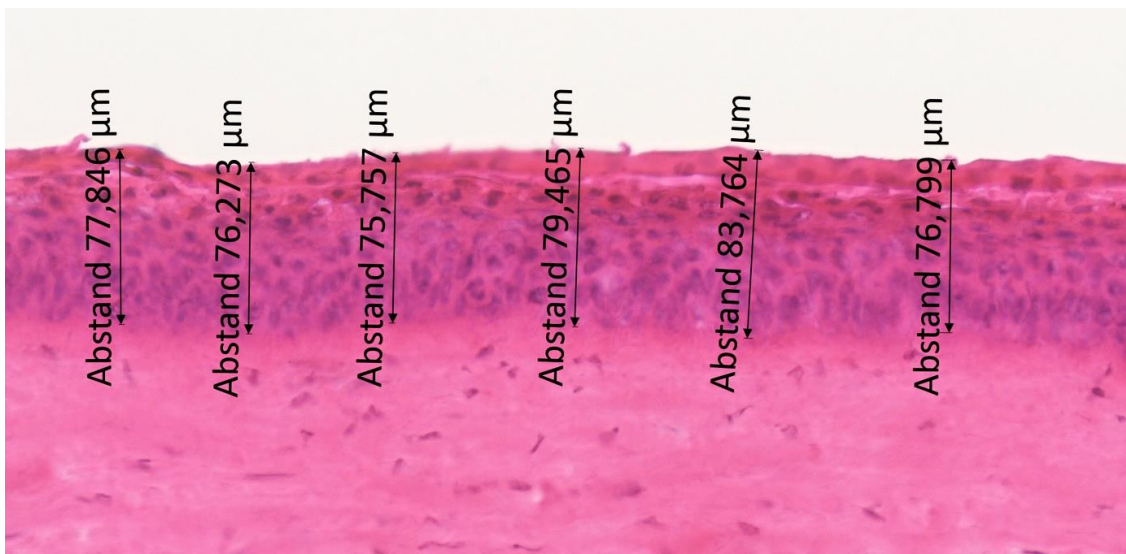


Figure 9: **The virtual meter used for corneal epithelial measurement.**

2.2.5.6 Histological analysis: analysis of corneal epithelium integrity

The corneal epithelium integrity of porcine corneas was analyzed and rated according to the scale: 20% of integrity corresponded to damage to all layers of the corneal epithelium, 40% corresponded to damage to the superficial layer and wing cells, 60% corresponded to damage to the superficial layer, 80% correlated to light damage to the superficial layer and 100% correlated to an intact epithelium (Figure 10). PAS pictures were used for the analysis by blindly comparing each picture with the proposed scale. One to six pictures per sample were analyzed, and the average for each sample was calculated. The number of samples used for quantification was: $n = 6$ for HH + Atto 488, $n = 5$ for HH + NP-Atto 488, $n = 4$ for LH + Atto 488, $n = 5$ for LH + NP-Atto 488.

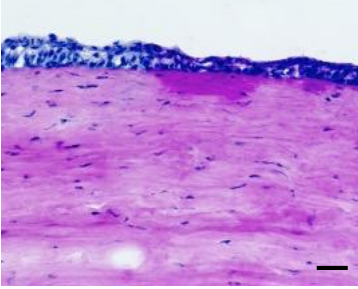
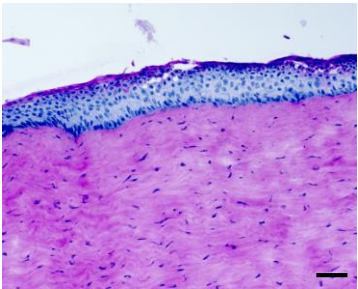
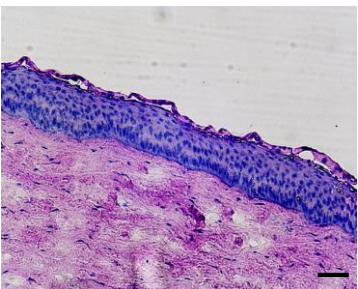
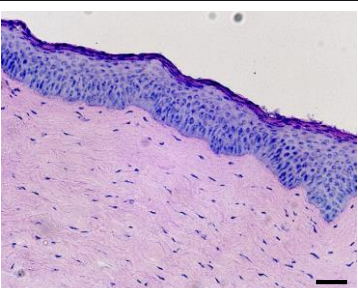
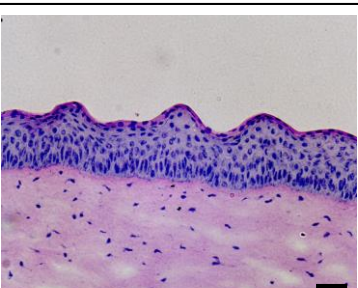
PAS	Evaluation
 <p>EP</p> <p>ST</p>	<p>20% - damage to all layers of the corneal epithelium</p>
 <p>EP</p> <p>ST</p>	<p>40% - damage to the superficial layer and wing cells</p>
 <p>EP</p> <p>ST</p>	<p>60% - damage to the superficial layer</p>
 <p>EP</p> <p>ST</p>	<p>80% - light damage to the superficial layer</p>
 <p>EP</p> <p>ST</p>	<p>100% - intact epithelium</p>

Figure 10: **Evaluation of the corneal epithelial integrity of PAS images.**

The lower corneal epithelial integrity was rated as 20% and corresponded to damage to all layers of the corneal epithelium. 40% corresponded to damage to the superficial layer and wing cells, 60% to damage to the superficial layer, 80% correlated to light damage to the superficial

layer, and 100% to an intact epithelium. PAS: Periodic acid-Schiff. EP: epithelium. ST: stroma. Scale bar = 50 μ m.

2.2.5.7 Analysis of NPs' fluorescence

The evaluation of the fluorescent area in each picture was performed with the help of the program ImageJ™ (Version 2.0.0-rc-68/1.52e). One to five pictures per sample were used for the evaluation, and an average was calculated per sample. The following protocol was used: ImageJ software was opened, and “Set Measurements” was clicked, so “Analyze”, “Integrated Density”, and “Area Fraction” were selected at the same time to set the evaluation settings. “TIFF Image” was opened. To convert the images to gray values, “32 bit” was selected under “Image” and “Type”. To edit the background, “Subtract Background” was clicked under “Process”, and “Rolling Ball Radius” was set to the pixel value of 50. The same threshold for every picture was determined under “Image”, “Adjust”, and finally, “Threshold”. For the analysis, “Analyze” and “Analyze Particles” were clicked, and 0-infinity was entered under “Size” so that all particles were counted. For “Circularity”, 0.00-1.00 was entered so that all shapes were included. The results were displayed in the “Summary” window. The interesting value was the “% Area” value. This value indicated, as a percentage, how much fluorescent area the NP-Atto 488 or pristine Atto 488 occupied in relation to the total image area.

2.2.6 Molecular methods

2.2.6.1 Quantitative Real-Time PCR of porcine corneas

The expression of molecular markers for inflammation, immune response, and apoptosis, like *NF- κ B*, *TNF- α* , *IL-1 β* , *IL-8*, and *NLRP3*, was analyzed. The mRNA expression of the tight junction's marker *occludin* and the

glycocalyx marker *galectin-3* was analyzed in the *ex vivo* model as well (Table 3).

The mRNA from porcine cornea explants was isolated and reverse transcribed using the MultiMACS™ mRNA Kit (Miltenyi Biotec), and cDNA synthesis was done with cDNA Synthesis Kit (Miltenyi Biotec) on the MultiMACS™ M96 Separator. Briefly, the porcine corneas were cut into 2-3 mm pieces and incubated in 800 µL of Lysis Buffer in an Eppendorf tube for 1 h at 37 °C on a shaker (Netto et al., 2022). The tubes were vortexed for 3 min, and syringes attached to 20G and 25G needles were used to shear the DNA completely by pulling up and down the barrel ten times for each size of needle. The tubes were centrifugated at 6000 x g at room temperature. The supernatant was transferred to another tube, and 30 µL of Oligo(dT) Microbeads was mixed by pipetting three times up and down. The MultiMACS™ M96 Separator was prepared with multi 8 columns, a washing plate, and multi 8 filter, and the program “cDNA synthesis without DNAase” was chosen. The filter was moisturized with 100 µL of Lysis/Binding Buffer. To isolate the mRNA, total lysate from beads and supernatant was pipetted on the filter. Two washing steps were performed with 200 µL of Lysis Binding Buffer, and the filter was removed. Four washing steps were conducted with 100 µL of Wash Buffer and two steps with 100 µL of Equilibration/Wash Buffer. To synthesize cDNA, 20 µL of Resuspension Buffer was added to each well of the Synthesis mix, and the mix was added to the columns. cDNA synthesis was done at 42 °C for 1 h. After 1 h, 100 µL of Equilibration/Wash Buffer was added twice in the columns. To elute cDNA, 20 µL of cDNA Release Solution was pipetted in the columns, and samples were incubated at 42 °C for 10 min. To apply pre-elution, 10 µL of cDNA Elution Buffer was added to the columns. A 96-well plate was placed under the columns, and 30 µL of Elution Buffer was added to the columns. cDNA samples were transferred from the 96-well plate to Eppendorf tubes. cDNA concentration was measured at M200 NanoQuant spectrophotometer (Tecan) in duplicates, and the average of these two values was calculated.

Quantitative real-time PCR (qRT-PCR) was performed using the SsoAdvanced Universal SYBR® Green Supermix or the iTaq Universal SYBR®

Green Supermix in a thermal cycler (Bio-Rad CFX96™ Real-Time System). For this step, the cDNA from the samples was diluted to 1 ng/μL, and a reaction mix was prepared with 5 μL of cDNA, Milli-Q water, forward and reverse primers (Table 3), and Supermix solution in a total of 15 μL per well. The samples were measured in duplicates. *β-actin* (*ACTB*), *Ribosomal protein L 4* (*RPL4*), and *glyceraldehyde 3-phosphate dehydrogenase* (*GAPDH*) were used as housekeeping genes (Netto et al., 2022).

Table 3: Primer pairs in 5'-3' directions used for a quantitative real-time PCR of porcine corneas.

Primer	Forward	Reverse
<i>NLRP3</i>	CAGCACGAACCAGAATCTCA	AGCAGCAGTGTGATGTGAGG
<i>NF-κB</i>	AGGATGGGATCTGCACTGTC	ATCAGGGTGCACCAAAGTC
<i>TNF-α</i>	CCCCTGTCCATCCCTTTATT	AAGCCCAGTTCCAATTCTT
<i>IL-1β</i>	CAGCCATGGCCATAGTACCT	CAGCCATGGCCATAGTACCT
<i>IL-8</i>	TGGCAGTTTTCTGCTTTCT	CAGTGGGGTCCACTCTCAAT
<i>Occludin</i>	TCGGACTATGCGGAGAGAGT	TTTGAAGACGCCTCCAAGTT
<i>Galectin-3</i>	CTGGAAAACCAAACCCTCAA	CCAGGATAACCAGGTGCTGT
<i>RPL4</i>	CAAGAGTAACTACAACCTTC	GAACTCTACGATGAATCTTC
<i>GAPDH</i>	GGGCATGAACCATGAGAAGT	AAGCAGGGATGATGTTCTGG
<i>ACTB</i>	CAGCCATCCTGCGTCTGGA	AGCACCGTGTTGGCGTAGAG

2.2.6.2 Quantitative Real-Time PCR of corneal cell cultures

The epithelial cell marker *cytokeratin 12* (*CK12*) and the keratocyte marker *keratocan* had their mRNA expression investigated. After cultivation of the cell cultures, they were split, and 200,000 cells per Eppendorf tube were frozen in 900 μL of Lysis Buffer. The mRNA was isolated from cell cultures and reverse transcribed using the MultiMACS mRNA, and cDNA synthesis was performed with a cDNA Synthesis Kit (Miltenyi Biotec) on the MultiMACS™ M96 Separator as described in section 2.2.6.1. After cDNA synthesis, a quantitative real-time PCR (qRT-PCR) was performed using the iTaq Universal SYBR® Green Supermix in a thermal cycler (Bio-Rad CFX96™ Real-Time System), as described in section 2.2.6.1. “*β-actin* (*ACTB*) and *glyceraldehyde 3-phosphate*

dehydrogenase (GAPDH) were used as housekeeping genes (Table 4) (Netto et al., 2023, p. 8).”

Table 4: “**Primer pairs in 5’-3’ directions used for quantitative real-time PCR of corneal cells (Netto et al., 2023, p. 9)**”.

Primer	Forward	Reverse
<i>CK12</i>	TGGTCTCATCGCAAGTTCAG	TAAAGACCAACATGGCCACA
<i>Keratocan</i>	TCCCAGGGAGTGTTTCTGTC	GCATTCTCGAATGGCTTCTC
<i>ACTB</i>	CACGCCATCCTGCGTCTGGA	AGCACCGTGTTGGCGTAGAG
<i>GAPDH</i>	GGGCATGAACCATGAGAAGT	AAGCAGGGATGATGTTCTGG

2.2.6.3 IL-1 β enzyme-linked immunosorbent assay (ELISA)

A quantification of IL-1 β levels in the cultivation media of porcine cornea explants was performed using the Lumit™ IL-1 β Human Immunoassay. First, to make a calibration curve, a dilution series of Human IL-1 β Standard was prepared in a culture medium and applied in the first and second columns of the 96-well plate. For that, an initial concentration of 40 ng/mL for human IL-1 β was prepared by diluting Human IL-1 β Standard (10 μ g/mL) 1:250 in cell culture medium (Culture medium II). For example, 500 μ L of 40 ng/mL human IL-1 β was prepared by adding 2 μ L of the Human IL-1 β Standard stock to 498 μ L of Culture medium II. Seven tubes were set up with 500 μ L of Culture medium II in each. A 3.5-fold serial dilution of the standard was performed. For that, 200 μ L from the 40 ng/mL stock was transferred to 500 μ L of Culture medium II for the second dilution. After mixing, the procedure was repeated five times to form seven standard dilutions with a range of 40 ng/mL - 22 pg/mL. The last well contained only medium as background control. An antibody mixture was prepared by diluting Anti-hIL-1 β mAb-SmBiT and Anti-hIL-1 β mAb-LgBiT 1:500 into a single volume of Culture medium II. 50 μ L of porcine cornea’s cell culture medium was applied in duplicate in a 96-well plate together with a 50 μ L antibody mixture. The plate was mixed in a plate shaker for 10 seconds and was incubated at 37 °C for 1 h. Afterward, a 20-fold dilution of Lumit™ Detection

Substrate B in Lumit™ Detection Buffer B was performed, and 25 µL was added to the samples after equilibrating the 96-well plate to room temperature for 10 min. The plate was mixed in a plate shaker for 10 seconds. The luminescence was measured within 5 min with a Tecan Spark (Netto et al., 2022).

2.2.6.4 TdT-Mediated dUTP-Biotin Nick End Labeling (TUNEL) Assay

Corneal epithelial apoptosis was analyzed using fluorescent *in situ* terminal deoxynucleotidyl transferase (TdT)-mediated uridine 5'-triphosphate-biotin nick end labeling (TUNEL assay). To perform the TUNEL assay, the cryosections were fixated with 4% paraformaldehyde (PFA) for 20 min and washed for 30 min with TBS. Permeabilization solution was pipetted onto the slides and incubated for 2 min. The samples were washed twice with TBS for 5 min. A reaction mixture of labeling solution with enzyme solution was pipetted, and samples were incubated at 37 °C and 95% humidity for 1 h. Cryosections were washed three times with TBS, and DAPI staining was performed. For controls terminal deoxynucleotidyl transferase enzyme was either excluded from the labeling solution (negative control), or sections were pre-treated for 10 min with DNase I in 50 mM Tris-HCl, pH 7.5, 1 mg/mL bovine serum albumin (BSA) to induce DNA strand breaks (positive control). While negative control had no staining, positive control stained all nuclei at the cornea. The Zeiss Axio Imager Z1 Apotome Microscope with Mrm digital camera was used for imaging. The semi-automated counter software ImageJ™ was used to execute a cell count. A percentage of the number of apoptotic epithelial corneal cells per total of corneal cells was calculated for each picture. To reduce variability, the mean of three sections per sample and of three to six pictures per sample of 200-fold magnification was used for analysis (Netto et al., 2022). The number of samples used was: $n = 8$ for 12 h LH and HH, $n = 4$ for 24h LH, $n = 6$ for 24 h HH, $n = 9$ for 48 h LH, $n = 6$ for 48h HH, $n = 6$ for HH, $n = 5$ for HH + buffer, $n = 5$ for HH + NP, $n = 5$ for LH, $n = 5$ for LH + buffer, $n = 5$ for LH + NP.

2.2.6.5 Porcine cytokine antibody array

For the simultaneous detection of multiple cytokines in the different corneal culture media (HH vs. LH), a semiquantitative Porcine Cytokine Array was performed (RayBio® C Series Porcine Cytokine Array 1). The media from six samples per condition (24 h HH/ 24 h LH/ 48 h HH/ 48 h LH) were pooled, and 500 μ L per array was used. The assay was performed according to the manufacturer's protocol. Briefly, 1 mL of Blocking Buffer was pipetted into each well and incubated for 30 min. After aspirating the Blocking Buffer, a total of 500 μ L of culture media per condition was added to the antibody arrays and incubated at room temperature for 5 h. Samples were aspirated from each well, and washing steps were conducted. For that, the 20x Wash Buffer Concentrates I and II were diluted 20-fold before use. 2 mL of 1x Wash Buffer I was pipetted into each well and incubated for 5 min at room temperature. After aspirating the buffer, this procedure was repeated two more times. 2 mL of 1x Wash Buffer II was pipetted into each well and incubated for 5 min at room temperature. This procedure was repeated one more time. 500 μ L of Biotinylated Antibody Cocktail was pipetted into each well containing an antibody array and incubated overnight at 4 °C. After a second washing step with 1x Wash Buffer I and 1x Wash Buffer II as described previously, 2 mL HRP-Streptavidin was added into each well and incubated for 2 h at room temperature. A third washing step was carried out similarly to the first and second washing steps, and chemiluminescence detection was performed. To perform data analysis, on each array the background signal was subtracted from the raw data for each cytokine spot, mean values for every investigated cytokine were calculated, and normalized to the positive control signals. Considering the signal intensity of each cytokine secreted at LH media a fold increase or decrease was calculated in relation to HH. It was considered that the cytokine was increased in the media of stressed samples in relation to controls when higher than 1.5 and that it was decreased when lower than 0.5 (Netto et al., 2022).

2.2.6.6 Immunostaining of corneal cell cultures

"To confirm the cultivation of corneal epithelial cells, the expression of cytokeratin 3 (CK3), an epithelial cell marker, was analyzed. Moreover, antibodies for zonula occludens 1 (ZO-1) and occludin were used to investigate the presence of tight junctions. To verify the presence of keratocytes in the cultures, keratocan and lumican antibodies were used. To analyze the presence of mesenchymal cells and undifferentiated epithelial cells in the cultures, a vimentin antibody was applied. Cells at first passage were seeded in chamber slides and were first fixed in 4% PFA for 10 min and then washed four times with PBS for 3 min. The cells were permeabilized with 0.1% Triton X-100 in PBS for 5 min at room temperature. Afterward, they were blocked for 1 h with a blocking solution (5% (w/v) BSA in PBS). The primary antibody was diluted in 5% (w/v) BSA in PBS, according to the concentrations in Table 5, and pipetted into the samples. The samples were incubated on a shaker overnight at 4 °C. After the incubation, the cells were washed three times for 5 min each with PBS. Next, 100 µL of secondary antibody diluted in 5% (w/v) in PBS (Table 5) was pipetted on the chamber slides and incubated at room temperature for 1 h in darkness (Netto et al., 2023, p. 7)." The chamber slides were then washed three times with PBS for 5 min, and 1 µg/mL of DAPI was applied to them for 5 min. Finally, the chamber slides were washed once with PBS and Milli-Q water for 5 min. After drying in air, the chamber slides were disassembled with the help of a plastic device, and three drops of FluorSave™ were placed on them. Next, a cover glass was placed on top of the chamber slides (Netto et al., 2023).

Table 5: Primary and secondary antibodies and dilutions used for immunostaining.

Primary antibody	Manufacturer and dilution	Secondary antibody	Manufacturer and dilution
Cytokeratin 3 (epithelial cell marker)	Biorbyt, Cambridge, UK Orb5866 1:50	AlexaFluor 488 anti-rabbit	Thermo-Fischer, Karlsruhe, Germany A11008 1:500
Occludin (tight junction marker)	Santa Cruz, Dallas, TX, USA sc-133256 1:50	AlexaFluor 488 anti-mouse	Thermo-Fischer, Karlsruhe, Germany A11001 1:500
Vimentin (undifferentiated epithelial cell and mesenchymal cell marker)	Sigma Aldrich, Taufenkirchen, Germany V2258 1:100	AlexaFluor 555 anti-mouse	Thermo-Fischer Karlsruhe, Germany A21422 1:500
Keratocan (keratocyte marker)	Santa Cruz Dallas, TX, USA sc-33243 1:50	AlexaFluor 488 anti-goat	Thermo-Fischer Karlsruhe, Germany A11055 1:500
Lumican (keratocyte marker)	Santa Cruz Dallas, TX, USA sc-27718 1:50	AlexaFluor 488 anti-goat	Thermo-Fischer, Karlsruhe, Germany A11055 1:500
ZO-1 (tight junction marker)	Santa Cruz, Dallas, TX, USA sc-33725 1:50	AlexaFluor 488 anti-rat	Invitrogen, Waltham, MA, USA 11006 1:500

2.2.7 Statistical analysis

GraphPad Prism™ Version 8.2.1 (GraphPad Software, San Diego, CA, USA) was used to perform statistical analysis. Normality was tested with Anderson Darling test, D`Agostino and Pearson test, Shapiro-Wilk test, or Kolmogorov-Smirnov test. The distribution was considered normal when at least one of the tests was positive. To compare two groups when normality was

confirmed the Student's t-test was applied. The Student's t-test with Welch's correction was performed when normality was assured, but variance was unequal. The Mann-Whitney test was used to compare two groups, when distribution was not normal. For multiple comparisons, one-way ANOVA was used, followed by a Tukey's post hoc test for equal groups when normality was attested. Welch's ANOVA test with Dunnett's multiple comparisons test were used when distribution was normal, but variance was unequal. For multiple comparisons when the distribution was not normal Kruskal Wallis with Dunn's post hoc test were used. Results are presented as mean \pm standard error of the mean (SEM). A p -value < 0.05 was considered to be statistically significant. The level of significance was set to * $p < 0.05$, ** $p < 0.01$ and *** $p < 0.001$ (Netto et al., 2022).

3 Results

3.1 Chapter 1: Development of an *ex vivo* porcine dry eye model

3.1.1 Corneal damage and corneal thinning are consequences of low humidity

To develop an *ex vivo* porcine dry eye model, low humidity (LH) was tested as a stressing factor, and the samples were analyzed histologically. Once porcine corneas were removed from the eyes, they were incubated for 12 h, 24 h, and 48 h at LH (30% humidity), and the controls were incubated at HH (95% humidity) for the same period of time (Netto et al., 2022).

HE and PAS stainings were carried out to analyze histological changes caused by LH. LH treatment for 12 h resulted in small desquamation of surface epithelial cells in comparison to the control group. In porcine corneas incubated at LH for 24 h, detachment of corneal epithelial cells was visualized in comparison to controls (Figure 11 A). Moreover, upon LH treatment for 24 h, the glycoprotein layer covering the apical epithelium detached from the apical layer, and this detachment was not observed in the control group (Figure 11 A). In addition, samples treated with LH for 12 h and for 24 h had a reduced epithelium thickness compared with those treated with HH for 12 h ($78.29 \mu\text{m} \pm 2.11$ for 12 h LH/ $89.77 \mu\text{m} \pm 3.17$ for 12 h HH; $p = 0.003$) and for 24 h ($60.34 \mu\text{m} \pm 3.98$ for 24 h LH/ $71.80 \mu\text{m} \pm 3.75$ for 24 h HH; $p = 0.009$) (Figure 11 B) (Netto et al., 2022).

The incubation of porcine corneas at LH for 48 h was also performed to investigate whether longer periods of incubation would also result in changes similar to DED, such as detachment of epithelial cells and corneal thinning. It was verified that aside from the detachment of superficial corneal cells, deeper epithelium layers were also damaged. These changes were observed in controls as well (Figure 11 A). In addition, no significant difference was verified in epithelial thickness in samples incubated at LH for 48 h and HH for the same period ($52.09 \mu\text{m} \pm 5.71$ for 48 h LH/ $60.90 \mu\text{m} \pm 7.21$ for 48 h HH; $p = 0.342$)

(Figure 11 B), most likely because both stressed samples and their controls presented severe epithelial deterioration (Netto et al., 2022).

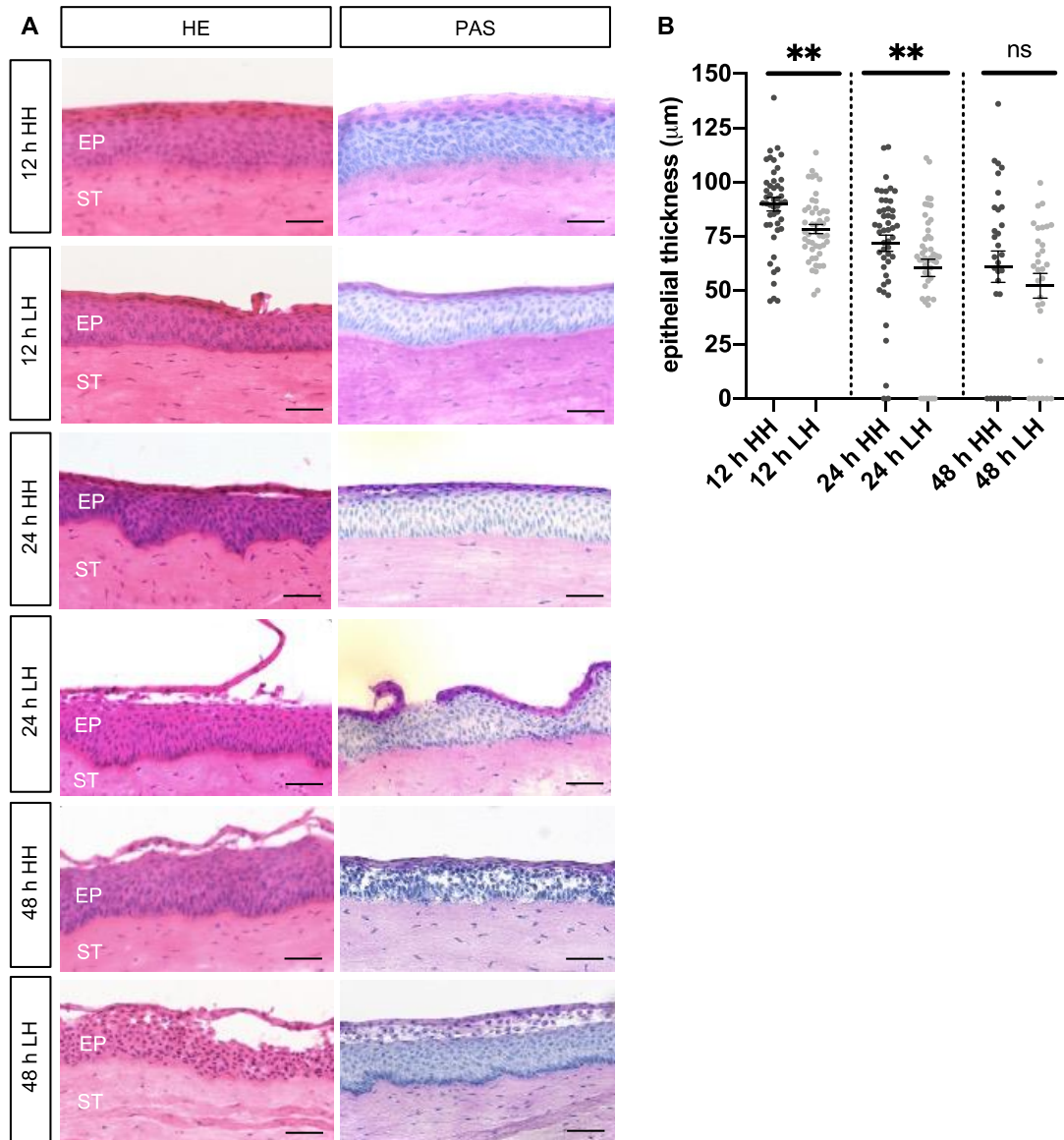


Figure 11: Corneal damage and corneal thinning occur as a consequence of exposure to LH.

(A) The images show porcine corneas exposed to LH and HH at different times. After incubation at LH for 12 h, samples stained with HE and PAS showed slight desquamation of surface corneal epithelial cells in comparison to controls. Porcine corneas incubated at LH for 24 h presented epithelial damage and detachment of the glycoprotein layer in comparison to HH samples. In addition, after 48 h of exposure to LH and HH, corneas demonstrated epithelial damage and detachment of the glycoprotein layer. (B) Epithelial thickness of corneas submitted to LH for 12 h and for 24 h was significantly reduced in comparison to their respective controls ($n = 8$ for 12 h LH and 12 h HH/ $n = 7$ for 24 h LH/ $n = 8$ for 24 h HH). No significant difference was seen between samples incubated at LH and at HH for 48 h ($n = 5$ for 48 h LH and 48 h HH). Each dot represents the thickness average of each picture. The horizontal bar represents the average thickness per condition. SEM is shown. Unpaired t-test was used for statistical

analysis between 12 h LH x 12 h HH and 48 h LH x 48 h HH. Mann-Whitney test was used for statistical analysis between 24 h LH x 24 h HH. Scale bar = 50 μ m. LH: low humidity. HH: high humidity. HE: Hematoxylin-Eosin. PAS: Periodic acid-Schiff. EP: epithelium. ST: stroma. ns: not significant. All data are shown as mean \pm SEM. ** $p < 0.01$. Figure published at <https://doi.org/10.3390/ijms23094567> (Netto et al. 2022).

3.1.2 Inflammation in the porcine model is induced by low humidity

As DED is characterized by an inflammatory process as described in 1.7.2., IL-1 β secretion was measured by ELISA assay to detect an inflammatory process caused by LH. An elevated secretion of IL-1 β was verified in the LH group incubated for 24 h (648.30 pg/mL \pm 20.30) compared to HH (558.20 pg/mL \pm 14.50; $p = 0.004$). This elevation in the inflammatory marker IL-1 β was also found in samples submitted to LH stress for 48 h (606.90 pg/mL \pm 49.35) when compared to HH samples (494.00 pg/mL \pm 21.31; $p = 0.05$) (Figure 12 A) (Netto et al., 2022).

Then, inflammatory markers were investigated by measuring qRT-PCR to certify that inflammation is induced in the model proposed. mRNA expression of pro-inflammatory markers *TNF- α* , *IL-1 β* , *NF- κ B*, and the inflammasome marker *NLRP3* were verified. Although no significant difference was observed in *IL-1 β* expression in corneas incubated at LH for 12 h (0.90-fold \pm 0.19; $p = 0.58$) and for 24 h (0.40-fold \pm 0.15; $p = 0.05$) in comparison to their controls (Figure 12 B), *IL-1 β* expression was 12.54-fold (\pm 2.69; $p = 0.001$) upregulated in samples incubated at LH for 48 h (Figure 12 B). Regarding the mRNA expression of *NF- κ B*, it was 2.40-fold (\pm 0.48; $p = 0.03$) upregulated in samples cultivated at LH for 12 h and 3.73-fold (\pm 0.36; $p < 0.001$) upregulated in the ones incubated at LH for 24 h compared to the corresponding controls (Figure 12 C). In corneas exposed to 48 h at LH (4.22-fold \pm 1.17; $p = 0.07$), a non-significant increase was found in *NF- κ B* expression in comparison to the controls (Figure 12 C). In relation to mRNA expression of *TNF- α* , significant downregulation in this marker was observed in samples incubated for 12 h at LH (0.44-fold \pm 0.12; $p = 0.01$) and for 24 h at LH (0.45-fold \pm 0.07; $p = 0.03$) in comparison to their controls (Figure 12 D). However, it was 8.44-fold (\pm 2.42; $p =$

0.006) upregulated in porcine corneas submitted to LH for 48 h compared to their corresponding controls (Figure 12 D). In corneas incubated for 12 h and 24 h, there was no significant difference in samples exposed to LH in the *NLRP3* expression (12 h LH = 0.72-fold \pm 0.14; p = 0.54/ 24 h LH = 0.73-fold \pm 0.16; p = 0.22) (Figure 12 E). Nonetheless, after 48 h, *NLRP3* was 16.43-fold (\pm 2.65; p < 0.001) upregulated in porcine corneas submitted to LH in comparison to their corresponding controls (Figure 12 E) (Netto et al., 2022).

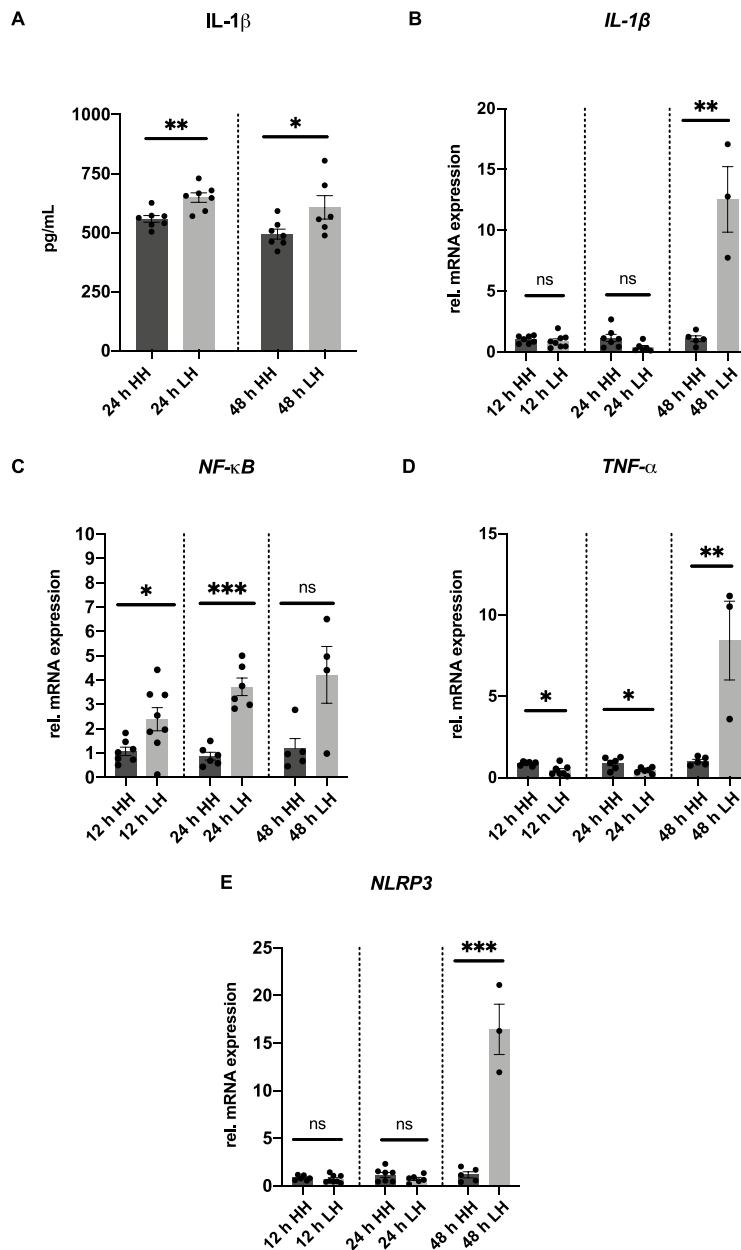


Figure 12: **Inflammatory markers are expressed in samples incubated at LH in comparison to the ones incubated at HH.**

(A) A significantly greater secretion of IL-1 β was verified in porcine corneas exposed to LH for 24 h when compared to 24 h HH ($n = 7$ for 24 h LH/ $n = 7$ for 24 h HH) and for 48 h LH in comparison to 48 h HH ($n = 6$ for 48 h LH/ $n = 7$ for 48 h HH). Unpaired t-test was used for statistical analysis between 24 h LH x 24 h HH and 48 h LH x 48 h HH. (B) *IL-1 β* mRNA expression was not changed in samples incubated at LH for 12 h and for 24 h in comparison to their controls. A significant upregulation of *IL-1 β* expression was observed in porcine corneas incubated at LH for 48 h. Unpaired t-test was used for statistical analysis between 12 h LH x 12 h HH and 48 h LH x 48 h HH. Welch's t test was used for statistical analysis between 24 h LH x 24 h HH. (C) mRNA expression of *NF- κ B* was 2.40-fold (± 0.48 ; $p = 0.03$) upregulated in corneas incubated at LH for 12 h and 3.73-fold (± 0.36 ; $p < 0.001$) upregulated in the ones submitted to LH for 24 h. A non-significant elevation was noticed between samples incubated at LH for 48 h compared to the respective HH samples. Unpaired t-test was used for statistical analysis between 12 h LH x 12 h HH and 24 h LH x 24 h HH. Welch's t-test was used for statistical analysis between 48 h LH x 48 h HH. (D) A downregulation of *TNF- α* mRNA expression in porcine corneas incubated at LH for 12 h and for 24 h in comparison to the corresponding HH samples was observed. However, *TNF- α* mRNA was 8.44-fold upregulated in samples incubated at LH for 48 h (± 2.42 ; $p = 0.006$). Unpaired t-test was used for statistical analysis between 12 h LH x 12 h HH, 24 h LH x 24 h HH and 48 h LH x 48 h HH. (E) Samples submitted to LH for 12 h and for 24 h conferred no significant difference in *NLRP3* expression in comparison to their HH controls. *NLRP3* expression was 16.43-fold (± 2.65 ; $p < 0.001$) upregulated in corneas cultivated at LH for 48 h. Unpaired t-test was used for statistical analysis between 12 h LH x 12 h HH, 24 h LH x 24 h HH and 48 h LH x 48 h HH. $n = 7-8$ for 12 h LH/ $n = 6-7$ for 12 h HH/ $n = 6$ for 24 h LH/ $n = 6-7$ for 24 h HH/ $n = 3-4$ for 48 h LH/ $n = 4-6$ for 48 h HH. LH: low humidity. HH: high humidity. ns: not significant. The dots represent the n numbers. The bars represent the mean values, and the SEM is shown. * $p < 0.05$ ** $p < 0.01$ *** $p < 0.001$. Figure published at <https://doi.org/10.3390/ijms23094567> (Netto et al., 2022).

Additionally, the protein levels of pro-inflammatory cytokines were measured in the culture media of porcine corneas stressed at LH and identified with a cytokine array. It was observed that pro-inflammatory cytokines were elevated in the culture media of samples incubated at LH. Interferon-gamma (IFN- γ) and macrophage migration inhibitory factor (MIF) were increased in the media of porcine corneas exposed to LH for 48 h (IFN- γ : 2.67-fold; MIF: 1.68-fold). Fibroblast growth factor 21 (FGF21), which triggers angiogenesis, and interferon-beta (IFN- β), which present either a pro- or anti-inflammatory effect, were elevated in the media of samples stressed at LH for 24 h (IFN- β : 4.92-fold; FGF21: 1.54-fold). Moreover, angiopoietin-1 (ang1), which stimulates angiogenesis and inflammation, was increased in the media of samples submitted to LH for 48 h (2.10-fold) (Table 6) (Netto et al., 2022).

As a result, it can be assumed that inflammation was activated in porcine corneas exposed to LH stress for 24 h and for 48 h in comparison with the respective HH samples (Netto et al., 2022).

Table 6: Cytokines released in the media of samples submitted to LH for 24 h and 48 h.

A calculation of the signal intensity ratio of each cytokine released at LH media in relation to HH was performed. A fold increase or decrease is demonstrated. LH: low humidity. HH: high humid.

Table published at <https://doi.org/10.3390/ijms23094567> (Netto et al., 2022).

Cytokine	Ratio 24 h LH/HH	Ratio 48 h LH/HH	Function
Erythropoietin	11.59	-	Decreases apoptosis and inflammation (Abri Aghdam et al., 2016)
Galectin-9	3.29	0.80	Anti-inflammatory/anti-angiogenic (AbuSamra & Argüeso, 2018)
Interferon-beta	4.92	1.25	Anti and pro-inflammatory (Benchabane et al., 2018)
Granulocyte-macrophage colony-stimulating factor	1.44	-	Pro-inflammatory (Dohlman et al., 2017)
Interferon-gamma	1.36	2.67	Pro-inflammatory (Jackson et al., 2016)
Macrophage migration inhibitory factor	1.01	1.68	Pro-inflammatory (Park et al., 2007)
Chemokine (C-C motif) ligand 3-like 1	0.71	1.41	Pro-inflammatory (Park et al., 2007)
Interleukin 22	0.01	0.63	Anti and pro-inflammatory (Pan et al., 2013)
Osteoprotegerin	1.43	-	Angiogenesis (Abu El-Asrar et al., 2017)
Fibroblast growth factor 21	1.54	0.44	Angiogenesis (Chen et al., 2020)
Angiopoietin-1	0.71	2.10	Angiogenesis/Inflammation (Kather et al., 2014)
Vascular endothelial growth factor	0.44	1.41	Angiogenesis/Inflammation (Liu et al., 2020)
Tissue inhibitor of metalloproteinase 2	0.83	3.37	Inhibits apoptosis and induces corneal epithelial cell proliferation (Sendon-Lago et al., 2019)
Transforming growth factor alpha	0.12	0.56	Cell proliferation, differentiation, and development (Luetteke & Lee, 1990)

3.1.3 Tight junctions and glycocalyx markers are upregulated in samples cultivated at LH

In order to understand why epithelial cells detach from corneal epithelium, especially in samples submitted to LH, the mRNA expression of *occludin*, a tight junction marker, was analyzed. In addition, mRNA expression of the glycocalyx marker *galectin-3* was investigated. In samples stressed at LH for 12 h, no difference in *occludin* expression was verified when compared to the controls (1.23-fold \pm 0.29; $p = 0.65$). However, it was noticed a 2.94-fold (\pm 0.69; $p = 0.02$) upregulation of *occludin* mRNA expression in porcine corneas submitted to LH stress for 24 h and a 2.56-fold (\pm 0.64; $p = 0.04$) upregulation was shown in the 48 h LH group compared to the respective HH corneas (Figure 13 A). Regarding *galectin-3*, no difference in mRNA expression was observed in samples cultivated at LH for 12 h (1.74-fold \pm 0.41; $p = 0.12$) in comparison to the 12 h HH controls. Nevertheless, mRNA expression of *galectin-3* was 2.25-fold (\pm 0.11; $p < 0.001$) upregulated in samples subjected to LH for 24 h and 5.16-fold (\pm 0.49; $p < 0.001$) upregulated in those incubated at LH for 48 h (Figure 13 B). In conclusion, upregulation of *occludin* and *galectin-3* mRNA expression was definitely induced in the porcine model incubated at LH for 24 h and 48 h (Netto et al., 2022).

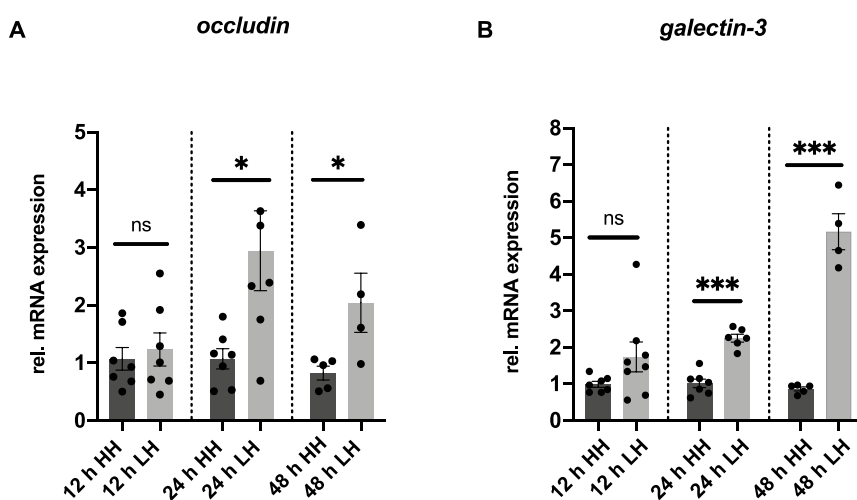


Figure 13: **Tight junction and glycocalyx markers are upregulated due to LH.**

(A) No difference in *occludin* expression was observed in samples cultivated at LH for 12 h in comparison to the 12 h HH controls. An upregulation of *occludin* expression of 2.94-fold (\pm 0.69;

$p = 0.02$) was verified in samples cultivated at LH for 24 h and 2.56-fold (± 0.64 ; $p = 0.04$) in the ones incubated for 48 h at LH. Unpaired t-test was used for statistical analysis between 12 h LH x 12 h HH, 24 h LH x 24 h HH and 48 h LH x 48 h HH. (B) *Galectin-3* mRNA expression was not significantly different in samples submitted to LH for 12 h in comparison to the 12 h HH controls. An upregulation of 2.25-fold (± 0.11 ; $p < 0.001$) of *galectin-3* mRNA was noticed in samples subjected to LH for 24 h, and an upregulation of 5.16-fold (± 0.49 ; $p < 0.001$) was observed in porcine corneas incubated at LH for 48 h. Unpaired t-test was used for statistical analysis between 12 h LH x 12 h HH, 24 h LH x 24 h HH and 48 h LH x 48 h HH. $n = 8$ for 12 h LH/ $n = 7$ for 12 h HH/ $n = 6-7$ for 24 h LH / $n = 7$ for 24 h HH / $n = 4$ for 48 h LH/ $n = 5$ for 48 h HH. LH: low humidity. HH: high humidity. ns: not significant. The dots represent the n numbers. The bars represent the mean values, and the SEM is shown. * $p < 0.05$ *** $p < 0.001$. Figure published at <https://doi.org/10.3390/ijms23094567> (Netto et al., 2022).

3.1.4 Apoptosis of porcine corneal cells is induced by LH

TUNEL staining was performed to analyze whether the loss of epithelial cells and the reduced thickness in the model were caused by apoptosis. After cultivating porcine corneas for 12 h and for 24 h at LH, it was observed a higher percentage of apoptotic epithelial cells in comparison to the respective controls (Figure 14 A). To verify these findings, a quantitative analysis of apoptotic cells to overall cell number was performed (12 h LH = $5.38\% \pm 0.48$ / 12 h HH = $3.87\% \pm 0.44$ apoptotic cells; $p = 0.036$) (24 h LH = $16.69\% \pm 3.79$ / 24 h HH = $6.98\% \pm 1.37$ apoptotic cells; $p = 0.0229$) (Figure 14 B). However, samples cultivated for 48 h presented no significant difference in the LH group compared to the controls (48 h LH = $28.23\% \pm 8.67$ / 48 h HH = $37.19\% \pm 9.53$ apoptotic cells; $p = 0.86$) (Figure 14 A and B). To summarize, the cultivation of porcine corneas at LH for 12 h and for 24 h induced apoptosis of corneal cells (Netto et al., 2022).

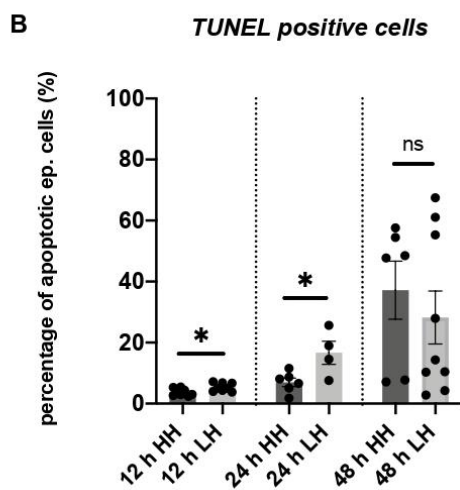
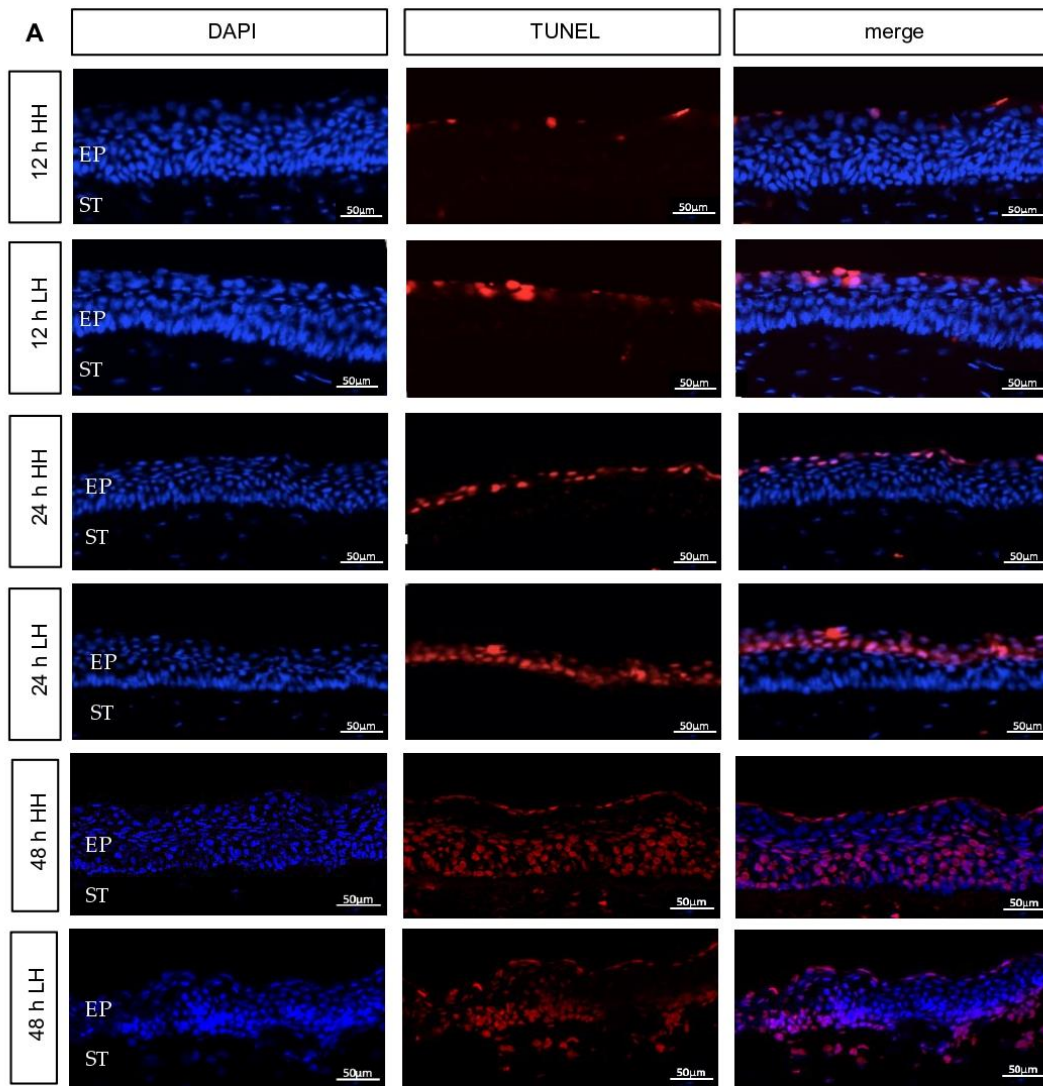


Figure 14: **Porcine corneas incubated for 12 h and for 24 h at LH had apoptosis of corneal epithelial cells stimulated.**

(A) Representative images of samples cultivated at LH for 12 h, 24 h, and 48 h and stained with TUNEL (red) and DAPI (blue) and controls cultivated at HH for the same time period. (B)

Samples cultivated at LH for 12 h and for 24 h presented an increased percentage of apoptotic epithelial cells in comparison to the respective controls ($n = 8$ for 12 h LH/ $n = 8$ for 12 h HH/ $n = 4$ for 24 h LH/ $n = 6$ for 24 h HH). No significant difference was verified between porcine corneas incubated at LH and HH for 48 h ($n = 9$ for 48 h LH / $n = 6$ for 48 h HH). Unpaired t-test was used for statistical analysis between 12 h LH x 12 h HH and 24 h LH x 24 h HH. Mann-Whitney test was used for statistical analysis between 48 h LH x 48 h HH. LH: low humidity. HH: high humidity. EP: epithelium. ST: stroma. DAPI: 4',6-diamidino-2-phenylindole. TUNEL: TdT-mediated dUTP-biotin nick end labeling. ns: not significant. Scale bar = 50 μm . The dots represent the n numbers. The bars represent the mean values, and the SEM is shown. All data are shown as mean \pm SEM. * $p < 0.05$. Figure published at <https://doi.org/10.3390/ijms23094567> (Netto et al, 2022).

3.1.5 Treatment with dexamethasone counteracts LH effects and with hyaluronic acid eye drops counteracts only partially

Important and robust effects of inflammation, corneal thinning, upregulation of tight junctions and glycocalyx markers, and apoptosis were triggered by 24 h incubation at LH compared to 12 h and 48 h incubation. For this reason, it was further explored whether the inflammation and changes caused by LH could be counteracted with eye drops that are used as a treatment option for DED. The eye drops investigated were composed either of dexamethasone 1.3 mg/mL (DexaEDO®, Bausch-Lomb, Heidelberg, Germany) (dexa) dropped every 12 h or of hyaluronic acid 0.2% (Artelac® Splash EDO®, Bausch-Lomb, Heidelberg, Germany) (HA) every 6 h (Netto et al., 2022).

As a corticosteroid, dexamethasone has a therapeutic effect against inflammation, while HA lubricates the cornea, thereby reducing inflammation triggered by DED. To investigate whether inflammatory processes could be counteracted, porcine corneas were divided in four groups: two incubated at LH, one with eye drop treatment and another without it, and two incubated at HH, one with eye drop treatment and another without it (Netto et al., 2022).

In order to assess the outcome of dexamethasone treatment on the LH induced inflammation, the secretion of IL-1 β and the mRNA expression of *NF- κ B*, *occludin* and *galectin-3* were analyzed. As shown previously (Figure 12 A), an increase of IL-1 β was observed in porcine corneas subjected to LH (718.10 pg/mL \pm 38.85) in comparison to the ones cultivated at HH (546.00 pg/mL \pm 19.49; $p = 0.02$) (Figure 15 A). No significant difference in IL-1 β secretion was found in porcine corneas cultivated at LH and treated with dexa, in comparison

to the ones cultivated at LH, though (LH + dexta = 658.10 pg/mL \pm 51.65/ LH = 718.10 pg/mL \pm 38.85; $p = 0.68$) (Figure 15 A). Treatment with dexamethasone in samples cultivated at LH could significantly prevent an augmentation in *NF- κ B* mRNA (0.18-fold \pm 0.05; $p < 0.001$) in comparison to the ones cultivated at LH (1.87-fold \pm 0.46) (Figure 15 B). Comparable to results described previously (Figure 13 A), an upregulation of *occludin* mRNA (5.56-fold \pm 0.91; $p < 0.001$) was verified in porcine corneas subjected to LH in comparison to the ones incubated at HH (Figure 15 C). Moreover, *occludin* mRNA expression (1.05-fold \pm 0.11; $p < 0.001$) was significantly inhibited in samples cultivated at LH + dexta in comparison to the ones submitted to LH (Figure 15 C). Also, *galectin-3* mRNA expression (LH: 6.85-fold \pm 1.07; $p < 0.001$) was significantly upregulated in porcine corneas cultivated at LH, and this fact could be significantly prevented by treatment with dexta (2.57-fold \pm 0.55; $p < 0.001$) (Figure 15 D). These findings endorse that dexamethasone counterbalances the mRNA increase in *NF- κ B*, *occludin*, and *galectin-3* caused by LH and can also diminish inflammatory processes at the transcriptional level in the *ex vivo* model (Netto et al., 2022).

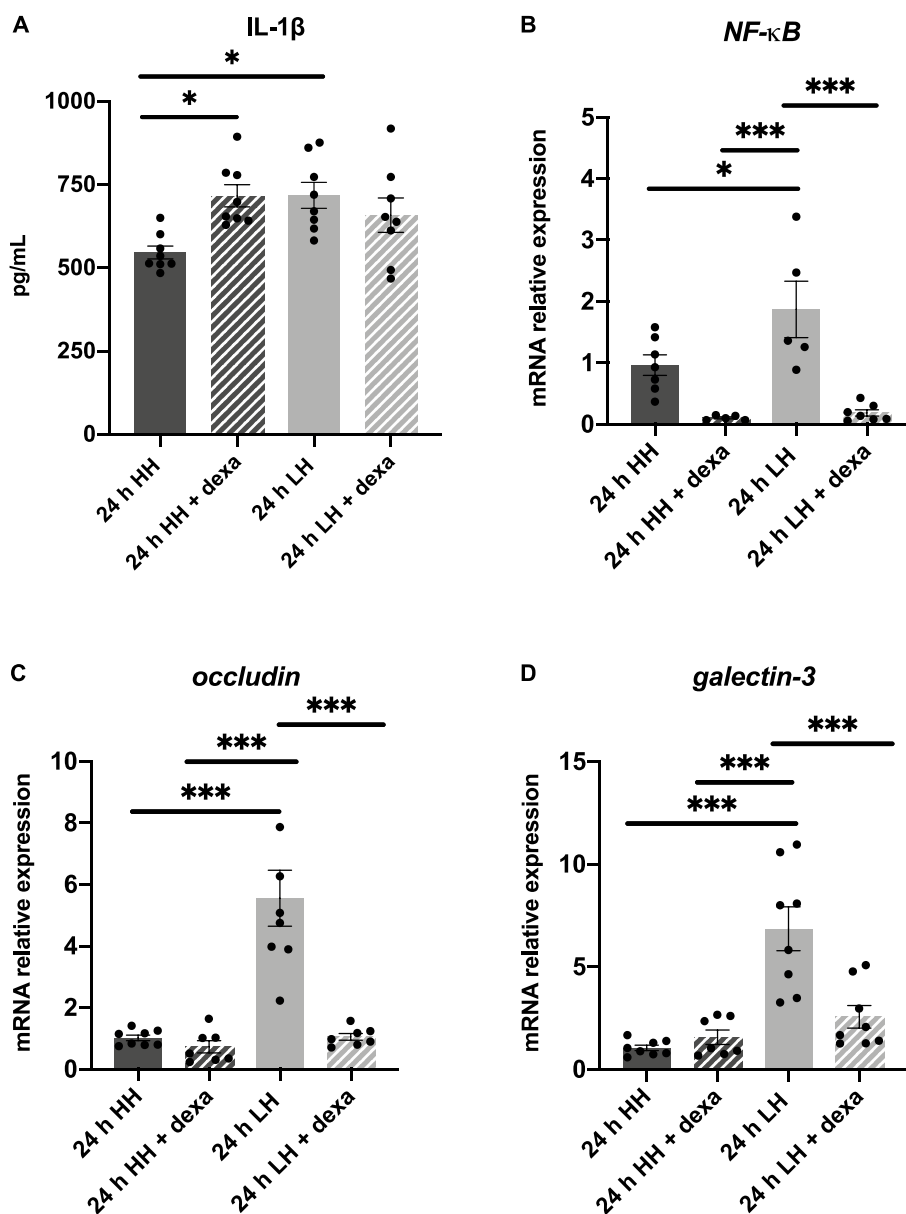


Figure 15: LH effects on porcine corneas are counteracted by dexa.

(A) IL-1 β secretion was not significantly different in corneas cultivated at LH + dexa in comparison to the LH group ($n = 8$ for LH/ $n = 8$ for LH + dexa/ $n = 8$ for HH/ $n = 8$ for HH + dexa). Ordinary one-way ANOVA followed by Tukey's multiple comparisons test were used for statistical analysis. (B) Significant suppression of increase of *NF- κ B* mRNA expression was noticed in the LH + dexa group in comparison to the LH group. Ordinary one-way ANOVA followed by Tukey's multiple comparisons test were used for statistical analysis. (C) The elevation of *occludin* mRNA expression caused by LH was significantly inhibited by dexa, in comparison to the LH group. Ordinary one-way ANOVA followed by Tukey's multiple comparisons test were used for statistical analysis. (D) LH significantly induced mRNA expression of *galectin-3*, and the treatment with dexa inhibited this outcome. Ordinary one-way ANOVA followed by Tukey's multiple comparisons test were used for statistical analysis. (B-D) $n = 5-8$ for LH/ $n = 7-8$ for LH + dexa/ $n = 7-8$ for HH/ $n = 5-7$ for HH + dexa. LH: low humidity. HH: high humidity. Dexa: dexamethasone. The dots represent the n numbers. The bars represent the mean values, and the SEM is shown. * $p < 0.05$ *** $p < 0.001$. Figure published at <https://doi.org/10.3390/ijms23094567> (Netto et al., 2022).

In order to investigate if treatment with HA could also inhibit the effects caused by LH, IL-1 β , *occludin*, and *galectin-3* were analyzed. In porcine corneas submitted to LH, to LH + HA, and to HH + HA, an increase of IL-1 β was noticed in comparison to the ones incubated at HH alone (LH: 638.60 pg/mL \pm 18.68/ LH + HA: 607.00 pg/mL \pm 37.54/ HH + HA: 571.20 pg/mL \pm 25.41/ HH: 406.10 pg/mL \pm 16.45; $p < 0.001$) (Figure 16 A). As shown previously, in this sample series an upregulation of *occludin* mRNA expression (2.48-fold \pm 0.19; $p < 0.001$) was also found in samples cultivated at LH in comparison to the ones incubated at HH only (Figure 16 B). In addition, treatment with HA could significantly inhibit the elevation of *occludin* mRNA expression in porcine corneas incubated at LH and treated with HA (1.75-fold \pm 0.18; $p = 0.03$) compared to the ones cultivated at LH without treatment (2.48-fold \pm 0.19) (Figure 16 B). Also, upregulation of *galectin-3* mRNA expression was found in samples cultivated at LH (1.66-fold \pm 0.21; $p = 0.04$) in comparison to the ones subjected to HH (Figure 16 C), but no counteracting effect of HA treatment could be identified (1.60-fold \pm 0.21; $p > 0.99$). According to this result, HA was able to partially inhibit the effects of incubation at LH at a transcriptional level (Netto et al., 2022).

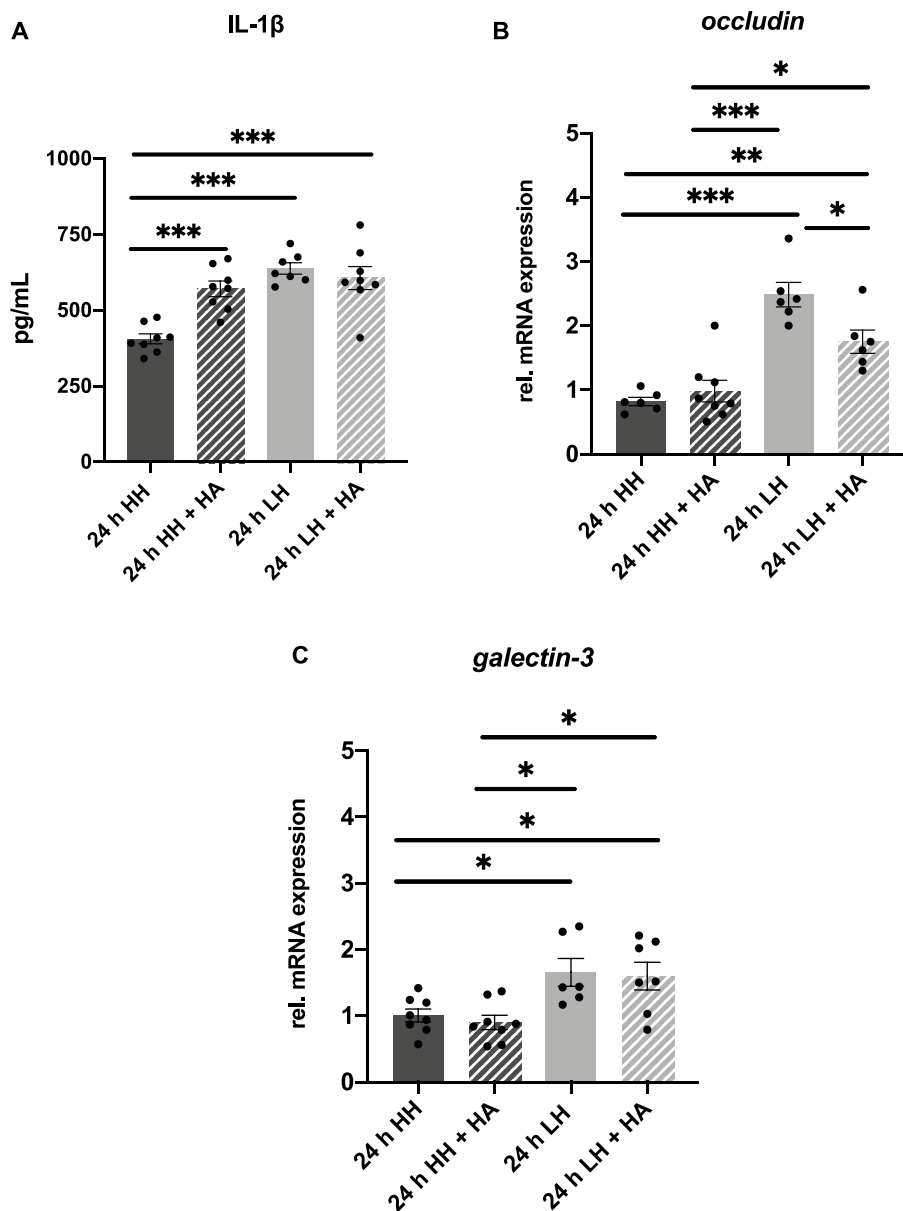


Figure 16: The effects caused by LH are partially neutralized by hyaluronic acid (HA). (A) IL-1 β secretion was not significantly different in the LH + HA group in comparison to the LH group. IL-1 β was elevated in porcine corneas incubated at LH, at LH + HA, and at HH + HA in comparison to the ones cultivated at HH ($n = 7$ for LH/ $n = 8$ for LH + HA/ $n = 8$ for HH/ $n = 8$ for HH + HA). Ordinary one-way ANOVA followed by Tukey's multiple comparisons test were used for statistical analysis. (B) Significant prevention of increase of *occludin* mRNA expression was noticed in the LH + HA group in comparison to LH. Ordinary one-way ANOVA followed by Tukey's multiple comparisons test were used for statistical analysis. (C) *Galectin-3* expression was not significantly different in the LH + HA group in comparison to the LH group. Ordinary one-way ANOVA followed by Tukey's multiple comparisons test were used for statistical analysis. (B-C) $n = 6$ for LH/ $n = 6-7$ for LH + HA/ $n = 6-8$ for HH/ $n = 8$ for HH + HA. LH: low humidity. HH: high humidity. HA: hyaluronic acid. The dots represent the n numbers. The bars represent the mean values, and the SEM is shown. * $p < 0.05$ ** $p < 0.01$ *** $p < 0.001$. Figure published at <https://doi.org/10.3390/ijms23094567> (Netto et al, 2022).

3.2 Chapter 2: Testing of DNA Nanoparticles in the dry eye model

Once the dry eye model was successfully established and tested with two usual therapeutic options for DED, DNA Nanoparticles (NPs) were verified as a treatment option for DED. Consequently, their effect on corneal preservation, inflammation, and cell apoptosis was examined. Therefore, as a preliminary step, the NPs were used to treat an *in vitro* corneal model (SkinEthic™ HCE), that is a 3D epithelial human corneal model. Afterward, porcine corneas were also treated with NPs and incubated for 24 h at LH, and the controls were treated with NPs and incubated at HH for the same period of time. Also, untreated controls were incubated at LH and HH for the same period.

3.2.1 The DNA-Nanoparticles protect the *in vitro* human corneal model by adhesion to the corneal epithelium

To evaluate if the NPs adhere to the tissues with damaged epithelium caused by LH, the *in vitro* human corneal model was treated with NPs attached to a fluorescent dye called Atto 488 (NP-Atto 488 50 μM), and it was submitted to an extreme LH stress (15% humidity at 37 °C) for 30 min. An extreme LH was applied because the incubation time was also shorter. The concentration of 50 μM was chosen for the NPs, after preliminary experiments with multiple concentrations (1 μM , 20 μM , 50 μM and 100 μM). Samples treated with NP-Atto 488 and incubated at HH (95% humidity at 37 °C) for the same period served as controls. Furthermore, additionally two groups of control samples received pristine Atto 488 and were also incubated at LH and HH simultaneously. Histological examination with HE staining revealed that the *in vitro* human corneal model underwent structural damage when cultivated at LH, while it remained intact at HH (Figures 17 A and C). The NP-Atto 488 treated tissues presented mild damage when the tissue was incubated at LH (Figure 17 D). The further evaluation indicated that pristine Atto 488 was unable to bind to

the tissue surface (Figures 17 A and C), while the NP-Atto 488 adhered to the tissue surface in the damage model, which can be verified by the green dye visualized on the surface of the tissue (Figure 17 D).

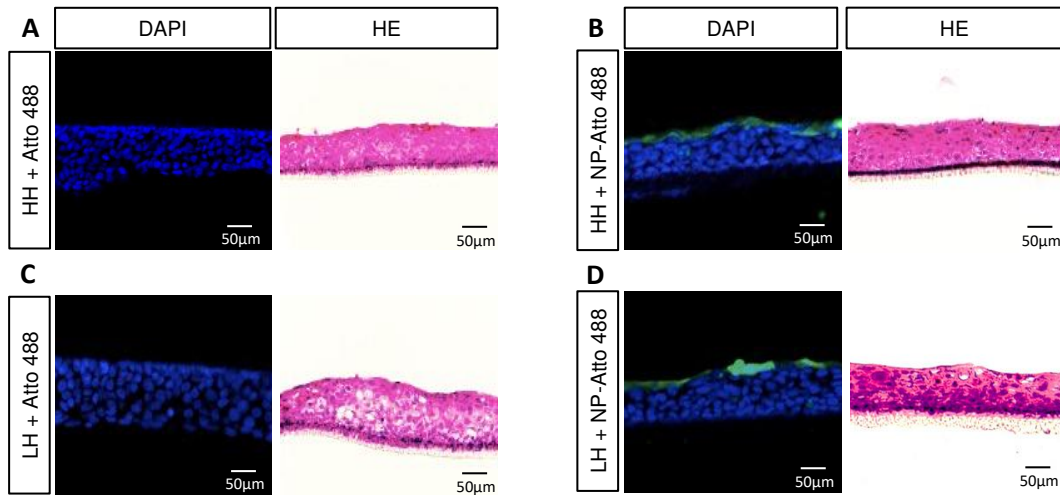


Figure 17: *In vitro* human corneal model (SkinEthic™ HCE) underwent structural damage when incubated with pristine Atto 488 at LH as control and presented mild damage when treated with NP-Atto 488 and incubated at LH.

(A) Control that received Atto 488 and was incubated at HH presented an undamaged structure, and the Atto 488 green signal was not visualized. (B) A control treated with NP-Atto 488 and cultivated at HH also showed an undamaged structure and green fluorescent signal was visualized. (C) The sample treated with Atto 488 and submitted to LH showed severe damage to the corneal epithelial tissue, and Atto 488 signal was not observed. (D) The sample treated with NP-Atto 488 and submitted to LH stress presented mild damage, and a green fluorescent signal was noticed. $n = 2$ for all groups. LH: low humidity. HH: high humidity. DAPI: 4',6-diamidino-2-phenylindole (blue). Atto 488: fluorescent dye (green). HE: hematoxylin eosin. NP-Atto 488: DNA-Nanoparticles attached to Atto 488. Scale bar = 50 μm .

3.2.2 The DNA-Nanoparticles adhere to the stressed *in vitro* human corneal model and to controls for up to 24 h

To verify if the NPs adhere to the tissue incubated at LH for a longer period of time, the *in vitro* human corneal model was treated with NPs attached to the fluorescent dye Atto 488, NP-Atto 488 50 μM , and it was submitted to LH stress (30% humidity at 37 $^{\circ}\text{C}$) for 24 h. Controls were treated with NP-Atto 488 and incubated for the same period at HH (95% humidity at 37 $^{\circ}\text{C}$). Samples that received pristine Atto 488 were also incubated at LH and HH simultaneously. The samples were frozen in liquid nitrogen and cut into slides for histological analysis, DAPI and HE staining were performed, and mosaic pictures were

taken to better access the whole *in vitro* human corneal tissue. As expected, it was verified that the pristine Atto 488 did not adhere to the *in vitro* corneal tissue, as no green fluorescent signal was observed (Figure 18 A and B). In both samples treated with NP-Atto 488 and incubated at HH or LH, green fluorescence was noticed, indicating that the NP-Atto 488 adhered strongly to the *in vitro* tissue up to 24 h of incubation (Figure 18 C and D). The integrity of the tissue was not evaluated because mosaic pictures aim to visualize the entire tissue but are not close enough to evaluate details.

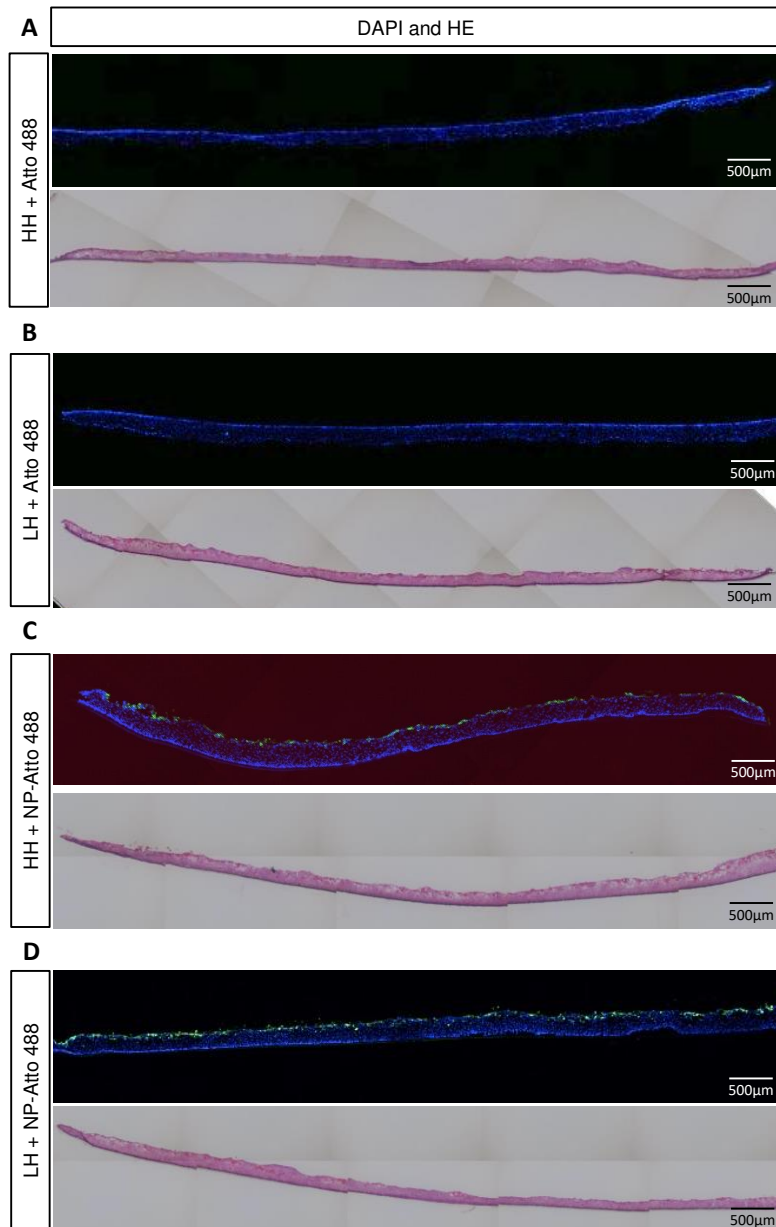


Figure 18: **NPs adhered to the stressed *in vitro* human corneal tissue for up to 24 h.** (A) A green fluorescent signal was not observed at the surface of the sample that received Atto 488 and was incubated at HH. (B) *In vitro* tissue that received Atto 488 and was cultivated at LH did not present a green fluorescent signal as well. (C) and (D) Tissues treated with NP-Atto 488 and incubated at HH (C) and at LH (D) showed a green fluorescent signal, indicating that the NP-Atto 488 could bind to the surface of the epithelial tissue for up to 24 h. $n = 4$. LH: low humidity. HH: high humidity. DAPI: 4',6-diamidino-2-phenylindole (blue). Atto 488: fluorescent dye (green). HE: hematoxylin eosin. NP-Atto 488: DNA-Nanoparticles attached to Atto 488. Scale bar = 500 μm.

3.2.3 The DNA-Nanoparticles adhere to the stressed porcine corneas

After confirming NPs binding to the *in vitro* human corneal epithelium up to 24 h and preventing the damage caused by LH, the NPs were tested in the porcine corneal model. To evaluate if the NPs adhere to the porcine corneas with stressed epithelium, the *ex vivo* porcine corneal model was treated with NP-Atto 488 50 μM , or with pristine Atto 488 and subjected to LH stress (37 °C and 30% humidity) for 24 h. Controls were treated with NP-Atto 488 50 μM or with pristine Atto 488 and were incubated at HH for the same period. Histological analysis was performed with HE and DAPI staining. Histological examination revealed that pristine Atto 488 cannot adhere to the tissue surface (Figure 19 A and C). However, in the tissues treated with NP-Atto 488 a green, fluorescent signal could be observed (Figures 19 B and D). The percentage of fluorescent area in each picture was analyzed. In accordance with the histological examination, in samples incubated with pristine Atto 488 at HH or LH, no fluorescence was observed. Porcine corneas treated with NP-Atto 488 50 μM and incubated at HH had an average of 3.66% (± 1.00) of fluorescent area in their pictures and the ones treated with NP-Atto 488 50 μM and submitted to LH had an average of 1.65% (± 0.16) (Figure 19 E). Although the percentage of fluorescent area in pictures of samples treated with NP-Atto 488 and incubated at LH was lower than the percentage of the ones treated with NP-Atto 488 and submitted to HH, this difference was not significant ($p > 0.99$).

Porcine corneas incubated at LH and treated with NP-Atto 488 or with pristine Atto 488 presented damage to the corneal epithelium (Figure 19 C and D). To confirm these findings, the integrity of the corneal epithelium was analyzed and graded after PAS staining, as described in section 2.2.5.6. Samples treated with Atto 488 and NP-Atto 488 50 μM and incubated at HH had a mean epithelial integrity of 86.94% (± 5.13) and 92.27% (± 3.80), respectively. Regarding the ones that received Atto 488 and were incubated at LH, the mean integrity was 56.67% (± 6.93), and porcine corneas treated with NP-Atto 488 50 μM and submitted to LH had a mean epithelial integrity of 61.33% (± 12.72 ; $p = 0.98$), and no significant difference between the two groups was observed. The

epithelial integrity of corneas treated with NP-Atto 488 and incubated at LH was significantly reduced when compared to the ones treated with NP-Atto 488 and subjected to HH ($p = 0.04$) (Figure 19 F).

In summary, the NPs adhered to the corneal epithelium of the samples incubated at LH or HH, while pristine Atto 488 was not able to adhere. However, the epithelial integrity of corneas treated with NP-Atto 488 and incubated at LH was not preserved by the NPs.

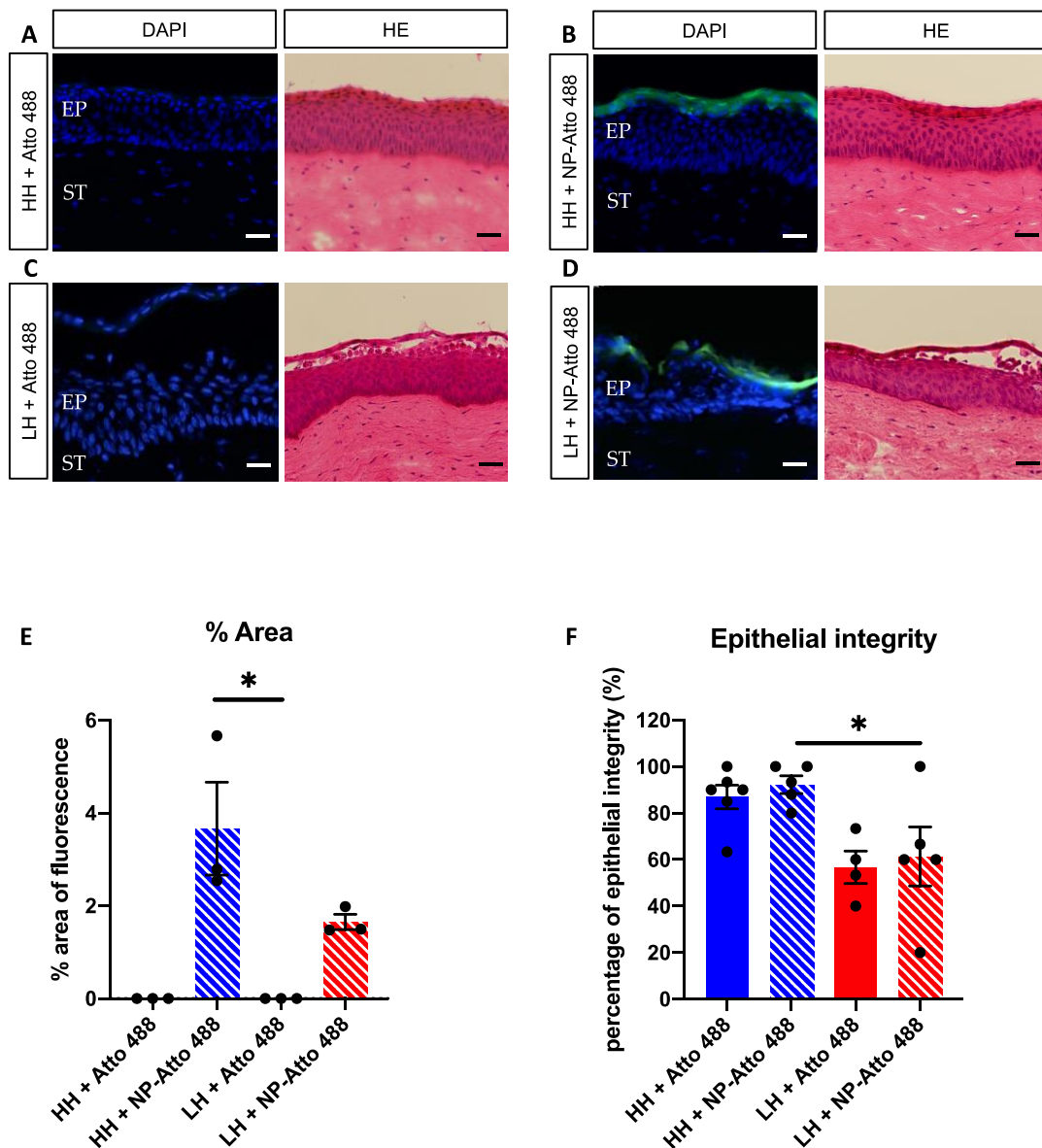


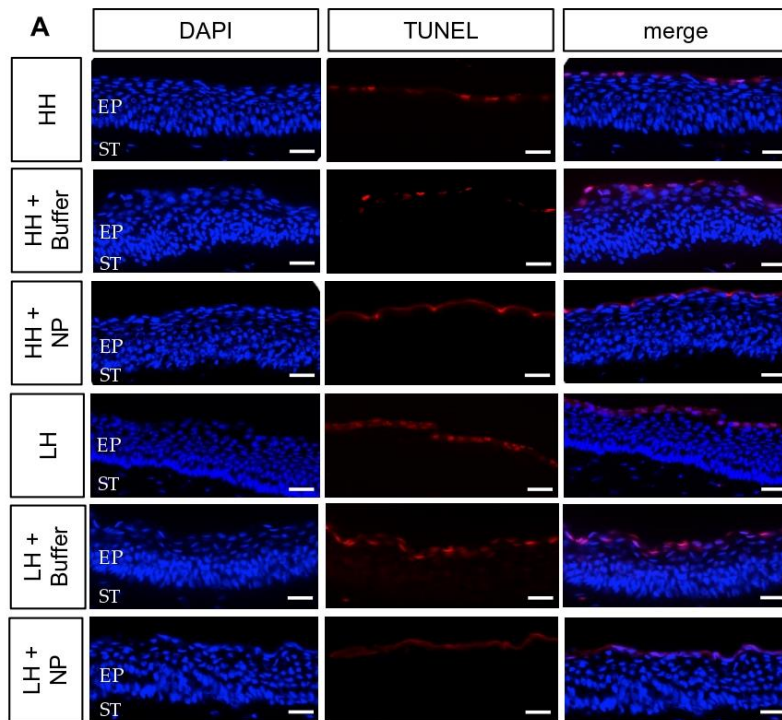
Figure 19: **NPs adhered to the stressed porcine corneal epithelium.** (A) Porcine corneas that received Atto 488 and were incubated at HH presented intact corneal epithelium, and no green fluorescence was visualized. (B) Corneas treated with NP-Atto 488

and submitted to HH showed intact corneal epithelium, and a green fluorescent signal was observed. (C) Samples that received Atto 488 and were subjected to LH presented a damaged epithelial layer, and no green signal was seen. (D) Porcine corneas treated with NP-Atto 488 and incubated at LH presented damage to the epithelial layer, and a green fluorescence was visualized. (E) Porcine corneas treated with NP-Atto 488 and incubated at HH had an average of 3.66% (± 1.00) of the fluorescent area in their pictures, and the ones treated with NP-Atto 488 and submitted to LH had an average of 1.65% (± 0.16). $n = 3$ for all groups. Kruskal-Wallis test followed by Dunn's multiple comparisons test were used for statistical analysis. (F) The epithelial integrity of corneas treated with NP-Atto 488 and incubated at LH was significantly reduced compared to the ones treated with NP-Atto 488 and subjected to HH. No significant difference in the epithelial integrity was observed between corneas treated with NP-Atto 488 and incubated at LH and those that received pristine Atto 488 and were incubated at LH. Ordinary one-way ANOVA followed by Tukey's multiple comparisons test were used for statistical analysis. $n = 6$ for HH + Atto 488/ $n = 5$ for HH + NP-Atto 488/ $n = 4$ for LH + Atto 488/ $n = 5$ for LH + NP-Atto 488. LH: low humidity. HH: high humidity. DAPI: 4',6-diamidino-2-phenylindole (blue). Atto 488: fluorescent dye (green). HE: hematoxylin eosin. NP-Atto 488: DNA-Nanoparticles attached to Atto 488. EP: epithelium. ST: stroma. The dots represent the n numbers. The bars represent the mean values. SEM is shown. * $p < 0.05$. Scale bar = 50 μm .

3.2.4 DNA-Nanoparticles hinder corneal epithelial apoptosis caused by low humidity

To analyze whether the NPs reduce corneal epithelial apoptosis caused by LH, a TUNEL assay was performed, and the apoptotic cells were quantified. After treating porcine corneas with NPs 50 μM or with buffer, samples were incubated at LH or HH for 24 h. Controls were incubated untreated at LH or HH. As expected, untreated corneas ($12.17\% \pm 0.68$, $p < 0.001$) or corneas treated with buffer ($15.32\% \pm 3.38$, $p = 0.25$) and incubated at LH contained almost three times more apoptotic epithelial cells than the untreated ones and incubated at HH ($4.87\% \pm 0.68$). This indicates that the buffer tested does not provide a protective effect against apoptosis on the corneal epithelium. However, a significant reduction in corneal epithelial apoptosis was observed in samples treated with NPs 50 μM and submitted to LH ($1.00\% \pm 0.38$) in comparison to the untreated ones incubated at HH ($4.87\% \pm 0.68$, $p = 0.01$). Moreover, no significant difference in corneal epithelial apoptosis was observed in samples treated with NPs 50 μM and submitted to LH ($1.00\% \pm 0.38$) in comparison to the ones treated with buffer ($4.52\% \pm 0.75$, $p = 0.05$) or treated with NPs ($1.49\% \pm 0.34$, $p > 0.99$) and incubated at HH. Porcine corneas treated with NPs and subjected to LH also showed significantly fewer apoptotic

cells ($1.00\% \pm 0.38$) compared to the untreated samples ($12.17\% \pm 0.68$, $p < 0.001$) incubated at LH (Figure 20 A and B). This fact demonstrates that NPs prevented corneal epithelial apoptosis that would be caused by LH.



B *TUNEL positive cells*

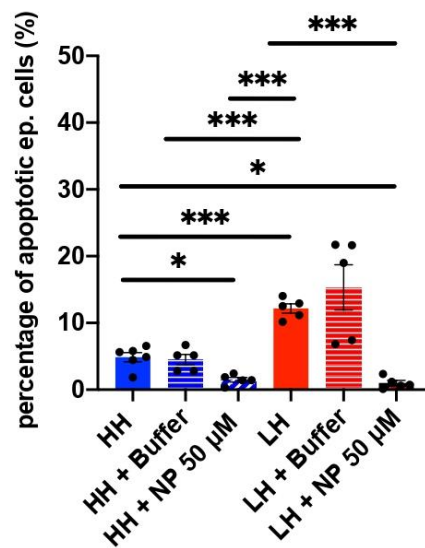


Figure 20: NPs hinder apoptosis caused by LH.

(A) Representative images of untreated porcine corneas, corneas treated with buffer or 50 μ M NPs and cultivated at LH or HH for 24 h and stained with TUNEL (red) and DAPI (blue). (B) A quantification was performed to assess the total number of apoptotic epithelial cells in each sample group in relation to DAPI-positive cells. Untreated porcine corneas or porcine corneas treated with buffer and incubated at LH showed more apoptotic cells than controls, untreated and submitted to HH. It was also possible to notice that corneas treated with NPs and incubated at LH had fewer apoptotic cells than the untreated ones and the ones treated with buffer and subjected to LH. Welch's ANOVA test followed by Dunnett's multiple comparisons test were used for statistical analysis. $n = 6$ for HH/ $n = 5$ for HH + buffer/ $n = 5$ for HH + NP/ $n = 5$ for LH/ $n = 5$ for LH + buffer/ $n = 5$ for LH + NP. LH: low humidity. HH: high humidity. DAPI: 4',6-diamidino-2-phenylindole. TUNEL: TdT-mediated dUTP-biotin nick end labelling. EP: epithelium. ST: stroma. Scale bar = 50 μ m. The dots represent the n numbers. The bars represent the mean values, and the SEM is shown. All data are shown as mean \pm SEM. * $p < 0.05$ *** $p < 0.001$.

3.2.5 Treatment with NPs 100 μ M counteracts upregulation of *galectin-3*

NPs have shown important effects in preventing apoptosis caused by LH. Therefore, it was investigated whether NPs at concentrations of 50 μ M and 100 μ M would prevent increased gene expression of *galectin-3* and *IL-8*, an inflammatory marker. NPs at concentrations of 100 μ M were used to investigate if a higher concentration would be more effective in preventing increased gene expression of those markers. As expected, an increased gene expression of *galectin-3* was observed in samples incubated at LH (3.48 ± 0.52) compared to the controls submitted to HH (1.35 ± 0.28 , $p = 0.001$). Interestingly, there was no statistically significant difference between samples incubated at LH and treated with NPs 50 μ M (2.26 ± 0.40 , $p = 0.62$) or 100 μ M (1.33 ± 0.28 , $p > 0.99$) and samples incubated at HH (1.35 ± 0.28). However, there was also no statistically significant difference in *galectin-3* expression in porcine corneas treated with buffer and subjected to LH (1.75 ± 0.45 , $p > 0.99$) and the ones incubated at HH. Moreover, a significant reduction in *galectin-3* expression was observed in samples treated with NP 100 μ M and incubated at LH (1.33 ± 0.28 , $p < 0.001$) compared to those untreated incubated at LH (Figure 21 A).

Regarding *IL-8* mRNA expression, no statistically significant difference was noticed between corneas treated with NP 100 μ M and incubated at LH (1.58 ± 0.32) and the controls, which were untreated and incubated at HH (1.20

± 0.24 , $p > 0.99$). Furthermore, an upregulation in *IL-8* was identified in samples treated with buffer and incubated at LH (2.83 ± 0.23) in comparison to the ones treated with NP 100 μM and incubated at HH (0.83 ± 0.18 , $p = 0.02$), which would be already expected since the buffer should not have any protective effect on porcine corneas, preventing damages caused by LH. An upregulation in *IL-8* gene expression was also observed in corneas treated with NP 50 μM (2.85 ± 0.72) in comparison to the ones treated with NP 100 μM and incubated at HH (0.83 ± 0.18 , $p = 0.01$). Furthermore, NPs at a concentration of 50 μM (2.85 ± 0.72 , $p = 0.92$) or 100 μM (1.58 ± 0.32 , $p = 0.90$) in samples incubated at LH had no significant influence on *IL-8* gene expression in comparison to untreated porcine corneas incubated at LH (2.20 ± 0.39) (Figure 21 B).

In conclusion, 100 μM NPs prevented the increase in gene expression of *galectin-3* that LH would cause, while 50 μM NPs did not prevent the increased expression of *galectin-3* and *IL-8* caused by LH.

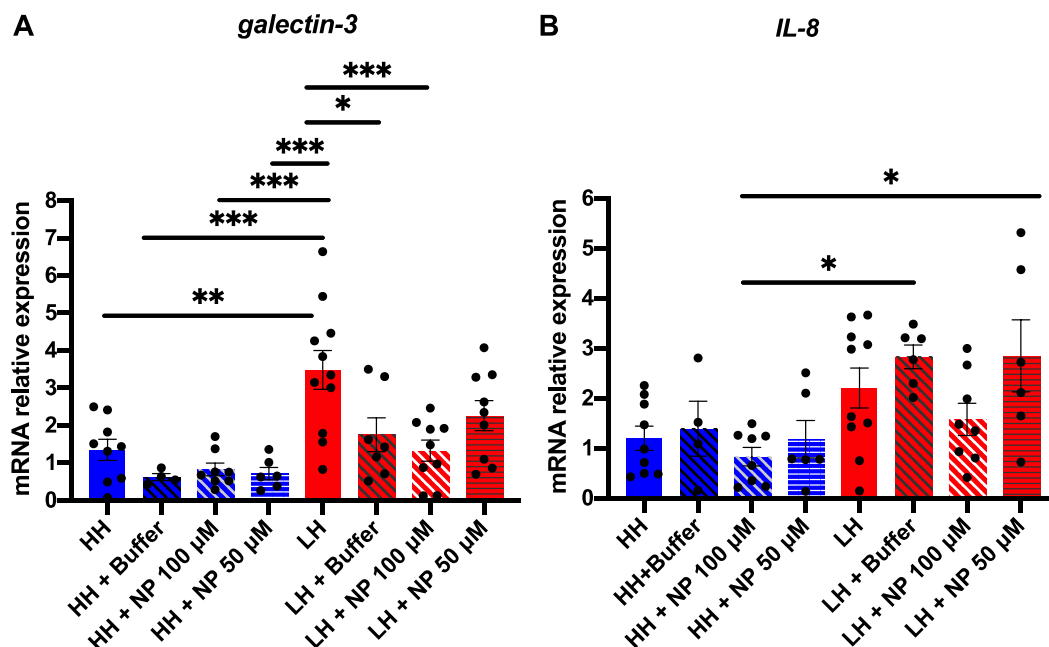


Figure 21: **Upregulation of *galectin-3* was prevented in corneas treated with NP 100 μM and submitted to LH.**

(A) An upregulation in *galectin-3* gene expression was noticed in samples incubated at LH in comparison to controls cultivated at HH. A statistically significant reduction in *galectin-3* gene expression was observed in corneas treated with NP 100 μM and incubated at LH in

comparison to untreated corneas incubated at LH. Ordinary one-way ANOVA followed by Tukey's multiple comparisons test were used for statistical analysis. (B) NPs at a concentration of 50 μM or 100 μM in samples incubated at LH had no influence on *IL-8* expression in comparison to untreated porcine corneas incubated at LH. Ordinary one-way ANOVA followed by Tukey's multiple comparisons test were used for statistical analysis. $n = 9$ for HH/ $n = 4$ for HH + buffer/ $n = 8$ for HH + NP 100 μM / $n = 6$ for HH + NP 50 μM / $n = 10-11$ for LH/ $n = 6-7$ for LH + buffer/ $n = 8-9$ for LH + NP 100 μM / $n = 6-9$ for LH + NP 50 μM . LH: low humidity. HH: high humidity. The dots represent the n numbers. The bars represent the mean values, and the SEM is shown. All data are shown as mean \pm SEM. * $p < 0.05$ ** $p < 0.01$ *** $p < 0.001$.

3.3 Chapter 3: Establishment of a porcine corneal cell culture

In ophthalmic research, there is a strong need for *in vitro* corneal cell models, to test new therapeutic options for corneal diseases, such as DED.

3.3.1 Establishment of the outgrowth method

To perform cell isolation and cultivation with the outgrowth method, the porcine cornea was extracted from the eyeball, and explants were produced of the limbus with a strip of approximately 2 mm of corneal tissue and 2 mm of sclera. The explants were placed in a culture flask and were incubated for four to five weeks. After isolation of the corneal limbal explants, the growth of corneal cells was observed with microscopy to compare the differences between the cultivation with and without FBS. Two days after the isolation of explants using cultivation methods with FBS and without it, cell growth from corneal explants was verified. At this time point, there were more cells growing out of the explants cultured with FBS, and the area of outgrowing cells around the explants was substantially diminished in cultures without FBS. On the fourth day of cultivation, it was verified the largest number of cells growing around the explants cultivated with FBS, and this difference could also be noticed in the following two weeks. After two weeks of incubation, changes in cell morphology became apparent. Cells incubated with 10% FBS were smaller, and there was a higher number of cells in these cultures, while cells grown with non-serum medium showed typical epithelium morphology in a cell order like roof tiles. In

the first two weeks of cultivation, almost the entire area surrounding the explants was occupied with cells. In the following weeks, cells of the cultivation group without FBS grew more in size of their cell bodies, showing an even more roof tile-like cell arrangement, and some stellate cells were also present. Regarding the cultivation group with FBS, some cells did not grow when it came to cell body size but developed fibrous-like structures. Therefore, the cell culture that was cultivated without FBS contained more homogenous cells with characteristics of corneal epithelial cells and some stellate cells with characteristics of keratocytes (Figure 22 A). While in the culture cultivated with FBS, some cells morphologically similar to fibroblasts and some epithelial cells were observed (Figure 22 B). In both methods, the cell cultures reached 70-80% of confluency in four to five weeks of incubation (Netto et al., 2023).

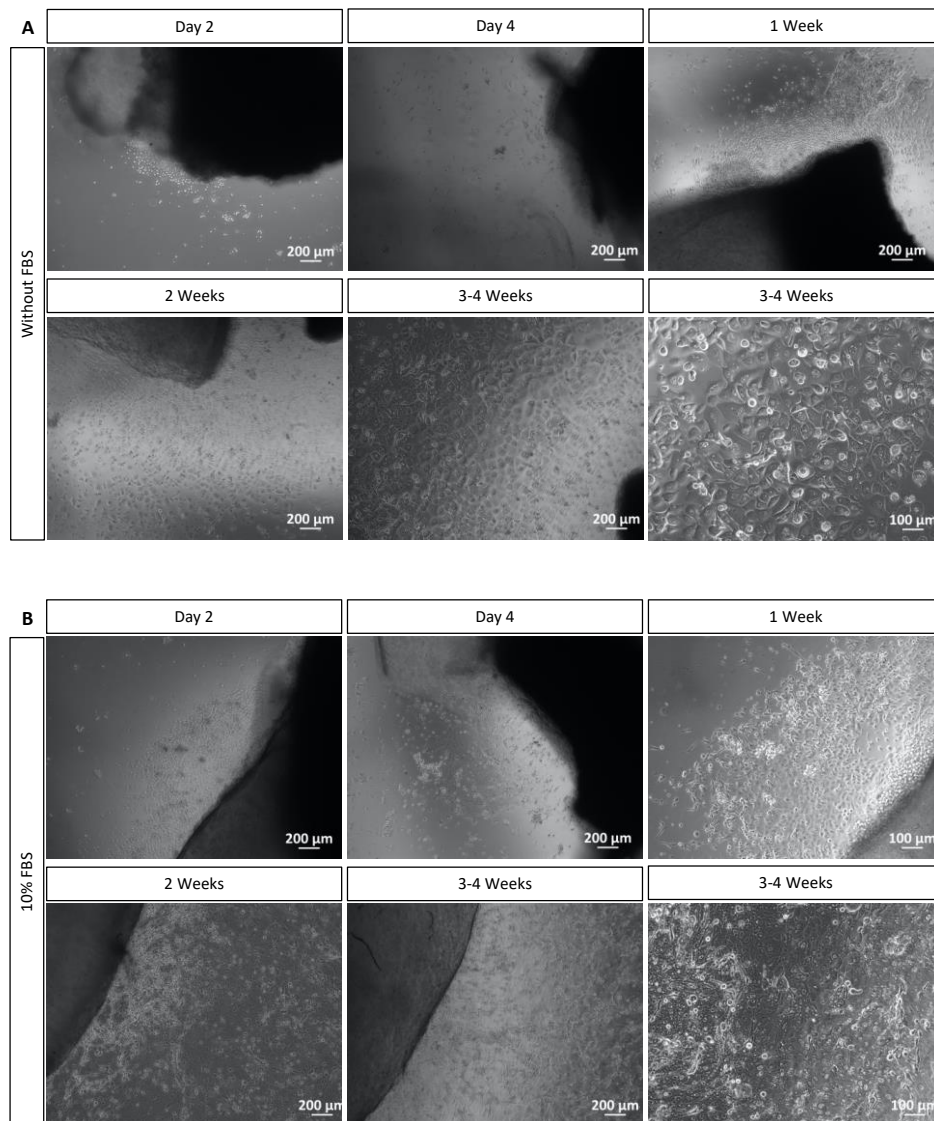


Figure 22: Corneal cell isolation with the outgrowth method.

Observation of cell outgrowth was possible two days after the explant isolation process. (A) A smaller number of cells grew around the explants of cultures cultivated without FBS, and most cells were morphologically like epithelial cells and some like keratocytes. (B) From day four until two weeks, more cells were growing in the culture with FBS, and some cells were morphologically similar to fibroblasts. After four to five weeks both cultures achieved 70-80% confluency and could be split. FBS: fetal bovine serum. Scale bar = 100 μm and 200 μm. Figure adapted from: <https://doi.org/10.3390/mps6030050> (Netto et al, 2023).

3.3.2 Cell cultures cultivated with FBS contain higher amounts of cells

To assess the number of cells in each cell culture, with or without FBS, at the outgrowth method, an automated cell counter (Olympus R1 SLI Cell counter, Olympus corporation) was used to quantify the number of cells per

flask after cells at passage zero were split. The cultivation of corneal explants from a single porcine eye resulted in the production of each flask. A minimum of three eyes per time point was evaluated, and the graph below demonstrates the average of cells per eye in each week of cultivation (Figure 23). It was observed that cultures incubated with FBS since the first week presented a higher number of cells, and the number of cells increased exponentially. The doubling cell time was approximately two weeks for cells cultivated with FBS and ten days for the ones cultivated without FBS. Compared to those without serum, the number of counted cells cultivated with serum was more than five times higher after five weeks (Netto et al., 2023).

Hence, to obtain a high number of corneal cells for an experiment, it is recommended to use FBS in the culture medium. Alternatively, if FBS is not used, the cell growth rate may be slow. As described in the previous results section, this fact correlates with microscopy observations.

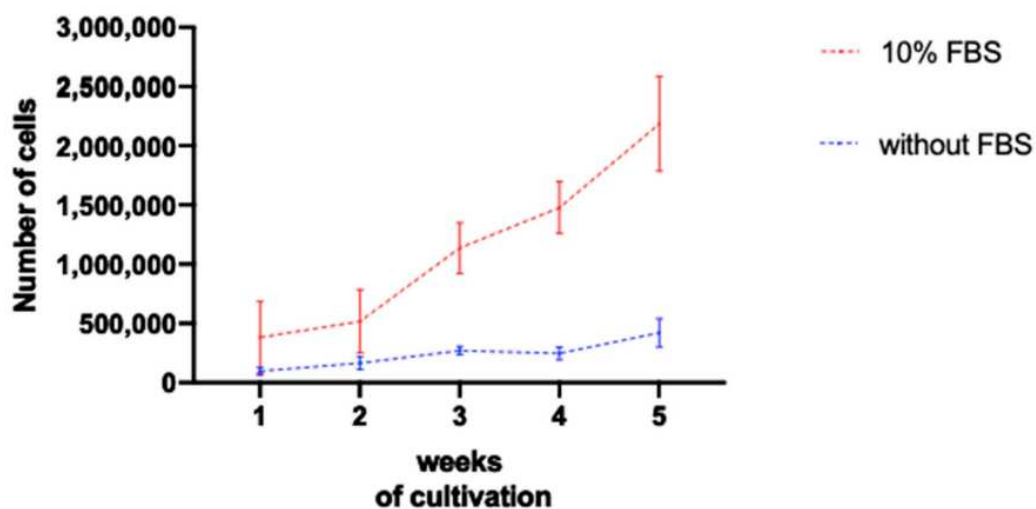


Figure 23: **The average number of cells per week during outgrowth cultivation.**

Cell amount in the cultures incubated with FBS was larger than in the ones without it, and the increase in the number of cells was significantly higher in the cultures with FBS. FBS: fetal bovine serum. The mean values and the SEM are shown. Figure published at: <https://doi.org/10.3390/mps6030050> (Netto et al, 2023).

3.3.3 Cultures cultivated without FBS contain mainly epithelial cells and keratocytes

To compare the cultivation method with 10% FBS and without it and to establish the different cell types, immunostaining, and qRT-PCR were performed. The expression of the epithelial cell marker, cytokeratin-3 (CK3), and the tight junctions' markers zonula occludens 1 (ZO-1) and occludin were evaluated to confirm the cultivation of corneal epithelial cells. The corneal epithelium contains a substantial amount of cytokeratin 12 (CK12) (Kasper et al., 1988). Therefore, to quantify the mRNA expression of *CK12*, qRT-PCR was performed. It was observed that cells from cultures with FBS and without it, expressed CK3 (Figure 24 A). Moreover, cells from both cultures expressed occludin and ZO-1, which are parts of tight junctions of epithelial cells (Figure 24 A). These facts confirm the hypothesis that both cultures permitted the growth of epithelial cells (Netto et al., 2023).

The mRNA expression of *CK12* was analyzed in cell cultures as well. The culture without FBS was considered as the control group, so upregulation of *CK12* gene expression was observed in the culture cultivated with FBS (10% FBS: 4.12 ± 0.88 ; without FBS: 1.23 ± 0.42 , $p = 0.02$) (Figure 24 B). Thus, it was concluded that the culture cultivated with FBS presented more cells that expressed the *CK12* gene (Netto et al., 2023).

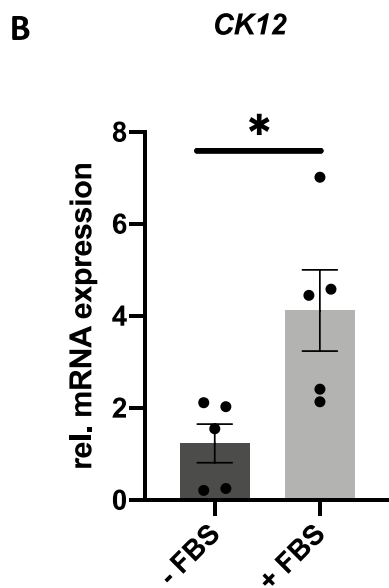
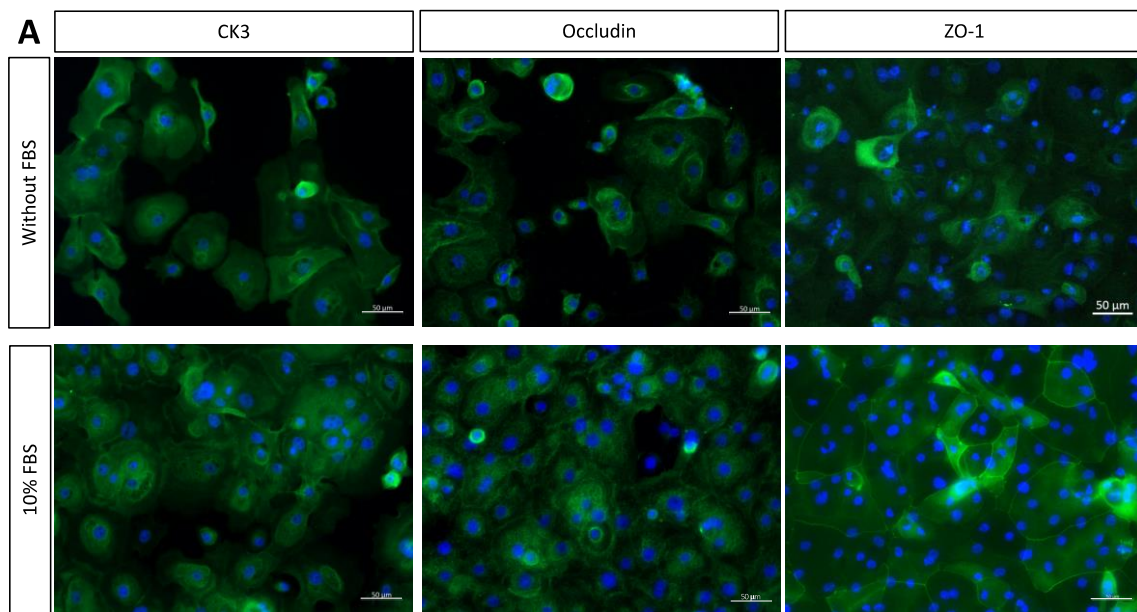


Figure 24: Cell cultures cultivated with FBS and without it contained corneal epithelial cells.

Antibodies targeting CK3, occludin, and ZO-1 were used to analyze the protein expression of those markers in corneal cell cultures, and *CK12* mRNA expression was investigated. Cells were cultured for four weeks, and then immunostained on chamber slides, or qRT-PCR was performed on frozen cells. ZO-1 and occludin were used as tight junction markers, while CK3 and CK12 were used as epithelial cell markers. (A) CK3, occludin, and ZO-1 positive cells were identified in both cell cultures, confirming the presence of corneal epithelial cells. (B) An upregulation of *CK12* was verified in the cell culture cultivated with FBS. Unpaired t-test was used for statistical analysis. $n = 5$ for without FBS/ $n = 5$ for with FBS. CK3 = green, ZO-1 = green, occludin = green, DAPI = blue. DAPI: 4',6-diamidino-2-phenylindole. FBS: fetal bovine serum. The bars represent the mean values, and the SEM is shown. The dots represent the n number in each group. Scale bar = 50 μm . * $p < 0.05$. Figure published at: <https://doi.org/10.3390/mps6030050> (Netto et al., 2023).

To analyze the amount of keratocytes in the cell cultures, antibodies targeting keratocyte markers, keratocan and lumican, were used. Moreover, the mRNA gene expression of *keratocan* was evaluated. Keratocan and lumican were more abundant in cultures cultivated without serum (Figure 25 A). Based on this finding, it is confirmed that keratocytes can grow in cultures without serum. McKay et al. also reported that exposure to low-serum conditions preserves the keratocyte phenotype (McKay et al., 2020 apud Netto et al., 2023).

Moreover, downregulation of *keratocan* expression was observed in the culture with FBS (0.30 ± 0.04 ; $p = 0.04$) in comparison to the one cultivated without serum (1.16 ± 0.44) (Figure 25 A). It is consistent with the hypothesis already discussed previously that low serum levels promote keratocyte proliferation (Netto et al., 2023).

Cell cultures were analyzed for the presence of mesenchymal cells and undifferentiated epithelial cells using an antibody targeting vimentin. The examination revealed that in both cultures, there were vimentin-positive cells present, indicating the existence of mesenchymal cells and undifferentiated epithelial cells, regardless of the presence or absence of serum (Figure 25 B) (Netto et al., 2023).

A quantification of CK3, lumican, and keratocan-positive cells was conducted to confirm the proportions of various cell types. In cultures grown without FBS, it was found that an average of 80.23% of the cells were epithelial, 19.31% were keratocytes, and 0.44% were other cell types. Moreover, cultures cultivated with 10% FBS, had an average of 67.36% epithelial cells, 9.86% keratocytes, and 22.76% of other cell types (Figure 26) (Netto et al., 2023).

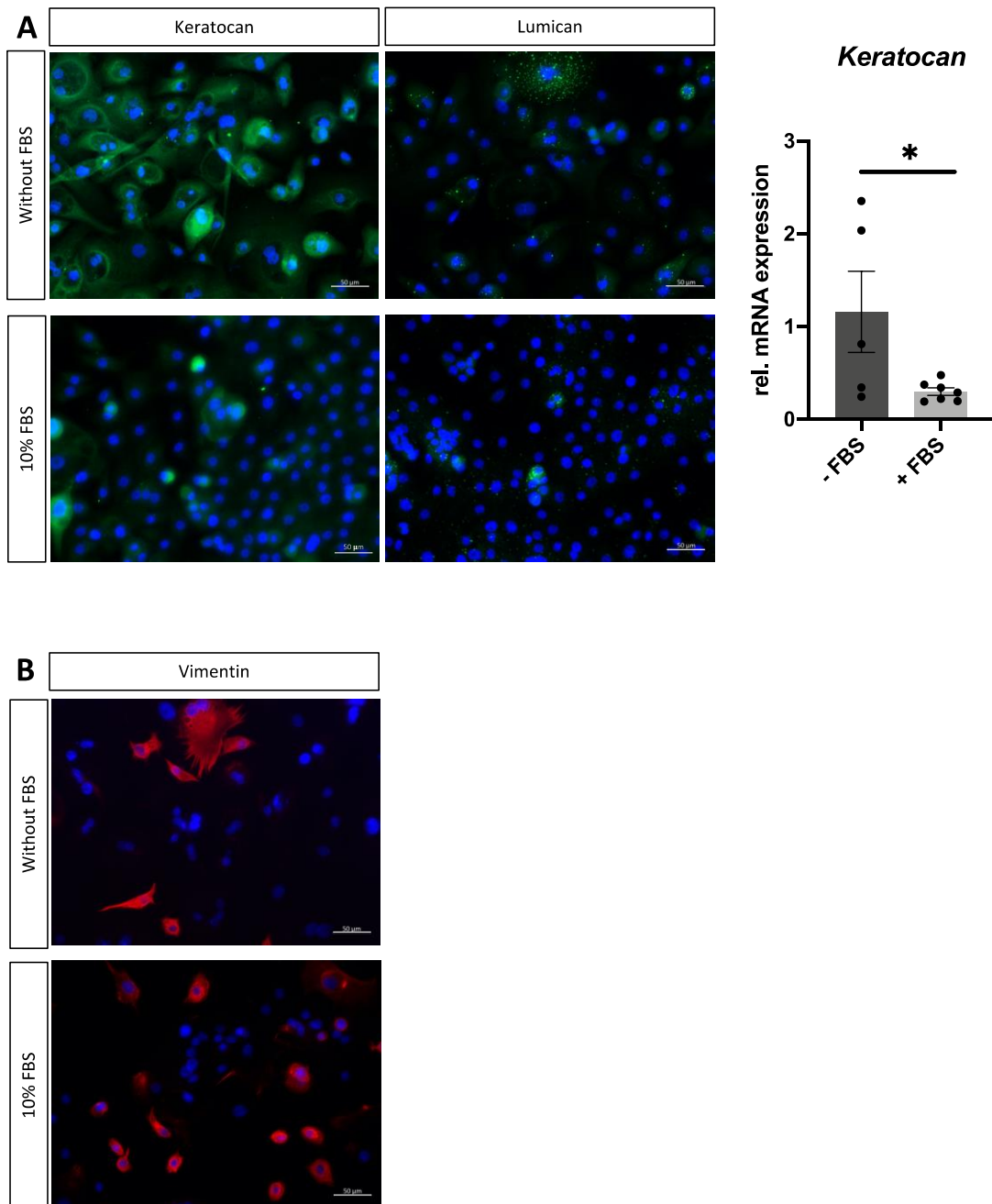


Figure 25: Cell cultures cultivated without FBS showed more keratocan and lumican expression.

Antibodies targeting keratocan and lumican were used in the cell cultures to identify expression of those keratocyte's markers, and quantification of *keratocan* mRNA expression was performed. (A) The cell culture cultivated without FBS had more keratocan and lumican-positive cells than the culture cultivated with FBS. This confirmed that there were more keratocytes in the culture cultivated without FBS. Compared with cultures without FBS, the culture with FBS showed a downregulation of *keratocan* mRNA expression. (B) An abundance of vimentin in cell cultures was verified. Cells that express vimentin and that are mainly mesenchymal cells and undifferentiated epithelial cells were positive in both cell cultures cultivated with FBS and without it. Unpaired t-test was used for statistical analysis. $n = 5$ for without FBS/ $n = 7$ for with FBS. Keratocan = green, Lumican = green, DAPI = blue, Vimentin = red. Scale bar = 50 μm . FBS: fetal bovine serum. DAPI: 4',6-diamidino-2-phenylindole. The bars represent the mean

values, and the SEM is shown. The dots represent the *n* number in each group. * $p < 0.05$. Figure adapted from: <https://doi.org/10.3390/mps6030050> (Netto et al. 2023).

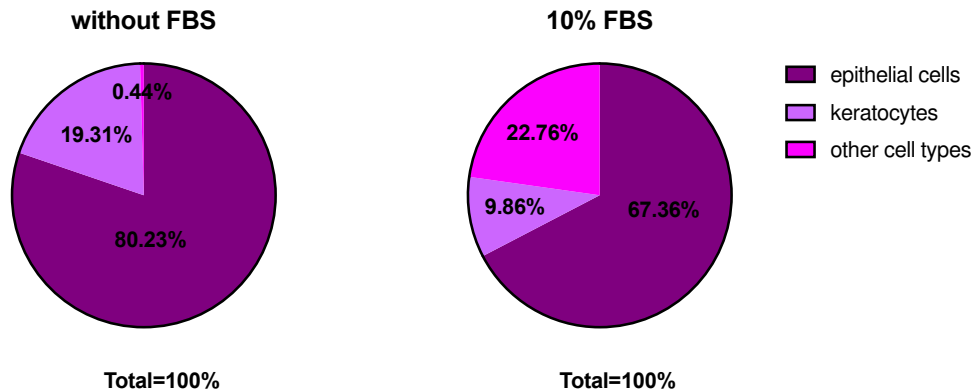


Figure 26: **Pie chart representing the proportion of distinct cell types.**

After single stainings were performed in a minimum of two wells per condition, a minimum of five pictures per staining and condition was used for analysis. The total number of cells per picture was counted, and the total number of CK3, lumican, and keratocan-positive cells was counted as well. CK3 was used as an epithelial cell marker, and keratocan and lumican as keratocytes markers. A percentage of positive cells for each marker was calculated in relation to the total number of cells. Finally, an average was calculated considering the cell type percentage of every picture per condition. The majority of cells in cultures cultivated without FBS were epithelial cells, some keratocytes, and a small proportion of other types of cells. Cultures cultivated with FBS mainly contained epithelial cells, but other cell types, probably fibroblasts and myofibroblasts, had a greater proportion than keratocytes. Figure published at: <https://doi.org/10.3390/mps6030050> (Netto et al., 2023).

To summarize, corneal cells isolated and cultivated using the outgrowth method with a medium containing FBS were mainly epithelial cells, and other cell types, probably fibroblasts and myofibroblasts, that were more abundant than keratocytes. Moreover, this culture presented a higher total amount of cells. Regarding corneal cells cultivated without FBS, they were mainly epithelial cells and keratocytes. Only a small percentage of other cell types was identified in this culture (Netto et al., 2023).

4 Discussion

4.1 An *ex vivo* model for dry eye disease

DED is very prevalent worldwide, and the main current treatment is the use of artificial tears (Zhang et al., 2017; Smith, 2007). Developing new therapies for DED is very important, as the worldwide disease burden is high. Nevertheless, robust models are required to test new therapies (Netto et al., 2022).

Although *in vivo* models for DED have already been developed, their cost is high, and the use of animals in research should be avoided due to ethical concerns (Barabino & Dana, 2004; Choi et al., 2015). In a review of animal models for DED, Barabino and Dana described several *in vivo* animal models to study this disease. By removing the lacrimal gland of dogs, cats, rabbits, mice, and monkeys, models were suggested. The implantation of a lid specula or sutures to avoid blinking was proposed in rabbit models as well. Furthermore, animal models developed from the cauterization of meibomian glands orifices or the application of scopolamine to reduce tear film aqueous production were described (Barabino & Dana, 2004). *Ex vivo* models were also previously developed with the use of pumping systems to simulate tears or mechanical arms to simulate blinking, for example (Chan et al., 2014; Schrage et al., 2012). These models, however, are difficult to reproduce, and special tools are needed (Netto et al., 2022).

This study aimed to establish a cheap and robust *ex vivo* dry eye model that will not only make it possible to test new therapies efficiently but will also reduce animal welfare concerns. Furthermore, porcine eyes are morphologically similar to the human eye (Menduni et al., 2018) and have a similar size (Schnichels et al., 2016). The structure of porcine corneas and human corneas are morphologically comparable because both species have a corneal epithelium constituted of stratified, non-keratinized squamous cell layer, Bowman's membrane, stroma with collagen fibers, Descemet's membrane and

corneal endothelia (Subasinghe et al., 2021). Therefore, a simple transfer of knowledge is possible. However, it is important to note that some authors do not agree with the existence of Bowman's membrane in porcine corneas (Menduni et al., 2018; Subasinghe et al., 2021 apud Netto et al., 2022).

One important risk factor for DED is the environmental LH (Rouen & White, 2018). Formerly, in an *in vivo* model and in an *in vitro* model, the humidity of 30% has already been used to trigger DED (Meloni et al., 2011). Here, to investigate the effect of LH, corneal epithelial tissues were incubated at 30% humidity for different durations of time. Incubation for 24 h at LH (37 °C and 30% humidity) triggered changes similar to DED, i.e., the characteristic epithelial features usually observed in DED. Former studies also described such conditions to be the ideal ones to stimulate DED (Meloni et al., 2011 apud Netto et al., 2022).

The air-lifting technique, which was used to culture porcine corneas, provides the advantage of maintaining the physiological barrier function of the corneal epithelium by humidifying the corneal surface, allowing a thin layer of medium to hydrate the surface and maintaining air contact above it. This technique had been used for the cultivation of *in vitro* corneal epithelial cells and was demonstrated to be superior when compared to the non-air-lifting technique, in which the cells are completely submerged in culture medium (Ban et al., 2003 apud Netto et al., 2022).

To evaluate the histological modifications in the porcine model, the epithelial thickness was measured, and disruption of the epithelial cells was analyzed with HE staining. Previous studies demonstrated that LH stimulates a reduction of epithelial thickness (Meloni et al., 2011; Pelegriano et al., 2012), and it is widely recognized that disruption of the epithelial cells is an important indicator of DED (Chen et al., 2008; Pelegriano et al., 2012). Here, porcine corneas submitted to stress at LH for 12 h demonstrated a significant reduction in epithelial thickness, but epithelial damage was mild (Figure 11 A and B). On the other hand, corneas cultivated at LH for 24 h exhibited epithelial damage, with detachment of the superficial cells of the cornea (Figure 11 A) and a significant reduction of the epithelial thickness (Figure 11 B). In a similar study,

Pelegriño et al. found that LH triggers changes in corneal barrier function, leading to a decrease in epithelial thickness (Pelegriño et al., 2012 apud Netto et al., 2022).

Severe epithelial damage, with detachment of not only the superficial cells of the cornea but also internal layers, was observed in porcine corneas submitted to stress at LH for 48 h, and these changes were also observed in controls (Figure 11 A). Nevertheless, no statistically significant reduction of the epithelial thickness between groups was observed (Figure 11 B). Therefore, it was concluded that incubation of porcine corneas for a period longer than 24 h may cause epithelial damage not only to stressed samples but also to controls. The origin, collection, and transportation of porcine eyes are different from the procedure associated with human donor eyes, and there are pre-damages that make longer cultivation times more difficult. Despite this, damage to superficial corneal epithelial cells and other DED markers increased after 24 h, and the effect could be counteracted. Furthermore, it is important to point out that in human corneas from donors that are incubated at cornea banks, damage of the corneal epithelia also arises in death-to-preservation time intervals longer than 6 h (Van Meter et al., 2005 apud Netto et al., 2022).

4.2 Inflammation is induced in the dry eye model

Patients with DED present increased secretion of IL-1 β in the tear film, an inflammatory cytokine (Solomon et al., 2001; Javadi & Feizi, 2011). Na et al. reported a correspondence between the increase in the concentration of IL-1 β in tears of patients with DED and the severity of the disease as well (Na et al., 2012). In addition, Okanobo et al. described that DED associated inflammation stimulates an augmentation in IL-1 β , but that could be contained in their *in vivo* model with the use of topical Interleukin-1 receptor antagonist (IL1-Ra) (Okanobo et al., 2012). An elevation of the inflammatory cytokine IL-1 β was observed in the stressed corneas when incubated at LH for 24 h and for 48 h (Figure 12 A). Accordingly, this important indicator of inflammation associated

with DED is also increased in samples incubated under the desiccation conditions proposed (Netto et al., 2022).

The transcription factor NF- κ B is well known for its roles in stress response, cytokine production, and free radical production (Tsubota et al., 2020). Furthermore, it triggers the production of TNF- α and IL-1 β , which finally activate MMP9 (Corrales et al., 2006; Bron et al., 2017). Because of this, the mRNA expression of these pro-inflammatory markers was evaluated in this study. An upregulation of *NF- κ B* was verified in porcine corneas submitted to LH for 12 h and 24 h (Figure 12 C). Moreover, mRNA of *IL-1 β* and *TNF- α* was upregulated in corneas incubated at LH for 48 h (Figure 12 B and D). This fact is in accordance with the literature because it has been described that pro-inflammatory cytokines such as IL-1 β and TNF- α increase in DED (De Paiva et al., 2006; Li et al., 2002). Furthermore, environmental stress, such as LH and high osmolarity, leads to activation of NLRP3. Activated NLRP3 ultimately stimulates the maturation and secretion of IL-1 β (Chi et al., 2017). Therefore, mRNA expression of *NLRP3* was also investigated in this study, and an upregulation in corneas incubated at LH for 48 h was verified (Figure 12 E) (Netto et al., 2022).

According to the literature, IFN- γ has been reported as a biomarker for DED (Jackson et al., 2016; Roda et al., 2020). In agreement with this fact, IFN- γ was elevated in the media of porcine corneas incubated at LH for 48 h. Moreover, the pro-inflammatory cytokine MIF and the pro-inflammatory and pro-angiogenic cytokine ang-1 were also elevated in the media of porcine corneas cultivated at LH for 48 h. An increase of a pro-angiogenic cytokine, FGF21, was found in the media of samples stressed at LH for 24 h. This evidence supports our hypothesis that inflammatory pathways are triggered in our porcine model. The fact that erythropoietin, galectin-9, and IFN- β , which are anti-inflammatory cytokines, were elevated in the media of samples incubated at LH for 24 h might suggest a protection mechanism against LH effects (Table 6) (Netto et al., 2022).

4.3 Upregulation of tight junctions and glycocalyx markers in the dry eye model

In addition to cleaving the epithelial basement membrane, the matrix metalloproteinase MMP9 also cleaves the proteins that are part of tight junctions, such as occludin (Meloni et al., 2011; Huet et al., 2011). Active MMP9 is responsible for the cleavage of galectin-3, which is part of the epithelial glycocalyx as well (Uchino et al., 2015). As a consequence of the cleavage of these proteins, their gene expression is stimulated. Moreover, the expression of *occludin* mRNA has been described as an early marker for corneal damage severity (Meloni et al., 2010 apud Netto et al., 2022).

Samples cultured at LH for 24 h and 48 h showed significant upregulation of *occludin* and *galectin-3* mRNA expression (Figure 13 A and B). This evidence corroborates the hypothesis that the upregulation of mRNA expression of *occludin* and *galectin-3* can be interpreted as an early marker that acts as a positive signal to stimulate their protein production. As a consequence of the cleavage of occludin and galectin-3, their gene expression is stimulated. Meloni et al. demonstrated the upregulation of *occludin* mRNA expression as an early biomarker for irritation as well. It was reported that strong irritants stimulate this upregulation, which can be corresponded to early signs of cell defense and recovery potential (Meloni et al., 2011 apud Netto et al., 2022).

4.4 Apoptosis is induced in the dry eye model

To evaluate if the loss of epithelial cells in the porcine model is due to apoptosis, a TUNEL assay was done. Porcine corneas cultivated at LH for 12 h and 24 h exhibited a higher percentage of apoptotic cells in comparison to controls (Figure 14 A), which could be confirmed by the quantification of the percentage of apoptotic epithelial cells (Figure 14 B). However, no significant difference was observed in samples incubated at LH for 48 h, so this

corroborates the hypothesis that 48 h is too long period of incubation for the porcine corneas (Netto et al., 2022).

To summarize, incubation at LH for 24 h is suggested as the best time point to incubate the dry eye model. At this time point, damage to the superficial corneal epithelial cells and thinning of the corneal epithelium were observed. Furthermore, elevated secretion of IL-1 β and upregulation of *NF- κ B*, *occludin*, and *galectin-3* were shown. Apoptosis of corneal epithelial cells was stimulated in corneas cultivated at LH for 24 h as well (Figure 27) (Netto et al., 2022).

	12h LH	24h LH	48h LH
Corneal thickness	↓	↓	—
IL-1 β secretion	x	↑	↑
IL-1 β expression	—	—	↑
<i>NF-κB</i> expression	↑	↑	—
<i>TNF-α</i> expression	↓	↓	↑
<i>NLRP3</i> expression	—	—	↑
<i>Occludin</i> expression	—	↑	↑
<i>Galectin-3</i> expression	—	↑	↑
INF- γ secretion	x	—	↑
MIF secretion	x	—	↑
FGF21 secretion	x	↑	↓
INF- β secretion	x	↑	—
Ang1 secretion	x	—	↑
EPO secretion	x	↑	★
Galectin-9 secretion	x	↑	—
Corneal cell death	↑	↑	—

↑ ↓ = vs. controls
 — no changes
 x not investigated
 ★ calculation not possible

Figure 27: **A summary of the results of *ex vivo* incubations of porcine corneas at LH for 12 h, 24 h, and 48 h.**

When the comparison between LH and HH was statistically significant an increase or decrease in each factor was considered. In the case of the Cytokine Antibody Array, when the ratio LH/HH was lower than 0.5 a decrease was considered, or higher than 1.5 an increase was considered. LH: low humidity. HH: high humidity.

Figure published at <https://doi.org/10.3390/ijms23094567> (Netto et al, 2022).

4.5 Treatment with dexamethasone can reverse the effects of low humidity, while hyaluronic acid partially reverses it

To treat DED, artificial tears comprised of hyaluronic acid (HA) to lubricate the cornea, and corticosteroids, such as dexamethasone, to diminish inflammation are commonly used. Artificial tears are prescribed for the

treatment of DED in ophthalmologists' daily routine. Nevertheless, it has been demonstrated that inflammation plays an important role in the pathophysiology of this disease. Therefore, corticosteroids, such as dexamethasone, are used for the treatment of DED, suppressing inflammatory mediators (Pflugfelder, 2004). Prevention of the increase in *NF-κB* mRNA expression in porcine corneas incubated at LH and treated with dexamethasone in comparison to those only incubated at LH was observed in the dry eye model proposed (Figure 15 B). The literature has shown that glucocorticoids act in different pathways to suppress NF-κB (Pflugfelder, 2004; Almawi & Melemedjian, 2002 apud Netto et al., 2022).

Prior studies have established that the use of dexamethasone prevents corneal epithelial damage (Nagelhout et al., 2005). Here, it was shown that treatment with dexamethasone could suppress LH-induced mRNA expression of *occludin* and *galectin-3* (Figure 15 C and D). These facts substantiate the hypothesis that dexamethasone has the potential to reverse the inflammatory response and corneal injury caused by LH in the model proposed (Netto et al., 2022). Hence, the functionality of the DED model proposed was tested. Moreover, similar drugs that are still in the testing phase can be studied with this model, and their action pathways can be analyzed.

The initial course of treatment for DED typically involves the administration of artificial tears due to their ability to alleviate symptoms and enhance the stability of the tear film (Choi et al., 2015). It was observed that porcine corneas incubated at LH and treated with HA exhibited a hindering of increase in the mRNA expression of *occludin* in comparison to the ones incubated at LH (Figure 16 B), which demonstrates that the damage caused by LH might regress with the treatment with HA. The absence of significant difference in *galectin-3* mRNA expression found in the LH + HA group in comparison to the LH group (Figure 16 C) suggests that the effects of the treatment with HA are less prominent than those of the treatment with dexamethasone or that it may require a longer period to yield a more efficacious therapeutic outcome. Consistent with our findings, Meloni et al. reported that in their 24 h *in vitro* dry eye model, only a corticosteroid exhibited the capacity to counteract

the impact of inflammatory genes, whereas artificial tears proved to be ineffective in this regard (Meloni et al., 2011 apud Netto et al., 2022).

Moreover, we noted that porcine corneas treated with HA at LH or HH exhibited an elevated secretion of IL-1 β in comparison to the HH group (Figure 16 A). Previous research has elucidated that low-molecular weight HA has the potential to induce inflammation by upregulating the expression of pro-inflammatory cytokine genes such as IL-1 β (Litwiniuk et al., 2016). Aragona et al. investigated the molecular weight of 18 commercially available artificial tears. Artelac® Splash was identified as having an average molecular weight of 533 kDa and was consequently categorized as medium-molecular weight HA. Eye drops possessing a molecular weight lower than 500 kDa were categorized as low-molecular weight products (Aragona et al., 2019). Considering these findings, we hypothesize that the increased IL-1 β secretion in our model might have been triggered by the eye drops containing HA used in our research (Netto et al., 2022).

Furthermore, we speculate that the augmented secretion of IL-1 β in the samples incubated at LH and treated with dexamethasone or HA was not prevented by these treatments in the porcine model due to the limited duration of 24 h, which may have been insufficient to trigger significant molecular modification of IL-1 β . Nevertheless, notable changes were observed at the transcriptional level, particularly in the case of porcine corneas treated with dexamethasone (Netto et al., 2022). In conclusion, the functionality of the model proposed was tested and confirmed with drugs currently used for the DED treatment, enabling the study of drugs that are still in the testing phase.

4.6 NPs adhere to the epithelial surface of stressed *in vitro* and *ex vivo* models

As mentioned previously, one of the main treatments for DED is the use of lubricating eye drops (Jones et al., 2017). However, these eye drops require multiple applications per day to ensure adequate moistening of the cornea, resulting in reduced compliance. Another disadvantage is the fact that many of

these eye drops can cause blurred vision due to their viscosity. An additional issue is that the short survival time of the drugs on the surface of the eye reduces the efficacy of eye drops (Willem de Vries et al., 2018). Therefore, DNA-nanoparticles (NPs) were tested with the goal of being an alternative to the use of lubricating eye drops.

In previous studies, it was demonstrated that NPs show very good biosafety properties *in vitro* and that kanamycin-loaded NPs present a superior efficacy in comparison to the pristine drug when tested in a pathogenic model (Willem de Vries et al., 2018). In living rats, kanamycin and neomycin-loaded NPs bind to the cornea for 2 h, while pristine antibiotics are not verified on corneas after 5 min (Willem de Vries et al., 2018). Furthermore, it was verified that the NPs increase the adherence time of an anti-glaucoma drug, travoprost, on the ocular surface. Experiments on *in vivo* rat corneas showed that travoprost-loaded NPs are present 60 min after the eye drop application (Schnichels et al., 2020).

Originally, the NPs were developed to be a carrier system that could connect lipophilic or hydrophilic ocular drugs using different loading strategies. Drugs can be incorporated into NPs by means of DNA or RNA aptamers, by means of hydrophobic interactions with the micelle's lipid core, and by covalent bonding with a complementary DNA strand (Willem de Vries et al., 2018). However, in the case of the present work, it was investigated whether pure NPs, without being linked to any drug, could contribute to the treatment of DED.

Therefore, three hypotheses for the possible action of NPs were formulated. The first hypothesis is that, due to its amphiphilic properties, the NP can help to support the aqueous and lipid layer. At concentrations below the critical micelle concentration (CMC), the NPs micelles disintegrate, and the hydrophobic lipid part of the NPs connects to the lipid layer of the tear film, while the hydrophilic part, composed of the DNA strand, connects to the aqueous layer of the tear film.

The second hypothesis is that due to the good water binding capacity of the NPs, it can help to stabilize the tear film. In this case, the NPs above the

CMC form micelles that remain intact after application to the ocular surface, and the hydrophilic corona binds to water molecules.

The third hypothesis is that the NPs may form a protective layer on damaged corneal epithelium. In DED, it occurs loss of cell-cell adhesion and apoptosis in the corneal epithelium (Pflugfelder et al., 2005; Stevenson et al., 2012; Tsubota et al., 2020). In this case, the NPs act by covering the damaged corneal epithelium and preventing more cells from detaching from this tissue.

These three mechanisms described would act reducing the desiccating stress that initiates the inflammatory events in DED. However, the first hypothesis could not be tested in this work because cell culture media are typically hydrophilic, differently from the tear film, that has layers with different polarities. So, here we worked mainly with the second and third hypotheses.

The NPs were first tested on an *in vitro* human corneal tissue (SkinEthic™ HCE) that resembles a corneal epithelium. This is because the *in vitro* corneal tissue is less complex than an entire cornea. The *in vitro* tissue was treated with NP-Atto 488 50 μ M and incubated at extremely low humidity (15%) for 30 min. Therefore, it was verified that the *in vitro* tissue that was treated with NP-Atto 488 and incubated at LH presented mild damage, while the one that received pristine Atto 488 and was submitted to the same humidity condition presented more extensive damage (Figures 17 C and D). Furthermore, it was observed that NP-Atto 488 adhered to the stressed *in vitro* tissue due to the green fluorescence visualized on the tissue's surface (Figure 17 D). This fact led us to think that perhaps the NPs would be protecting the epithelium from damage caused by LH.

To verify if the NPs would attach to the stressed *in vitro* tissue for a longer period, it was treated with NP-Atto 488 50 μ M and incubated at LH (30%) for 24 h. NP-Atto 488 green fluorescence was visualized at the surface of stressed *in vitro* tissue and also on the surface of controls (Figure 18 D). So, it was confirmed that the NPs attached to the stressed tissue's surface up to 24 h after application.

Next, the NPs were tested in the *ex vivo* porcine DED model. In contrast to *in vitro* tissue, which maintained its integrity after treatment with NPs despite

being subjected to LH, porcine corneas treated with NP-Atto 488 50 μ M and incubated at LH for 24 h presented damaged epithelium (Figure 19 D). This fact was also confirmed after analysis of several PAS staining pictures that were graded according to the epithelial integrity. It was demonstrated that porcine corneas treated with NP-Atto 488 and incubated at LH presented an average integrity significantly lower than the ones treated with NP-Atto 488 and incubated at HH and an average integrity not significantly lower than corneas that received Atto 488 and were incubated at HH. Moreover, no difference was observed between corneas incubated with Atto 488 at LH or those treated with NP-Atto 488 and incubated at LH (Figure 19 F). Such a difference between the integrity analysis of *in vitro* human corneal tissue and *ex vivo* porcine model can be attributed to the fact that the number of stressed and treated with NP-Atto 488 samples from the *in vitro* tissue was only two, while from porcine corneas it was five. Another hypothesis is that the NPs couldn't help to maintain the integrity of stressed porcine corneas due to the complexity of the corneal tissue in comparison to the *in vitro* tissue.

However, it was confirmed that the NPs adhered to stressed porcine corneas up to 24 h of incubation at LH, similar to adherence to the *in vitro* human corneal tissue. Such an adherence pattern on porcine corneas was also confirmed with an analysis of the fluorescent area of the pictures of porcine corneas treated with NP-Atto 488 50 μ M and incubated at LH. This area was increased compared to the fluorescent area of samples treated with pristine Atto 488, whose average was close to zero (Figure 19 E).

Compared to previous studies, it was already demonstrated that NPs attach to healthy corneas (Willem de Vries et al., 2018; Schnichels et al., 2021). Willem de Vries et al. detected with ocular fluorophotometry NPs on porcine corneas surface up to 4 h after application, even when the corneas were submitted to washing steps with PBS (Willem de Vries et al., 2018). Here, we showed by means of microscopy that the NPs also adhered to impaired corneas for an extended time period of 24 h.

Hypothesis for the adherence of the NPs to the ocular surface were already discussed in previous studies, and it might occur due to interactions of

the NPs with the mucous layer (Lai et al., 2009) or interactions with cell membranes (Weber et al., 2014; Selden et al., 2012; Willem de Vries et al., 2018).

4.7 NPs prevent apoptosis at *ex vivo* porcine DED model

Previous *in vivo* studies demonstrated that NPs at concentrations of 20 μM and 100 μM administrated once or four times with 1 h between each drop in rat's corneas did not induce apoptosis of corneal cells. Hence, it was confirmed the non-toxic character of the NPs (Willem de Vries et al., 2018). Here, we wanted to check if, additionally, the NPs would prevent cell apoptosis caused by LH. For that, porcine corneas treated with one drop of NP 50 μM were incubated at LH for 24 h. It was observed that these corneas presented a significantly lower percentage of apoptotic cells when compared to the untreated corneas incubated at LH (Figure 20). Therefore, it was concluded that the NPs prevented apoptosis in the *ex vivo* porcine DED model.

This might have happened due to the fact that NPs are able to bind water molecules, reducing the desiccating stress caused by LH. Consequently, the dry eye inflammatory vicious cycle that starts due to desiccating stress and hyperosmolarity of the tear fluid and culminates with cell apoptosis is attenuated. Another hypothesis is that the NPs may form a protective layer on damaged corneal epithelium, also reducing the desiccating stress triggered by LH.

4.8 NPs 100 μM prevent upregulation of *galectin-3* caused by LH

To verify whether the NPs help to prevent inflammation caused by LH, two different concentrations of NPs, 50 μM and 100 μM , were used to treat porcine corneas that were incubated at LH for 24 h. DED inflammatory pathway culminates with the activation of MMP9, which cleaves galectin-3, a glyocalyx

component (Uchino et al., 2015). As we showed previously, *galectin-3* mRNA expression is upregulated in corneas incubated at LH. Therefore, we speculated that mRNA expression *galectin-3* can be interpreted as an early marker that acts as a positive signal to induce its production. In porcine corneas treated with NP 100 μ M and incubated at LH, upregulation in *galectin-3* expression was hindered (Figure 21 A). This indicates that the NPs 100 μ M probably act to prevent at some stage the inflammatory mechanism caused by LH by preventing upregulation of *galectin-3* gene expression. Taking into consideration that we have shown that the NPs adhere to the surface of the corneal epithelium even when subjected to LH, one possible hypothesis may be that the NPs 100 μ M bind to the epithelial glycocalyx preventing the cleavage of *galectin-3*.

IL-8 is a pro-inflammatory cytokine secreted by epithelial cells and macrophages during the innate immune response (Tsubota et al., 2020). Because of that, mRNA expression of *IL-8* was investigated in porcine corneas treated with NPs in two different concentrations, 50 μ M and 100 μ M. An upregulation in *IL-8* gene expression was verified in corneas treated with NPs 50 μ M and incubated at LH in comparison to the ones treated with NPs 100 μ M and incubated at HH. Moreover, in samples treated with 50 μ M NPs or 100 μ M NPs and incubated LH, no significant difference in *IL-8* expression was observed in relation to porcine corneas incubated at LH (Figure 21 B), meaning that 100 μ M NPs and 50 μ M NPs were not able to prevent upregulation of *IL-8*.

To summarize, NPs 50 μ M preserved the epithelium of the *in vitro* tissue incubated at LH but did not preserve the epithelium of porcine corneas incubated at LH. However, in both models, NPs 50 μ M adhered to the corneal epithelium of samples incubated at HH or LH. Moreover, in porcine corneas, NPs 50 μ M prevented apoptosis that would be caused by LH. In addition, it was verified that NPs 100 μ M hindered upregulation of *galectin-3* in comparison to corneas incubated at LH. However, it is important to notice that further studies should be conducted to confirm if the NPs present an anti inflammatory role and to investigate in which exact stage of the DED inflammatory vicious cycle the NPs act.

In conclusion, it can be assumed that the effects described can be either due to the fact that the NPs are able to bind water molecules, maintaining the cornea lubricated and reducing the stress caused by LH that culminates with cell apoptosis or due to the adherence to corneal cells, preventing that more cells detach from the epithelium and suffer apoptosis.

4.9 Corneal cell isolation with the outgrowth method: differences in cell cultures cultured with FBS and without it

Previously in our laboratory, methods for isolation and cultivation of corneal cells were developed, involving isolation of corneal explants and the use of dispase (Yoeruek et al., 2007; Sobolewska et al., 2015). In this research, the outgrowth method was developed as an adaptation to the methods previously used. Limbal explants from porcine corneas were incubated in flasks with a culture medium containing 10% FBS or without FBS. FBS in cell cultures is a source of nutrients, growth factors, and other essential components that are necessary for the survival and growth of cultured cells. Moreover, it has been demonstrated that the use of FBS in corneal cell cultures stimulates the growth of fibroblasts, while low serum conditions induce the growth of keratocytes (McKay et al., 2020).

Regarding the cells cultures isolated with the outgrowth method, after a minimum of four weeks of incubation, it was observed microscopically that cell cultures cultivated without FBS presented cells in a roof tile arrangement that resembled epithelial cells and stellate cells similar to keratocytes. In contrast, cell cultures cultivated with FBS presented in addition to cells morphologically like epithelial cells, cells that formed fibrous-like structures that resembled fibroblasts (Netto et al., 2023).

To confirm the cell types that grew in each culture, immunostaining and qRT-PCR for specific cell markers were performed. CK3 and CK12 are considered specific epithelial cell markers (Kasper et al., 1988). CK3-positive cells were present in both cultures with FBS and without it. Moreover, occludin and ZO-1, which are proteins from epithelial cells' tight junctions, were also

observed in both cultures. *CK12* gene expression was quantified as well, and it was verified an upregulation of this gene in cultures cultivated with FBS in relation to the ones without it (Netto et al., 2023).

To attest the existence of keratocytes, keratocan and lumican were analyzed as they are specific keratocyte markers (Dunlevy et al., 2000). It was observed more keratocan and lumican-positive cells in cultures without FBS. Furthermore, mRNA expression of *keratocan* was upregulated in cultures without FBS (Netto et al., 2023). These facts are in accordance with the literature that already showed that maintaining keratocytes phenotype requires low serum levels (McKay et al., 2020).

Vimentin can be expressed by mesenchymal cells, as keratocytes and fibroblasts, and by undifferentiated epithelial cells (Chaurasia et al., 2009; Castro-Muñozledo et al., 2017). It was observed that in cell cultures cultivated with FBS and without it, vimentin-positive cells were present. This fact was already expected as it was observed with microscopy that the cultures were not pure of corneal epithelial cells (Netto et al., 2023).

CK3, lumican, and keratocan-positive cells were quantified to verify the proportion of different cell types. Cells cultivated without FBS primarily consisted of epithelial cells, some keratocytes, and a small number of other types of cells. Similarly, FBS-cultivated cultures contained mostly epithelial cells, but other cell types, probably fibroblasts, were more prevalent than keratocytes. This corroborates with the hypothesis already discussed previously that the low amount of serum allows the proliferation of keratocytes, while high serum conditions stimulate the proliferation of fibroblasts (McKay et al., 2019; McKay et al., 2020 apud Netto et al., 2023).

An evaluation of the number of cells in each cell culture, with or without FBS, was performed. From the first week of incubation with bovine serum, cultures exhibited a higher cell count that continued to increase even further after two weeks. Compared to the group without serum, the number of counted cells after five weeks was more than five times higher among the serum-cultivated cells (Netto et al., 2023).

Therefore, a major disadvantage of cultivating corneal cells without FBS is that they take a long time to grow and are less numerous. In this culture, however, epithelial cells and keratocytes are more prevalent, and the incidence of fibroblasts is lower. Hence, cells cultured without FBS are more appropriate to simulate healthy corneal tissue conditions, as normal corneal stroma contains more keratocytes, which are activated and differentiated into fibroblasts when injured. On the other hand, cells cultivated with FBS can be used to simulate scarring in corneal tissue by producing a large number of fibroblasts (Netto et al., 2023).

4.10 The outgrowth method provides a mixed cell culture that can be useful in studying toxicology of new ocular drugs

The outgrowth method is fast to be performed, taking about two hours for the corneal explants' isolation, and the explants with the limbal section provide a long-term outgrowth of corneal cells. Moreover, as the culture medium has to be changed directly in the flasks twice a week, this procedure does not take much time, different from if the explants were incubated in well-plates (Netto et al., 2023).

Previously in our laboratory, Yoeruek et al. received corneoscleral rims from the Tübingen Eye Bank and acquired epithelial cells from discoid samples from the limbus after incubation of these samples in dispase dissolved in the medium. Single-cell suspension was then seeded in 24-well plates. Additionally, corneal fibroblasts were prepared by cutting stroma pieces and incubating them with a medium containing collagenase A. Next, the cells were also seeded in 24-well plates (Yoeruek et al., 2007). Sobolewska et al. used a similar method to isolate human corneal epithelial cells by removing small explants from the epithelial layer under a microscope and incubating them with dispase dissolved in a medium with 5% FBS and PS. Cells were seeded in 24-well plates as well (Sobolewska et al., 2015).

In relation to the outgrowth method, it is important to highlight that with this method, more than one corneal cell type is cultured, so a pure culture of

corneal epithelial cells cannot be obtained. In the case that a pure culture of corneal epithelial cells is desired, various techniques can be employed. These techniques include the use of differential trypsinization, density gradient centrifugation, or magnetic bead sorting using specific antibodies against cell surface markers, among others. Incorporating these additional purification steps can effectively enhance the purity of the culture (Okumura et al., 2015; Nakatsu & Deng, 2013; García-Posadas et al., 2013 apud Netto et al., 2023).

Conversely, in certain experimental contexts, a corneal cell culture that is not pure may offer some advantages. *In vivo*, corneal epithelial cells coexist in close proximity with stromal cells, and the interactions between these two cell types play a crucial role in sustaining the health of the cornea. A mixed corneal cell culture may better replicate the *in vivo* environment and offer a more physiologically relevant model for investigating corneal biology. Corneal epithelial cells and stromal cells interact with each other through diverse signaling pathways. A mixed cell culture may facilitate cross-talk between these cell types, thereby offering more precise and informative outcomes in particular experimental contexts (Yu et al., 2010; Joris et al., 2013 apud Netto et al., 2023).

Another limitation of the outgrowth method is that as the cells were isolated from porcine eyes, there is a greater chance of contamination with this method. Hence, to minimize the likelihood of contamination, it is imperative to carry out the complete cellular isolation process under a strictly aseptic environment. This requirement underscores the criticality of maintaining sterile conditions throughout the isolation procedure. Additionally, it is important to notice that despite the similarities between porcine and human eyes (Menduni et al., 2018), interspecies variations do exist (Netto et al., 2023).

In conclusion, the outgrowth method holds promising potential for investigating disorders that result in limbal insufficiency, as the corneal explants are abundant in limbal epithelial stem cells (Bremond-Gignac et al., 2018). Furthermore, the method can also be used to test the toxicology of new ocular drugs *in vitro* (Netto et al., 2023).

4.11 Conclusion

A novel, cheap, and easy-to-reproduce *ex vivo* corneal model for DED is presented. By incubating porcine corneas at 30% humidity and 37 °C, changes similar to the ones found in DED are triggered. It was verified that 24 h incubation is the best time point to stimulate such changes, in comparison to 12 h and 48 h. After treatment with eye drops currently used for DED, HA, and dexamethasone, it was observed that HA was able to partially prevent the effects of incubation at LH, while dexamethasone reduced the effects triggered by LH (Netto et al., 2022).

To treat DED, NPs were tested in the established *ex vivo* porcine dry eye model and in an *in vitro* human corneal tissue. The NPs presented a good adherence profile to both damage models up to 24 h of incubation. Moreover, the NPs showed reduced apoptosis at the *ex vivo* porcine model and reduced mRNA expression of *galectin-3*.

Finally, a method to isolate corneal epithelial cells was established, and the differences of cultivation with FBS and without it were investigated. It was shown that cell cultures cultivated with FBS were more numerous and presented mainly epithelial cells and other cell types, probably fibroblasts, while cultures cultivated without serum were formed mainly of epithelial cells and keratocytes. Therefore, using the outgrowth method, *in vitro* models to study DED can be established, and testing of new drugs for ocular diseases can be performed (Netto et al., 2023).

5 Summary

Dry eye disease (DED) has a prevalence of 5-35% in the general population worldwide. Intrinsic factors such as age, sex steroids imbalance, autoimmune diseases, and extrinsic factors such as refractive surgery, allergy, use of contact lenses, and dry environment contribute to this disease. DED affects both the surface of the eye and the tear film. Therefore, chronic dry eye is characterized by increased osmolarity of the tear film, and it is associated with inflammation of the lacrimal gland and the surface of the eye (Yamaguchi, 2018). To treat DED, the current and most common option includes several daily applications of lubricant eye drops. Nevertheless, these eye drops usually lead to local side effects, including ocular allergies and blurred vision.

To study DED, the development of a robust dry eye model is essential to testing new treatments. Here, an *ex vivo* porcine model of dry eye was established by incubating porcine corneas at low humidity (LH). The model was characterized by histological damage evaluation, epithelial thickness, and relevant dry eye markers such as interleukin 1 beta (IL-1 β), nuclear factor kappa-light-chain-enhancer of activated B cells (NF- κ B), occludin and galectin-3. In the dry eye model proposed, it was verified a rise in the secretion of IL-1 β , along with a mRNA expression upregulation of *NF- κ B*, *occludin*, and *galectin-3*. Furthermore, it was observed a higher apoptosis rate in the dry eye model in comparison to controls (Netto et al., 2022).

Next, eye drops that are currently used to treat DED, composed of hyaluronic acid and dexamethasone, were used to determine if they were therapeutically effective in the established porcine dry eye model. Hence, it was demonstrated that the low humidity-induced effects could be partially reversed with the use of hyaluronic acid eye drops and successfully reversed with treatment with dexamethasone. As a result, the dry eye model proposed simulates the *in vivo* condition and enables animal-free testing of dry eye treatments, as the porcine eyes came from a local abattoir, and the animals were euthanized for nutritional purposes (Netto et al., 2022).

The further step in this research was to evaluate if the DNA-Nanoparticles (NPs), developed initially to function as a drug delivery platform, would also behave as a treatment option for DED. For that, the *ex vivo* porcine dry eye model and an *in vitro* human corneal model were submitted to LH stress and treated with the NPs. Therefore, it was verified that the NPs attached to the stressed *in vitro* and *ex vivo* models up 24 h of incubation at LH, demonstrating their affinity to bind damaged tissue as well. Moreover, the NPs prevented apoptosis caused by LH at the porcine model and hindered mRNA expression upregulation of *galectin-3*. However, the exact mechanisms for an anti-inflammatory role should still be investigated in further research.

The last aim of this project was to improve a method of isolation and cultivation of corneal cells so that *in vitro* models can be established for the study of DED and other corneal diseases. For that, the outgrowth method was defined with the use of porcine corneas that came from a local abattoir. Small explants of the corneal limbus were isolated and cultivated in flasks in two different conditions: with the use of fetal bovine serum (FBS) and without it. It was verified that cultures cultivated with FBS were more numerous and were composed mainly of epithelial cells and other cell types, probably fibroblasts. As for the cultures incubated without FBS, the cells were predominantly epithelial cells and keratocytes. Therefore, cell isolation with the outgrowth method and the use of FBS can be used to study injury processes, while cell isolation and cultivation without FBS can be useful to develop an *in vitro* model similar to healthy corneal conditions (Netto et al., 2023).

In conclusion, important steps for the study of DED were developed with this project, allowing the expansion of knowledge about models for studying DED *ex vivo* and *in vitro*, and a possible new therapy for the disease was investigated.

6 German Summary

Die Prävalenz des Trockenen Auges (DED) liegt in der Allgemeinbevölkerung weltweit bei 5-35%. Intrinsische Faktoren wie Alter, ein Ungleichgewicht der Geschlechtssteroiden, Autoimmunerkrankungen bzw. extrinsische Faktoren wie refraktive Chirurgie, Allergien, Verwendung von Kontaktlinsen oder eine trockene Umgebung tragen zu dieser Krankheit bei. Das DED betrifft sowohl die Augenoberfläche als auch den Tränenfilm. Daher ist das chronisch trockene Auge durch eine erhöhte Osmolarität des Tränenfilms gekennzeichnet und geht mit einer Entzündung der Tränendrüse und der Augenoberfläche einher (Yamaguchi, 2018). Die derzeit gängigste Option zur Behandlung des trockenen Auges ist die mehrmalige tägliche Anwendung von Augentropfen, die als Lubrikationsmittel dienen. Diese Augentropfen führen jedoch in der Regel zu lokalen Nebenwirkungen, wie Augenallergien und verschwommenem Sehen.

Zur Untersuchung der Erkrankung ist die Entwicklung eines robusten Modells unerlässlich, um neue Behandlungen testen zu können. Indem Hornhäute von Schweinen bei niedriger Luftfeuchtigkeit (LH) inkubiert wurden, konnte ein *ex vivo*-Schweinmodell des trockenen Auges etabliert werden. Das Modell ist durch die Bewertung histologischer Schäden, der Epitheldicke und relevanter Marker des trockenen Auges, wie Interleukin 1 beta (IL-1 β), Nuklearfaktor kappa-light-chain-enhancer of activated B cells (NF- κ B), Occludin und Galektin-3 charakterisiert. In dem vorgeschlagenen Modell des trockenen Auges wurde ein Anstieg der Sekretion von IL-1 β nachgewiesen, zusammen mit einer Hochregulierung der mRNA-Expression von *NF- κ B*, *Occludin* und *Galektin-3*. Außerdem wurde im Modell des trockenen Auges im Vergleich zu den Kontrollen eine höhere Apoptoserate beobachtet (Netto et al., 2022).

Anschließend wurden Augentropfen, die derzeit zur Behandlung eingesetzt werden und aus Hyaluronsäure und Dexamethason bestehen, verwendet, um festzustellen, ob sie in dem etablierten Modell des trockenen Auges beim Schwein therapeutisch wirksam sind. So konnte gezeigt werden, dass die durch die niedrige Luftfeuchtigkeit hervorgerufenen Effekte durch die

Verwendung von Hyaluronsäure-Augentropfen teilweise und durch die Behandlung mit Dexamethason erfolgreich rückgängig gemacht werden konnten. Das vorgeschlagene Modell des trockenen Auges simuliert die *in vivo*-Bedingungen und ermöglicht die tierversuchsfreie Untersuchung von Therapieoptionen, da die Schweineaugen aus einem örtlichen Schlachthof stammen und die Tiere zur Fleischversorgung geschlachtet wurden (Netto et al., 2022).

In einem weiteren Schritt wurde untersucht, ob die DNA-Nanopartikel (NPs), die ursprünglich als Plattform für die Verabreichung von Medikamenten entwickelt wurden, auch als Behandlungsoption für das trockene Auge geeignet sind. Zu diesem Zweck wurden das *ex vivo*-Modell des trockenen Auges beim Schwein und ein *in vitro*-Modell der menschlichen Hornhaut einer LH-Belastung ausgesetzt und mit den NPs behandelt. Es konnte nachgewiesen werden, dass die NPs an den gestressten *in vitro*- und *ex vivo*-Modellen bis zu 24 Stunden nach LH-Schädigung anhafteten, was ihre Affinität zu geschädigtem Gewebe beweist. Außerdem verhinderten die NPs die durch LH verursachte Apoptose im Schweinemodell, ebenso wie die Hochregulierung der mRNA-Expression von *Galektin-3*. Die genauen Mechanismen für eine entzündungshemmende Wirkung sollten jedoch in weiteren Forschungen noch untersucht werden.

Das letzte Ziel dieses Projekts war die Verbesserung einer Methode zur Isolierung und Kultivierung von Hornhautzellen, damit *in vitro*-Modelle für die Untersuchung des trockenen Auges und anderen Hornhauterkrankungen erstellt werden können. Zu diesem Zweck wurde die Auswuchs-Methode unter Verwendung von Schweinehornhäuten entwickelt, die aus einem örtlichen Schlachthof stammten. Kleine Explantate des Hornhautlimbus wurden isoliert und in Flaschen unter zwei verschiedenen Bedingungen kultiviert: mit und ohne fötales Rinderserum (FBS). Es wurde festgestellt, dass die mit FBS kultivierten Zellen zahlreicher waren und hauptsächlich aus Epithelzellen und anderen Zelltypen, wahrscheinlich Fibroblasten, bestanden. Bei den Kulturen, die ohne FBS inkubiert wurden, handelte es sich überwiegend um Epithelzellen und Keratozyten. Die Zellisolierung mit der Auswuchs-Methode und die Verwendung von FBS können daher zur Untersuchung von Verletzungsprozessen verwendet

werden, während die Zellisolierung und Kultivierung ohne FBS zur Entwicklung eines *in vitro*-Modells, das den Bedingungen der gesunden Hornhaut ähnelt, nützlich sein kann (Netto et al., 2023).

Zusammengefasst gelang es dem Projekt, wichtige Schritte für eine bessere und praxistauglichere Erforschung des trockenen Auges zu entwickeln, indem die Modelle zur Untersuchung von trockenen Augen *ex vivo* und *in vitro* erweitert wurden, welche als Plattform dienen können, um eine neue Therapie für die Heilung des Syndroms zu entwickeln.

7 Bibliography

- Abri Aghdam, K., Soltan Sanjari, M., & Ghasemi Falavarjani, K. (2016). Erythropoietin in ophthalmology: A literature review. *Journal of current ophthalmology*, 28(1), 5–11. <https://doi.org/10.1016/j.joco.2016.01.008>
- Abu El-Asrar, A. M., Struyf, S., Mohammad, G., Gouwy, M., Rytinx, P., Siddiquei, M. M., Hernández, C., Alam, K., Mousa, A., De Hertogh, G., Opdenakker, G., & Simó, R. (2017). Osteoprotegerin Is a New Regulator of Inflammation and Angiogenesis in Proliferative Diabetic Retinopathy. *Investigative Ophthalmology & Visual Science*, 58(7), 3189–3201. <https://doi.org/10.1167/iovs.16-20993>
- AbuSamra, D. B., & Argüeso, P. (2018). Lectin-Glycan Interactions in Corneal Infection and Inflammation. *Frontiers in Immunology*, 9. <https://www.frontiersin.org/article/10.3389/fimmu.2018.02338>
- Alépée, N., Leblanc, V., Adriaens, E., Grandidier, M. H., Lelièvre, D., Meloni, M., Nardelli, L., Roper, C. S., Santirocco, E., Toner, F., Van Rompay, A., Vinall, J., & Cotovio, J. (2016). Multi-laboratory validation of SkinEthic HCE test method for testing serious eye damage/eye irritation using liquid chemicals. *Toxicology in vitro: An International Journal Published in Association with BIBRA*, 31, 43–53. <https://doi.org/10.1016/j.tiv.2015.11.012>
- Almawi, W. Y., & Melemedjian, O. K. (2002). Negative regulation of nuclear factor-kappaB activation and function by glucocorticoids. *Journal of Molecular Endocrinology*, 28(2), 69–78. <https://doi.org/10.1677/jme.0.0280069>
- Anderson, J. M., & Van Itallie, C. M. (2009). Physiology and Function of the Tight Junction. *Cold Spring Harbor Perspectives in Biology*, 1(2), a002584–a002584. <https://doi.org/10.1101/cshperspect.a002584>
- Aragona, P., Simmons, P. A., Wang, H., & Wang, T. (2019). Physicochemical Properties of Hyaluronic Acid-Based Lubricant Eye Drops. *Translational Vision Science & Technology*, 8(6), 2. <https://doi.org/10.1167/tvst.8.6.2>
- Araújo Filho, A., Salomão, S. R., Berezovsky, A., Cinoto, R. W., Morales, P. H. A., Santos, F. R. G., & Belfort, R. (2008). Prevalence of visual impairment, blindness, ocular disorders and cataract surgery outcomes in low-income elderly from a metropolitan region of São Paulo-Brazil. *Arquivos Brasileiros De Oftalmologia*, 71(2), 246–253. <https://doi.org/10.1590/s0004-27492008000200021>
- Arora, S., Rajwade, J. M., & Paknikar, K. M. (2012). Nanotoxicology and *in vitro* studies: the need of the hour. *Toxicology and applied pharmacology*, 258(2), 151–165. <https://doi.org/10.1016/j.taap.2011.11.010>
- Ban, Y., Cooper, L. J., Fullwood, N. J., Nakamura, T., Tsuzuki, M., Koizumi, N., Dota, A., Mochida, C., & Kinoshita, S. (2003). Comparison of ultrastructure, tight junction-related protein expression and barrier function of human corneal epithelial cells cultivated on amniotic membrane with and without air-lifting. *Experimental Eye Research*, 76(6), 735–743. [https://doi.org/10.1016/S0014-4835\(03\)00033-2](https://doi.org/10.1016/S0014-4835(03)00033-2)

- Barabino, S., & Dana, M. R. (2004). Animal models of dry eye: A critical assessment of opportunities and limitations. *Investigative Ophthalmology & Visual Science*, 45(6), 1641–1646. <https://doi.org/10.1167/iovs.03-1055>
- Barabino, S., Chen, Y., Chauhan, S., & Dana, R. (2012). Ocular surface immunity: homeostatic mechanisms and their disruption in dry eye disease. *Progress in retinal and eye research*, 31(3), 271–285. <https://doi.org/10.1016/j.preteyeres.2012.02.003>
- Bäumli, G. (2008). *Interaktion des humanen Tight Junction Proteins ZO-1 mit dem Ras-Effektor AF6 und Untersuchungen am Zellwandprotein Aga2 von Saccharomyces cerevisiae*. Universität Regensburg
- Benchabane, S., Belkhef, M., Belguendouz, H., Zidi, S., Boudjelida, A., Youinou, P., & Touil-Boukoffa, C. (2018). Interferon- β inhibits inflammatory responses mediators via suppression of iNOS signaling pathway in PBMCs from patients with primary Sjögren's syndrome. *Inflammopharmacology*, 26(5), 1165–1174. <https://doi.org/10.1007/s10787-018-0499-4>
- Bremond-Gignac, D., Copin, H., & Benkhalifa, M. (2018). Corneal epithelial stem cells for corneal injury. *Expert Opinion on Biological Therapy*, 18(9), 997–1003. <https://doi.org/10.1080/14712598.2018.1508443>
- Bron, A. J., de Paiva, C. S., Chauhan, S. K., Bonini, S., Gabison, E. E., Jain, S., Knop, E., Markoulli, M., Ogawa, Y., Perez, V., Uchino, Y., Yokoi, N., Zoukhri, D., & Sullivan, D. A. (2017). TFOS DEWS II pathophysiology report. *The Ocular Surface*, 15(3), 438–510. <https://doi.org/10.1016/j.jtos.2017.05.011>
- Castro-Muñozledo, F., Meza-Aguilar, D. G., Domínguez-Castillo, R., Hernández-Zequinely, V., & Sánchez-Guzmán, E. (2017). Vimentin as a Marker of Early Differentiating, Highly Motile Corneal Epithelial Cells. *Journal of Cellular Physiology*, 232(4), 818–830. <https://doi.org/10.1002/jcp.25487>
- Cavas-Martínez, F., Bataille, L., Fernández-Pacheco, D. G., Cañavate, F. J. F., & Alió, J. L. (2017). A new approach to keratoconus detection based on corneal morphogeometric analysis. *PLoS ONE*, 12(9), e0184569. <https://doi.org/10.1371/journal.pone.0184569>
- Chan, K. Y., Cho, P., & Boost, M. (2014). Corneal epithelial cell viability of an ex vivo porcine eye model. *Clinical & experimental optometry*, 97(4), 337–340. <https://doi.org/10.1111/cxo.12128>
- Chaurasia, S. S., Kaur, H., de Medeiros, F. W., Smith, S. D., & Wilson, S. E. (2009). Dynamics of the expression of intermediate filaments vimentin and desmin during myofibroblast differentiation after corneal injury. *Experimental Eye Research*, 89(2), 133–139. <https://doi.org/10.1016/j.exer.2009.02.022>
- Chen, W., Zhang, X., Zhang, J., Chen, J., Wang, S., Wang, Q., & Qu, J. (2008). A murine model of dry eye induced by an intelligently controlled environmental system. *Investigative Ophthalmology & Visual Science*, 49(4), 1386–1391. <https://doi.org/10.1167/iovs.07-0744>
- Chen, Y. S., Hung, Y. C., Liao, I., & Huang, G. S. (2009). Assessment of the *In vivo* Toxicity of Gold Nanoparticles. *Nanoscale research letters*, 4(8), 858–864. <https://doi.org/10.1007/s11671-009-9334-6>

- Chen, M., Bao, L., Zhao, M., Cao, J., & Zheng, H. (2020). Progress in Research on the Role of FGF in the Formation and Treatment of Corneal Neovascularization. *Frontiers in Pharmacology*, 11. <https://www.frontiersin.org/article/10.3389/fphar.2020.00111>
- Chi, W., Hua, X., Chen, X., Bian, F., Yuan, X., Zhang, L., Wang, X., Chen, D., Deng, R., Li, Z., Liu, Y., de Paiva, C. S., Pflugfelder, S. C., & Li, D.-Q. (2017). Mitochondrial DNA Oxidation Induces Imbalanced Activity of NLRP3/NLRP6 Inflammasomes by Activation of Caspase-8 and BRCC36 in Dry Eye. *Journal of Autoimmunity*, 80, 65–76. <https://doi.org/10.1016/j.jaut.2017.02.006>
- Choi, J. H., Kim, J. H., Li, Z., Oh, H. J., Ahn, K. Y., & Yoon, K. C. (2015). Efficacy of the Mineral Oil and Hyaluronic Acid Mixture Eye Drops in Murine Dry Eye. *Korean Journal of Ophthalmology*, 29(2), 131. <https://doi.org/10.3341/kjo.2015.29.2.131>
- Choy, E. P. Y., Cho, P., Benzie, I. F. F., Choy, C. K. M., & To, T. S. S. (2004). A novel porcine dry eye model system (pDEM) with simulated lacrimation/blinking system: Preliminary findings on system variability and effect of corneal drying. *Current Eye Research*, 28(5), 319–325. <https://doi.org/10.1076/ceyr.28.5.319.28681>
- Choy, E. P. Y., To, T. S. S., Cho, P., Benzie, I. F. F., & Choy, C. K. M. (2004). Viability of porcine corneal epithelium ex vivo and effect of exposure to air: A pilot study for a dry eye model. *Cornea*, 23(7), 715–719. <https://doi.org/10.1097/01.icc.0000127475.29551.56>
- Choy, E. P. Y., Cho, P., Benzie, I. F. F., & Choy, C. K. M. (2006). Investigation of corneal effect of different types of artificial tears in a simulated dry eye condition using a novel porcine dry eye model (pDEM). *Cornea*, 25(10), 1200–1204. <https://doi.org/10.1097/01.icc.0000243960.14651.95>
- Choy, E. P. Y., Cho, P., Benzie, I. F. F., & Choy, C. K. M. (2008). Dry eye and blink rate simulation with a pig eye model. *Optometry and Vision Science: Official Publication of the American Academy of Optometry*, 85(2), 129–134. <https://doi.org/10.1097/OPX.0b013e31816225ed>
- Contreras-Ruiz, L., Schulze, U., García-Posadas, L., Arranz-Valsero, I., López-García, A., Paulsen, F., & Diebold, Y. (2012). Structural and functional alteration of corneal epithelial barrier under inflammatory conditions. *Current Eye Research*, 37(11), 971–981. <https://doi.org/10.3109/02713683.2012.700756>
- Corrales, R. M., Stern, M. E., De Paiva, C. S., Welch, J., Li, D.-Q., & Pflugfelder, S. C. (2006). Desiccating stress stimulates expression of matrix metalloproteinases by the corneal epithelium. *Investigative Ophthalmology & Visual Science*, 47(8), 3293–3302. <https://doi.org/10.1167/iovs.05-1382>
- Davies N. M. (2000). Biopharmaceutical considerations in topical ocular drug delivery. *Clinical and experimental pharmacology & physiology*, 27(7), 558–562. <https://doi.org/10.1046/j.1440-1681.2000.03288.x>
- DelMonte, D. W., & Kim, T. (2011). Anatomy and physiology of the cornea. *Journal of Cataract & Refractive Surgery*, 37(3), 588–598. <https://doi.org/10.1016/j.jcrs.2010.12.037>
- De Paiva, C. S., Corrales, R. M., Villarreal, A. L., Farley, W. J., Li, D.-Q., Stern, M. E., & Pflugfelder, S. C. (2006). Corticosteroid and doxycycline suppress MMP-9 and inflammatory cytokine expression, MAPK activation in the corneal epithelium in experimental dry eye. *Experimental Eye Research*, 83(3), 526–535. <https://doi.org/10.1016/j.exer.2006.02.004>

- De Paiva, C. S., Pangelinan, S. B., Chang, E., Yoon, K. C., Farley, W. J., Li, D. Q., & Pflugfelder, S. C. (2009). Essential role for c-Jun N-terminal kinase 2 in corneal epithelial response to desiccating stress. *Archives of ophthalmology (Chicago, Ill. : 1960)*, *127*(12), 1625–1631. <https://doi.org/10.1001/archophthalmol.2009.316>
- Dohlman, T. H., Ding, J., Dana, R., & Chauhan, S. K. (2017). T Cell-Derived Granulocyte-Macrophage Colony-Stimulating Factor Contributes to Dry Eye Disease Pathogenesis by Promoting CD11b+ Myeloid Cell Maturation and Migration. *Investigative Ophthalmology & Visual Science*, *58*(2), 1330–1336. <https://doi.org/10.1167/iovs.16-20789>
- Dua, H. S., & Azuara-Blanco, A. (2000). Limbal Stem Cells of the Corneal Epithelium. *Survey of Ophthalmology*, *44*(5), 415–425. [https://doi.org/10.1016/S0039-6257\(00\)00109-0](https://doi.org/10.1016/S0039-6257(00)00109-0)
- Dua, H. S., Faraj, L. A., Said, D. G., Gray, T., & Lowe, J. (2013). Human corneal anatomy redefined: A novel pre-Descemet's layer (Dua's layer). *Ophthalmology*, *120*(9), 1778–1785. <https://doi.org/10.1016/j.ophtha.2013.01.018>
- Dunlevy, J. R., Beales, M. P., Berryhill, B. L., Cornuet, P. K., & Hassell, J. R. (2000). Expression of the Keratan Sulfate Proteoglycans Lumican, Keratocan and Osteoglycin/Mimecan During Chick Corneal Development. *Experimental Eye Research*, *70*(3), 349–362. <https://doi.org/10.1006/exer.1999.0789>
- Dursun, D., Wang, M., Monroy, D., Li, D. Q., Lokeshwar, B. L., Stern, M. E., & Pflugfelder, S. C. (2002). A mouse model of keratoconjunctivitis sicca. *Investigative ophthalmology & visual science*, *43*(3), 632–638.
- Enríquez-de-Salamanca, A., Castellanos, E., Stern, M. E., Fernández, I., Carreño, E., García-Vázquez, C., Herreras, J. M., & Calonge, M. (2010). Tear cytokine and chemokine analysis and clinical correlations in evaporative-type dry eye disease. *Molecular Vision*, *16*, 862–873.
- Espana, E. M., He, H., Kawakita, T., Di Pascuale, M. A., Raju, V. K., Liu, C.-Y., & Tseng, S. C. G. (2003). Human Keratocytes Cultured on Amniotic Membrane Stroma Preserve Morphology and Express Keratocan. *Investigative Ophthalmology & Visual Science*, *44*(12), 5136–5141. <https://doi.org/10.1167/iovs.03-0484>
- Fujihara, T., Nagano, T., Nakamura, M., & Shirasawa, E. (1995). Establishment of a rabbit short-term dry eye model. *Journal of Ocular Pharmacology and Therapeutics: The Official Journal of the Association for Ocular Pharmacology and Therapeutics*, *11*(4), 503–508. <https://doi.org/10.1089/jop.1995.11.503>
- Fukuda, K. (2020). Corneal fibroblasts: Function and markers. *Experimental Eye Research*, *200*, 108229. <https://doi.org/10.1016/j.exer.2020.108229>
- García-Posadas, L., Arranz-Valsero, I., López-García, A., Soriano-Romaní, L., & Diebold, Y. (2013). A new human primary epithelial cell culture model to study conjunctival inflammation. *Investigative Ophthalmology & Visual Science*, *54*(10), 7143–7152. <https://doi.org/10.1167/iovs.13-12866>
- Gilbard, J. P., Carter, J. B., Sang, D. N., Refojo, M. F., Hanninen, L. A., & Kenyon, K. R. (1984). Morphologic effect of hyperosmolarity on rabbit corneal epithelium. *Ophthalmology*, *91*(10), 1205–1212.

- Gilbard, J. P., Rossi, S. R., & Heyda, K. G. (1989). Tear film and ocular surface changes after closure of the meibomian gland orifices in the rabbit. *Ophthalmology*, *96*(8), 1180–1186. [https://doi.org/10.1016/s0161-6420\(89\)32753-9](https://doi.org/10.1016/s0161-6420(89)32753-9)
- Gipson, I. K. (2007). The Ocular Surface: The Challenge to Enable and Protect Vision: The Friedenwald Lecture. *Investigative Ophthalmology & Visual Science*, *48*(10), 4391. <https://doi.org/10.1167/iovs.07-0770>
- Hamrah, P., Sahin, A., Dastjerdi, M. H., Shahatit, B. M., Bayhan, H. A., Dana, R., & Pavan-Langston, D. (2015). *In vivo* Confocal Microscopic Changes of the Corneal Epithelium and Stroma in Patients With Herpes Zoster Ophthalmicus. *American Journal of Ophthalmology*, *159*(6), 1036-1044.e1. <https://doi.org/10.1016/j.ajo.2015.03.003>
- Hasegawa, T., Amako, H., Yamamoto, T., Tazawa, M., & Sakamoto, Y. (2014). Corneal-protective effects of an artificial tear containing sodium hyaluronate and castor oil on a porcine short-term dry eye model. *The Journal of Veterinary Medical Science*, *76*(9), 1219–1224. <https://doi.org/10.1292/jvms.14-0143>
- Hermann, M. M., Bron, A. M., Creuzot-Garcher, C. P., & Diestelhorst, M. (2011). Measurement of adherence to brimonidine therapy for glaucoma using electronic monitoring. *Journal of Glaucoma*, *20*(8), 502–508. <https://doi.org/10.1097/IJG.0b013e3181f3eb4a>
- Huet, E., Vallée, B., Delbé, J., Mourah, S., Prulière-Escabasse, V., Tremouilleres, M., Kadomatsu, K., Doan, S., Baudouin, C., Menashi, S., & Gabison, E. E. (2011). EMMPRIN modulates epithelial barrier function through a MMP-mediated occludin cleavage: Implications in dry eye disease. *The American Journal of Pathology*, *179*(3), 1278–1286. <https://doi.org/10.1016/j.ajpath.2011.05.036>
- Hurst, J., Mueller-Buehl, A. M., Hofmann, L., Kuehn, S., Herms, F., Schnichels, S., & Joachim, S. C. (2020). iNOS-inhibitor driven neuroprotection in a porcine retina organ culture model. *Journal of Cellular and Molecular Medicine*, *24*(7), 4312–4323. <https://doi.org/10.1111/jcmm.15091>
- Jackson, D. C., Zeng, W., Wong, C. Y., Mifsud, E. J., Williamson, N. A., Ang, C.-S., Vingrys, A. J., & Downie, L. E. (2016). Tear Interferon-Gamma as a Biomarker for Evaporative Dry Eye Disease. *Investigative Ophthalmology & Visual Science*, *57*(11), 4824–4830. <https://doi.org/10.1167/iovs.16-19757>
- Javadi, M.-A., & Feizi, S. (2011). Dry eye syndrome. *Journal of Ophthalmic & Vision Research*, *6*(3), 192–198.
- Jones, L., Downie, L. E., Korb, D., Benitez-Del-Castillo, J. M., Dana, R., Deng, S. X., Dong, P. N., Geerling, G., Hida, R. Y., Liu, Y., Seo, K. Y., Tauber, J., Wakamatsu, T. H., Xu, J., Wolffsohn, J. S., & Craig, J. P. (2017). TFOS DEWS II Management and Therapy Report. *The Ocular Surface*, *15*(3), 575–628. <https://doi.org/10.1016/j.jtos.2017.05.006>
- Joris, F., Manshian, B. B., Peynshaert, K., Smedt, S. C. D., Braeckmans, K., & Soenen, S. J. (2013). Assessing nanoparticle toxicity in cell-based assays: Influence of cell culture parameters and optimized models for bridging the *in vitro*–*in vivo* gap. *Chemical Society Reviews*, *42*(21), 8339–8359. <https://doi.org/10.1039/C3CS60145E>
- Kasper, M., Moll, R., Stosiek, P., & Karsten, U. (1988). Patterns of cytokeratin and vimentin expression in the human eye. *Histochemistry*, *89*(4), 369–377. <https://doi.org/10.1007/BF00500639>

- Kather, J. N., Friedrich, J., Woik, N., Sticht, C., Gretz, N., Hammes, H.-P., & Kroll, J. (2014). Angiopoietin-1 Is Regulated by miR-204 and Contributes to Corneal Neovascularization in KLEIP-Deficient Mice. *Investigative Ophthalmology & Visual Science*, *55*(7), 4295–4303. <https://doi.org/10.1167/iovs.13-13619>
- Kels, B. D., Grzybowski, A., & Grant-Kels, J. M. (2015). Human ocular anatomy. *Clinics in Dermatology*, *33*(2), 140–146. <https://doi.org/10.1016/j.clindermatol.2014.10.006>
- Kinoshita, S., Koizumi, N., Ueno, M., Okumura, N., Imai, K., Tanaka, H., Yamamoto, Y., Nakamura, T., Inatomi, T., Bush, J., Toda, M., Hagiya, M., Yokota, I., Teramukai, S., Sotozono, C., & Hamuro, J. (2018). Injection of Cultured Cells with a ROCK Inhibitor for Bullous Keratopathy. *New England Journal of Medicine*, *378*(11), 995–1003. <https://doi.org/10.1056/NEJMoa1712770>
- Lai, S. K., Wang, Y.-Y., & Hanes, J. (2009). Mucus-penetrating nanoparticles for drug and gene delivery to mucosal tissues. *Advanced Drug Delivery Reviews*, *61*(2), 158–171. <https://doi.org/10.1016/j.addr.2008.11.002>
- Lemp, M. A., & Foulks, G. N. (2007). The definition and classification of dry eye disease. *Ocul Surf*, *5*(2), 75–92.
- Leong, Y.-Y., & Tong, L. (2015). Barrier Function in the Ocular Surface: From Conventional Paradigms to New Opportunities. *The Ocular Surface*, *13*(2), 103–109. <https://doi.org/10.1016/j.jtos.2014.10.003>
- Li, D.-Q., Chen, Z., Song, X. J., Farley, W., & Pflugfelder, S. C. (2002). Hyperosmolarity Stimulates Production of MMP-9, IL-1 β and TNF- by Human Corneal Epithelial Cells Via a c-Jun NH2-terminal Kinase Pathway. *Investigative Ophthalmology & Visual Science*, *43*(13), 1981–1981.
- Litwiniuk, M., Krejner, A., Speyrer, M. S., Gauto, A. R., & Grzela, T. (2016). Hyaluronic Acid in Inflammation and Tissue Regeneration. *Wounds: A Compendium of Clinical Research and Practice*, *28*(3), 78–88.
- Liu, C., Song, Y., Wang, X., Lai, Z., Li, C., Wan, P., Xu, N., Huang, D., Liu, Y., & Wang, Z. (2020). The Key Role of VEGF in the Cross Talk between Pterygium and Dry Eye and Its Clinical Significance. *Ophthalmic Research*, *63*(3), 320–331. <https://doi.org/10.1159/000503636>
- Luetteke, N. C., & Lee, D. C. (1990). Transforming growth factor alpha: Expression, regulation and biological action of its integral membrane precursor. *Seminars in Cancer Biology*, *1*(4), 265–275
- McKay, T. B., Karamichos, D., Hutcheon, A. E. K., Guo, X., & Zieske, J. D. (2019). Corneal Epithelial–Stromal Fibroblast Constructs to Study Cell–Cell Communication *in vitro*. *Bioengineering*, *6*(4), 110. <https://doi.org/10.3390/bioengineering6040110>
- McKay, T. B., Guo, X., Hutcheon, A. E. K., Karamichos, D., & Ciolino, J. B. (2020). Methods for Investigating Corneal Cell Interactions and Extracellular Vesicles *In vitro*. *Current Protocols in Cell Biology*, *89*(1), e114. <https://doi.org/10.1002/cpcb.114>
- Meloni, M., Pauly, A., Servi, B. D., Varlet, B. L., & Baudouin, C. (2010). Occludin gene expression as an early *in vitro* sign for mild eye irritation assessment. *Toxicology in vitro*, *24*(1), 276–285. <https://doi.org/10.1016/j.tiv.2009.08.016>

- Meloni, M., De Servi, B., Marasco, D., & Del Prete, S. (2011). Molecular mechanism of ocular surface damage: Application to an *in vitro* dry eye model on human corneal epithelium. *Molecular Vision*, *17*, 113–126.
- Menduni, F., Davies, L. N., Madrid-Costa, D., Fratini, A., & Wolffsohn, J. S. (2018). Characterisation of the porcine eyeball as an in-vitro model for dry eye. *Contact Lens & Anterior Eye: The Journal of the British Contact Lens Association*, *41*(1), 13–17. <https://doi.org/10.1016/j.clae.2017.09.003>
- Milner, M. S., Beckman, K. A., Luchs, J. I., Allen, Q. B., Awdeh, R. M., Berdahl, J., Boland, T. S., Buznego, C., Gira, J. P., Goldberg, D. F., Goldman, D., Goyal, R. K., Jackson, M. A., Katz, J., Kim, T., Majmudar, P. A., Malhotra, R. P., McDonald, M. B., Rajpal, R. K., ... Yeu, E. (2017). Dysfunctional tear syndrome: Dry eye disease and associated tear film disorders - new strategies for diagnosis and treatment. *Current Opinion in Ophthalmology*, *27* Suppl 1(Suppl 1), 3–47. <https://doi.org/10.1097/01.icu.0000512373.81749.b7>
- Na, K.-S., Mok, J.-W., Kim, J. Y., Rho, C. R., & Joo, C.-K. (2012). Correlations between Tear Cytokines, Chemokines, and Soluble Receptors and Clinical Severity of Dry Eye Disease. *Investigative Ophthalmology & Visual Science*, *53*(9), 5443–5450. <https://doi.org/10.1167/iovs.11-9417>
- Nagelhout, T. J., Gamache, D. A., Roberts, L., Brady, M. T., & Yanni, J. M. (2005). Preservation of tear film integrity and inhibition of corneal injury by dexamethasone in a rabbit model of lacrimal gland inflammation-induced dry eye. *Journal of Ocular Pharmacology and Therapeutics: The Official Journal of the Association for Ocular Pharmacology and Therapeutics*, *21*(2), 139–148. <https://doi.org/10.1089/jop.2005.21.139>
- Nakatsu, M. N., & Deng, S. X. (2013). Enrichment of human corneal epithelial stem/progenitor cells by magnetic bead sorting using SSEA4 as a negative marker. *Methods in Molecular Biology (Clifton, N.J.)*, *1014*, 71–77. https://doi.org/10.1007/978-1-62703-432-6_5
- Nelson, J. D., Craig, J. P., Akpek, E. K., Azar, D. T., Belmonte, C., Bron, A. J., Clayton, J. A., Dogru, M., Dua, H. S., Foulks, G. N., Gomes, J. A. P., Hammitt, K. M., Holopainen, J., Jones, L., Joo, C.-K., Liu, Z., Nichols, J. J., Nichols, K. K., Novack, G. D., ... Sullivan, D. A. (2017). TFOS DEWS II Introduction. *The Ocular Surface*, *15*(3), 269–275. <https://doi.org/10.1016/j.jtos.2017.05.005>
- Netto, A. R. T., Hurst, J., Bartz-Schmidt, K.-U., & Schnichels, S. (2022). Porcine Corneas Incubated at Low Humidity Present Characteristic Features Found in Dry Eye Disease. *International Journal of Molecular Sciences*, *23*(9), Article 9. <https://doi.org/10.3390/ijms23094567>
- Netto, A. R. T., Hrusa, M. D., Bartz-Schmidt, K.-U., Schnichels, S., & Hurst, J. (2023). Two Methods for the Isolation and Cultivation of Porcine Primary Corneal Cells. *Methods and Protocols*, *6*(3), 50. <https://doi.org/10.3390/mps6030050>
- Okanobo, A., Chauhan, S. K., Dastjerdi, M. H., Kodati, S., & Dana, R. (2012). Efficacy of topical blockade of interleukin-1 in experimental dry eye disease. *American Journal of Ophthalmology*, *154*(1), 63–71. <https://doi.org/10.1016/j.ajo.2012.01.034>
- Okumura, N., Kusakabe, A., Hirano, H., Inoue, R., Okazaki, Y., Nakano, S., Kinoshita, S., & Koizumi, N. (2015). Density-gradient centrifugation enables the purification of cultured corneal endothelial cells for cell therapy by eliminating senescent cells. *Scientific Reports*, *5*, 15005. <https://doi.org/10.1038/srep15005>

- Ong Tone, S., Kocaba, V., Böhm, M., Wylegala, A., White, T. L., & Jurkunas, U. V. (2021). Fuchs endothelial corneal dystrophy: The vicious cycle of Fuchs pathogenesis. *Progress in Retinal and Eye Research*, 80, 100863. <https://doi.org/10.1016/j.preteyeres.2020.100863>
- Pan, H.-F., Li, X.-P., Zheng, S. G., & Ye, D.-Q. (2013). Emerging role of Interleukin-22 in autoimmune diseases. *Cytokine & Growth Factor Reviews*, 24(1), 51–57. <https://doi.org/10.1016/j.cytogfr.2012.07.002>
- Park, C. Y., Zhuang, W., Lekhanont, K., Zhang, C., Cano, M., Lee, W.-S., Gehlbach, P. L., & Chuck, R. S. (2007). Lacrimal gland inflammatory cytokine gene expression in the botulinum toxin B-induced murine dry eye model. *Molecular Vision*, 13, 2222–2232.
- Park, B., Jo, K., Lee, T. G., Hyun, S.-W., Kim, J. S., & Kim, C.-S. (2019). Polydatin Inhibits NLRP3 Inflammasome in Dry Eye Disease by Attenuating Oxidative Stress and Inhibiting the NF-κB Pathway. *Nutrients*, 11(11), 2792. <https://doi.org/10.3390/nu11112792>
- Pelegriño, F. S. A., Pflugfelder, S. C., & De Paiva, C. S. (2012). Low humidity environmental challenge causes barrier disruption and cornification of the mouse corneal epithelium via a c-jun N-terminal kinase 2 (JNK2) pathway. *Experimental Eye Research*, 94(1), 150–156. <https://doi.org/10.1016/j.exer.2011.11.022>
- Pflugfelder, S. C. (2004). Antiinflammatory therapy for dry eye. *American Journal of Ophthalmology*, 137(2), 337–342. <https://doi.org/10.1016/j.ajo.2003.10.036>
- Pflugfelder, S. C., de Paiva, C. S., Tong, L., Luo, L., Stern, M. E., & Li, D. Q. (2005). Stress-activated protein kinase signaling pathways in dry eye and ocular surface disease. *The ocular surface*, 3(4 Suppl), S154–S157. [https://doi.org/10.1016/s1542-0124\(12\)70244-6](https://doi.org/10.1016/s1542-0124(12)70244-6)
- Pflugfelder, S. C., & de Paiva, C. S. (2017). The Pathophysiology of Dry Eye Disease: What We Know and Future Directions for Research. *Ophthalmology*, 124(11S), S4–S13. <https://doi.org/10.1016/j.ophtha.2017.07.010>
- Porth, J. M., Erin Deiotte, Dunn, M., & Bashshur, R. (2019). A Review of the Literature on the Global Epidemiology of Corneal Blindness. *Cornea*, 38(12), 1602–1609. <https://doi.org/10.1097/ICO.0000000000002122>
- Rajalakshmy, A. R., Malathi, J., & Madhavan, H. N. (2014). HCV core and NS3 proteins mediate toll like receptor induced innate immune response in corneal epithelium. *Experimental eye research*, 128, 117–128. <https://doi.org/10.1016/j.exer.2014.09.011>
- Ramadhani, A. M., Derrick, T., Holland, M. J., & Burton, M. J. (2016). Blinding Trachoma: Systematic Review of Rates and Risk Factors for Progressive Disease. *PLOS Neglected Tropical Diseases*, 10(8), e0004859. <https://doi.org/10.1371/journal.pntd.0004859>
- Robin, A. L., & Muir, K. W. (2019). Medication adherence in patients with ocular hypertension or glaucoma. *Expert Review of Ophthalmology*, 14:4-5, 199-210, DOI: <https://doi.org/10.1080/17469899.2019.1635456>
- Roda, M., Corazza, I., BacchiReggiani, M. L., Pellegrini, M., Taroni, L., Giannaccare, G., & Versura, P. (2020). Dry Eye Disease and Tear Cytokine Levels—A Meta-Analysis. *International Journal of Molecular Sciences*, 21(9), Article 9. <https://doi.org/10.3390/ijms21093111>

- Rouen, P. A., & White, M. L. (2018). Dry Eye Disease: Prevalence, Assessment, and Management. *Home Healthcare Now*, 36(2), 74–83. <https://doi.org/10.1097/NHH.0000000000000652>
- Santodomingo-Rubido, J., Carracedo, G., Suzaki, A., Villa-Collar, C., Vincent, S. J., & Wolffsohn, J. S. (2022). Keratoconus: An updated review. *Contact Lens & Anterior Eye: The Journal of the British Contact Lens Association*, 45(3), 101559. <https://doi.org/10.1016/j.clae.2021.101559>
- Schrage, N., Frentz, M., & Spoeler, F. (2012). The Ex Vivo Eye Irritation Test (EVEIT) in evaluation of artificial tears: Purite-preserved versus unpreserved eye drops. *Graefes archive for clinical and experimental ophthalmology = Albrecht von Graefes Archiv fur klinische und experimentelle Ophthalmologie*, 250(9), 1333–1340. <https://doi.org/10.1007/s00417-012-1999-3>
- Schlötzer-Schrehardt, U., & Kruse, F. E. (2005). Identification and characterization of limbal stem cells. *Experimental Eye Research*, 81(3), 247–264. <https://doi.org/10.1016/j.exer.2005.02.016>
- Schnichels, S., Dorfi, T., Schultheiss, M., Arango-Gonzalez, B., Bartz-Schmidt, K. U., Januschowski, K., Spitzer, M. S., & Ziemssen, F. (2016). Ex-vivo-examination of ultrastructural changes in organotypic retina culture using near-infrared imaging and optical coherence tomography. *Experimental eye research*, 147, 31–36. <https://doi.org/10.1016/j.exer.2016.04.011>
- Schnichels, S., Hurst, J., de Vries, J. W., Ullah, S., Gruszka, A., Kwak, M., Löscher, M., Dammeier, S., Bartz-Schmidt, K.-U., Spitzer, M. S., & Herrmann, A. (2020). Self-assembled DNA nanoparticles loaded with travoprost for glaucoma-treatment. *Nanomedicine: Nanotechnology, Biology, and Medicine*, 29, 102260. <https://doi.org/10.1016/j.nano.2020.102260>
- Schnichels, S., Hurst, J., de Vries, J. W., Ullah, S., Fröβl, K., Gruszka, A., Löscher, M., Bartz-Schmidt, K.-U., Spitzer, M. S., & Herrmann, A. (2021). Improved Treatment Options for Glaucoma with Brimonidine-Loaded Lipid DNA Nanoparticles. *ACS Applied Materials & Interfaces*, 13(8), 9445–9456. <https://doi.org/10.1021/acsami.0c18626>
- Selden, N. S., Todhunter, M. E., Jee, N. Y., Liu, J. S., Broaders, K. E., & Gartner, Z. J. (2012). Chemically programmed cell adhesion with membrane-anchored oligonucleotides. *Journal of the American Chemical Society*, 134(2), 765–768. <https://doi.org/10.1021/ja2080949>
- Sendon-Lago, J., Seoane, S., Martinez-Ordoñez, A., Eiro, N., Saa, J., Vizoso, F. J., Gonzalez, F., Perez-Fernandez, R., & Bermudez, M. A. (2019). Corneal regeneration by conditioned medium of human uterine cervical stem cells is mediated by TIMP-1 and TIMP-2. *Experimental Eye Research*, 180, 110–121. <https://doi.org/10.1016/j.exer.2018.12.004>
- Shi, L., Stachon, T., Käsmann-Kellner, B., Seitz, B., Szentmáry, N., & Latta, L. (2020). Keratin 12 mRNA expression could serve as an early corneal marker for limbal explant cultures. *Cytotechnology*, 72(2), 239–245. <https://doi.org/10.1007/s10616-020-00373-z>
- Smith, J. (2007). The epidemiology of dry eye disease. *Acta Ophthalmologica Scandinavica*, 85(s240), 0–0. <https://doi.org/10.1111/j.1600-0420.2007.01063.2858.x>
- Snell, R., & Lemp, M. (1998). *Clinical Anatomy of the eye* (Second). Blackwell Science.

- Sobolewska, B., Guerel, G., Hofmann, J., Tarek, B., Bartz-Schmidt, K.-U., & Yoeruek, E. (2015). Cytotoxic Effect of Voriconazole on Human Corneal Epithelial Cells. *Ophthalmic Research*, 54(1), 41–47. <https://doi.org/10.1159/000371712>
- Solomon, A., Dursun, D., Liu, Z., Xie, Y., Macri, A., & Pflugfelder, S. C. (2001). Pro- and anti-inflammatory forms of interleukin-1 in the tear fluid and conjunctiva of patients with dry-eye disease. *Investigative Ophthalmology & Visual Science*, 42(10), 2283–2292.
- Sridhar M. S. (2018). Anatomy of cornea and ocular surface. *Indian journal of ophthalmology*, 66(2), 190–194. https://doi.org/10.4103/ijo.IJO_646_17
- Stapleton, F., Alves, M., Bunya, V. Y., Jalbert, I., Lekhanont, K., Malet, F., Na, K.-S., Schaumberg, D., Uchino, M., Vehof, J., Viso, E., Vitale, S., & Jones, L. (2017). TFOS DEWS II Epidemiology Report. *The Ocular Surface*, 15(3), 334–365. <https://doi.org/10.1016/j.its.2017.05.003>
- Stevenson, W., Chauhan, S. K., & Dana, R. (2012). Dry eye disease: An immune-mediated ocular surface disorder. *Archives of Ophthalmology (Chicago, Ill.: 1960)*, 130(1), 90–100. <https://doi.org/10.1001/archophthamol.2011.364>
- Subasinghe, S. K., Ogbuehi, K. C., Mitchell, L., & Dias, G. J. (2021). Animal model with structural similarity to human corneal collagen fibrillar arrangement. *Anatomical Science International*, 96(2), 286–293. <https://doi.org/10.1007/s12565-020-00590-8>
- Takahashi, M., Ishimaru, N., Yanagi, K., Haneji, N., Saito, I., & Hayashi, Y. (1997). High incidence of autoimmune dacryoadenitis in male non-obese diabetic (NOD) mice depending on sex steroid. *Clinical and Experimental Immunology*, 109(3), 555–561. <https://doi.org/10.1046/j.1365-2249.1997.4691368.x>
- Tsubota, K., Pflugfelder, S. C., Liu, Z., Baudouin, C., Kim, H. M., Messmer, E. M., Kruse, F., Liang, L., Carreno-Galeano, J. T., Rolando, M., Yokoi, N., Kinoshita, S., & Dana, R. (2020). Defining Dry Eye from a Clinical Perspective. *International Journal of Molecular Sciences*, 21(23), 9271. <https://doi.org/10.3390/ijms21239271>
- Uchino, Y., Mauris, J., Woodward, A. M., Dieckow, J., Amparo, F., Dana, R., Mantelli, F., & Argüeso, P. (2015). Alteration of *galectin-3* in tears of patients with dry eye disease. *American Journal of Ophthalmology*, 159(6), 1027-1035.e3. <https://doi.org/10.1016/j.ajo.2015.02.008>
- Van Blokland, S. C. A., & Versnel, M. A. (2002). Pathogenesis of Sjögren's syndrome: Characteristics of different mouse models for autoimmune exocrinopathy. *Clinical Immunology (Orlando, Fla.)*, 103(2), 111–124. <https://doi.org/10.1006/clim.2002.5189>
- Van Meter, W. S., Katz, D. G., White, H., & Gayheart, R. (2005). Effect of death-to-preservation time on donor corneal epithelium. *Transactions of the American Ophthalmological Society*, 103, 209–224.
- Vogel, R., Crockett, R. S., Oden, N., Laliberte, T. W., Molina, L., & Sodium Hyaluronate Ophthalmic Solution Study Group. (2010). Demonstration of efficacy in the treatment of dry eye disease with 0.18% sodium hyaluronate ophthalmic solution (vismed, rejena). *American Journal of Ophthalmology*, 149(4), 594–601. <https://doi.org/10.1016/j.ajo.2009.09.023>
- Weber, R. J., Liang, S. I., Selden, N. S., Desai, T. A., & Gartner, Z. J. (2014). Efficient targeting of fatty-acid modified oligonucleotides to live cell membranes through stepwise assembly. *Biomacromolecules*, 15(12), 4621–4626. <https://doi.org/10.1021/bm501467h>

- Wentz-Hunter, K., Cheng, E. L., Ueda, J., Sugar, J., & Yue, B. Y. J. T. (2001). Keratocan Expression Is Increased in the Stroma of Keratoconus Corneas. *Molecular Medicine*, 7(7), 470–477. <https://doi.org/10.1007/BF03401852>
- Willem de Vries, J., Schnichels, S., Hurst, J., Strudel, L., Gruszka, A., Kwak, M., Bartz-Schmidt, K. U., Spitzer, M. S., & Herrmann, A. (2018). DNA nanoparticles for ophthalmic drug delivery. *Biomaterials*, 157, 98–106. <https://doi.org/10.1016/j.biomaterials.2017.11.046>
- Yamaguchi, T. (2018). Inflammatory Response in Dry Eye. *Investigative Ophthalmology & Visual Science*, 59(14), DES192. <https://doi.org/10.1167/iovs.17-23651>
- Yoeruek, E., Spitzer, M. S., Tatar, O., Aisenbrey, S., Bartz-Schmidt, K. U., & Szurman, P. (2007). Safety Profile of Bevacizumab on Cultured Human Corneal Cells. *Cornea*, 26(8), 977. <https://doi.org/10.1097/ICO.0b013e3180de1d0a>
- Yoon, J. J., Ismail, S., & Sherwin, T. (2014). Limbal stem cells: Central concepts of corneal epithelial homeostasis. *World Journal of Stem Cells*, 6(4), 391–403. <https://doi.org/10.4252/wjsc.v6.i4.391>
- Yu, F.-S. X., Yin, J., Xu, K., & Huang, J. (2010). Growth factors and corneal epithelial wound healing. *Brain Research Bulletin*, 81(2–3), 229–235. <https://doi.org/10.1016/j.brainresbull.2009.08.024>
- Zeev, M. S., Miller, D. D., & Latkany, R. (2014). Diagnosis of dry eye disease and emerging technologies. *Clinical ophthalmology (Auckland, N.Z.)*, 8, 581–590. <https://doi.org/10.2147/OPHTH.S45444>
- Zhang, X., Jeyalatha M, V., Qu, Y., He, X., Ou, S., Bu, J., Jia, C., Wang, J., Wu, H., Liu, Z., & Li, W. (2017). Dry Eye Management: Targeting the Ocular Surface Microenvironment. *International Journal of Molecular Sciences*, 18(7). <https://doi.org/10.3390/ijms18071398>.

8 Declaration of own contributions

The study was conceived by Dr. Sven Schnichels and Dr. José Hurst. The work was carried out at the Institute for Ophthalmic Research in Tübingen.

All experiments were performed and analysed by me (Alice Rocha Teixeira Netto) under the supervision of Dr. José Hurst and Dr. Sven Schnichels, except for:

The DNA strands of the DNA Nanoparticles were synthesized by Dr. Jan Willem de Vries and the DNA Nanoparticles micelles were synthesized by Dr. José Hurst and Alice Rocha Teixeira Netto.

The samples of the human corneal *in vitro* model (Episkin™) incubated at 15% LH for 30 minutes were cultivated and incubated by Dr. José Hurst. Karin Tiedermann performed cryocut. Alice Rocha Teixeira Netto performed HE and DAPI staining, imaging and prepared the figures.

The samples of the human corneal *in vitro* model (Episkin™) incubated at 30% LH for 24 h were cultivated and incubated by Dr. José Hurst and Alice Rocha Teixeira Netto. Karin Tiedermann performed cryocut. Alice Rocha Teixeira Netto performed HE and DAPI staining, imaging and prepared the figures.

Alice Rocha Teixeira Netto and Marc Hrusa prepared the photos that exemplify how to develop the corneal cell outgrowth method (Figure 8). Alice Rocha Teixeira Netto prepared figure 8. Alice Rocha Teixeira Netto improved the method previously established at Schnichels lab, by washing a porcine eye five times in PBS with 2% PS after its extraction from the eye to reduce contamination of the culture and by incubating one entire porcine cornea cut into pieces of approximately 2 mm of corneal tissue and 2 mm of sclera in a T25 culture flask with ventilation screw cap. Marc Hrusa developed the method of cutting the porcine cornea in half and then each half in three parts to extract the center of the cornea. Previously, Alice Rocha Teixeira Netto used to extract first the center of the cornea with a scalpel and leave a strip with 2 mm of corneal tissue and 2 mm of sclera. Then the strip used to be cut in 2 mm pieces and

incubated in a T25 culture flask. The two ways of cutting the corneal pieces are possible for the outgrowth method.

Alice Rocha Teixeira Netto and Marc Hrusa performed the corneal cell isolation method and performed imaging of the cell outgrowth (day 2, day 4, 1 week, 2 weeks, 3-4 weeks) demonstrated at figure 22. Marc Hrusa quantified number of cells in each week of cell culture. Alice Rocha Teixeira Netto and Marc Hrusa performed data analysis. Alice Rocha Teixeira Netto developed the graph that shows “The average number of cells per week during outgrowth cultivation” and prepared figure 23.

Alice Rocha Teixeira Netto and Marc Hrusa performed immunostaining (CK3, occludin, ZO-1, keratocan, lumican and vimentin) and imaging of corneal cells after cultivation with the outgrowth method. Alice Rocha Teixeira Netto counted the total number of cells per picture and the number of cells that expressed CK3, occludin, ZO-1, keratocan, lumican and vimentin per picture, performed data analysis and developed the “Pie chart representing the proportion of distinct cell types”.

Marc Hrusa isolated and cultivated corneal cells with the outgrowth method for qRT-PCR. Alice Rocha Teixeira Netto performed cDNA synthesis, qRT-PCR, data analysis, graphs and prepared the figures.

Statistical analysis was carried out after consulting Dr. Torsten Strasser and under the supervision of Dr. José Hurst and Dr. Sven Schnichels.

I certify that I have written this thesis and all papers derived from it in which I am first author after the guidance by Dr. Hurst and Dr. Schnichels and that I have not used any sources other than those indicated by me.

Niterói, 05.02.24

Alice Rocha Teixeira Netto

9 Publications

Netto, Alice Rocha Teixeira, José Hurst, Karl-Ulrich Bartz-Schmidt, and Sven Schnichels. 2022. "Porcine Corneas Incubated at Low Humidity Present Characteristic Features Found in Dry Eye Disease". *International Journal of Molecular Sciences* 23, no. 9: 4567. <https://doi.org/10.3390/ijms23094567>

Netto*, Alice Rocha Teixeira, Marc Dieter Hrusa*, Karl-Ulrich Bartz-Schmidt, Sven Schnichels, and José Hurst. 2023. "Two Methods for the Isolation and Cultivation of Porcine Primary Corneal Cells". *Methods and Protocols* 6, no. 3: 50. <https://doi.org/10.3390/mps6030050>

*first shared authors

10 Acknowledgements

I started this research project with many challenges. As I studied medicine and worked for four years as a doctor, attending patients and performing surgeries, I had no previous experience in the area of basic research. Therefore, I would like to thank everyone who trusted in me, in my ability to learn new methods and to develop the skills necessary to carry out this doctoral research.

I would like to express my sincere thanks to Prof. Bartz-Schmidt for giving me the opportunity to do this Ph.D. and for agreeing to supervise me. I also want to express my gratitude to Jose Hurst for guiding and supporting me through the most challenging moments and for being so considerate. In addition, I thank Sven Schnichels for allowing me to conduct the research in his research group as well as for the numerous feedbacks on my Ph.D. project. Moreover, I thank all the members of my research group who were present in my daily life in the laboratory: Manuela, Heidi, Karin, Marc, Agnes, Peter, Nicolas, Helen, David, Julian, Marina, and many others that were in this research group during the time I developed this research.

I would like to express my thanks to the members of my advisory board, Prof. Tatagiba and Prof. Schaeffel, who gave me several inputs on my research project and for supporting me during these years. I also want to thank Prof. Tatagiba for being so kind and caring at crucial moments and the neurosurgery team for caring for my health during critical times of intense pain.

I thank Rodrigo Pegado and IBAP for all the support and trust since the beginning and Paulo Pfeil and Roswitha Meyer for the great opportunity to participate in the International Program of Ophthalmology. I acknowledge financial support from Coordenação de Aperfeiçoamento de Pessoal de Nível Superior-Brasil (CAPES) - Doutorado CAPES/DAAD - File number 88881.199770/2018-01 - Full Doctorate and Sandwich Doctorate -Call No. 22/2018 - Finance Code 001, without which it would not be possible to carry out this doctorate. In addition, I thank the coordination of the Ph.D. Program in

Experimental Medicine, Inka and Lina, for their support and patience in always answering numerous questions.

I also thank Jan de Vries, who, despite not having met him personally, contributed enormously to the development of DNA-Nanoparticles and left me with a lot of knowledge through his thesis and papers.

I would like to thank my friends Arianna, Eduardo, Lia, and Henriette, who supported me with countless conversations and encouragement. Furthermore, I would like to thank all my friends from Germany and Brazil who accompanied me on this journey and supported me in times of happiness or difficulty.

Finally, I want to thank my family, Roseli, Joaquim, and Elisa, who are my example of dedication and hard work, in addition to motivating and supporting me in every decision. Without the help of my family, I certainly would not have reached the end of this journey. Most importantly, I thank God and Jesus Christ, who supported and guided me at all moments.